

**PLASMA ENHANCED CHEMICAL VAPOUR
DEPOSITION OF CARBON NITRIDE FILMS FROM
ETHANE AND NITROGEN GAS MIXTURES**

MAISARA BINTI OTHMAN

**DISSERTATION SUBMITTED IN FULFILLMENT OF
THE REQUIREMENT FOR THE DEGREE OF
MASTERS OF SCIENCE**

**DEPARTMENT OF PHYSICS
FACULTY OF SCIENCE
UNIVERSITY OF MALAYA
KUALA LUMPUR**

2012

UNIVERSITI MALAYA

ORIGINAL LITERARY WORK DECLARATION

Name of Candidate: **Maisara binti Othman** (I.C/Passport No: **860417-56-5614**)

Registration/Matric No: **SGR090098**

Name of Degree: **Master of Science (Dissertation)**

Title of Project ~~Paper/Research Report~~/Dissertation/Thesis ("this Work"):

**PLASMA ENHANCED CHEMICAL VAPOUR DEPOSITION OF CARBON NITRIDE FILMS
FROM ETHANE AND NITROGEN GAS MIXTURES**

Field of Study: **Low Dimensional Materials**

I do solemnly and sincerely declare that:

- (1) I am the sole author/writer of this Work;
- (2) This Work is original;
- (3) Any use of any work in which copyright exists was done by way of fair dealing and for permitted purposes and any excerpt or extract from, or reference to or reproduction of any copyright work has been disclosed expressly and sufficiently and the title of the Work and its authorship have been acknowledged in this Work;
- (4) I do not have any actual knowledge nor do I ought reasonably to know that the making of this work constitutes an infringement of any copyright work;
- (5) I hereby assign all and every rights in the copyright to this Work to the University of Malaya ("UM"), who henceforth shall be owner of the copyright in this Work and that any reproduction or use in any form or by any means whatsoever is prohibited without the written consent of UM having been first had and obtained;
- (6) I am fully aware that if in the course of making this Work I have infringed any copyright whether intentionally or otherwise, I may be subject to legal action or any other action as may be determined by UM.

Candidate's Signature:

Date:

Subscribed and solemnly declared before,

Witness's Signature:

Date:

ABSTRACT

The fabrication and characterization of amorphous carbon nitride $a\text{-CN}_x$ thin films are intensively studied in this work. These films were obtained using radio frequency (rf) plasma enhanced chemical vapour deposition. In the first part of this work, $a\text{-CN}_x$ films were deposited either from methane and nitrogen ($\text{CH}_4\text{:N}_2$) or ethane and nitrogen ($\text{C}_2\text{H}_6\text{:N}_2$) mixtures under identical deposition conditions. The effects of varying the N_2 flow rate in each mixture were studied. It was observed that the use of different hydrocarbon gas produce either graphitic or polymeric $a\text{-CN}_x$ films. It was found that each set of films demonstrate its own unique characteristic. For films produced from $\text{CH}_4\text{:N}_2$, the sp^2 clusters increased due to high N incorporation into the films. This leads to the formation of graphitic-like structure. The nitrogen also distorts the carbon network and induced the increase in nitrile and/or isonitrile $\text{C}\equiv\text{N}$ bonds. This bonding influences the structure of the films by becoming more disordered and more porous. In contrast, low nitrogen incorporation was observed for films produced from $\text{C}_2\text{H}_6\text{:N}_2$ mixture. In these films, CH_n bonds are preferred which leads to the formation of more sp^3 sites in the films. This results in the films having higher E_g (2.8 eV) compared to films deposited from $\text{CH}_4\text{:N}_2$ which exhibits average E_g values of 1.9 eV. The increase in CH_n bonds indicates high H content which was found to be approximately 50 a.t%. This value suggests the films to be polymeric-like $a\text{-CN}_x$ films. A significant increase in PL intensity with increase in N incorporation was observed from both sets of films. However, the PL intensity of films produced from $\text{C}_2\text{H}_6\text{:N}_2$ is generally higher compared to films produced from $\text{CH}_4\text{:N}_2$. From these results it seems that the $\text{C}_2\text{H}_6\text{:N}_2$ mixture may be a better alternative to the popular $\text{CH}_4\text{:N}_2$, as it shows a significantly higher PL emission and low porosity. The disadvantage is the lower growth rate and N incorporation of the films formed using $\text{C}_2\text{H}_6\text{:N}_2$ mixture. In order to solve these problems and further improve the properties of these films, hydrogen were introduced into the $\text{C}_2\text{H}_6\text{:N}_2$ mixture. As a result, the films produced from $\text{C}_2\text{H}_6\text{:N}_2\text{:H}_2$ shows enhancement in their growth rate and N incorporation with the increase in hydrogen dilution. Increase of the film's growth rate and N incorporation, while retaining low porosity and high PL properties was possible if low H_2 dilution was applied. At high H_2 dilution, N incorporation increases but this leads to the increase in porosity and quenching of the PL intensities of the films. However, even the PL efficiency decreases, these films still generally exhibit much higher PL emission intensities compared to those $\text{CH}_4\text{:N}_2$. This work concludes that the $\text{C}_2\text{H}_6\text{:N}_2\text{:H}_6$ mixture with low H_2 dilution is an excellent alternative to the popular $\text{CH}_4\text{:N}_2$ mixture in the deposition of rf PECVD CN_x films to obtain high PL intensities, high N incorporation and low porosity.

ABSTRAK

Fabrikasi dan pencirian filem nipis amorfus karbon nitrida ($a\text{-CN}_x$) dikaji secara intensif di dalam kajian ini. Filem ini telah dihasilkan dengan menggunakan kaedah pemendapan frekuensi radio wap kimia secara peningkatan plasma. Dalam bahagian pertama kajian ini, filem $a\text{-CN}_x$ telah dimendapkan sama ada daripada campuran metana dan nitrogen ($\text{CH}_4:\text{N}_2$) atau campuran etana dan nitrogen ($\text{C}_2\text{H}_6:\text{N}_2$) di bawah keadaan pemendapan yang sama. Kesan pengubahan kadar alir gas N_2 kepada setiap campuran gas dikaji. Penggunaan gas hidrokarbon yang berlainan diperhatikan telah menghasilkan jenis filem $a\text{-CN}_x$ yang berbeza sama ada bersifat grafitik atau filem yang bersifat polimerik. Setiap set filem menunjukkan ciri-ciri unik mereka yang tersendiri. Bagi filem yang terhasil daripada campuran $\text{CH}_4:\text{N}_2$, kelompok sp^2 meningkat akibat penglibatan nitrogen yang tinggi di dalam filem. Ini mendorong kepada pembentukan struktur seperti grafitik terhasil. Nitrogen juga mengganggu rangkaian karbon dan mendorong peningkatan ikatan nitril dan/atau isonitril $\text{C}\equiv\text{N}$. Ikatan ini mempengaruhi struktur filem menjadi lebih tak tertib dan lebih berliang. Berbeza dengan filem yang dihasilkan daripada campuran $\text{C}_2\text{H}_6:\text{N}_2$, penglibatan nitrogen ke dalam filem didapati lebih rendah. Ikatan CH_n bagi filem ini adalah lebih banyak dan mendorong kepada peningkatan penghasilan sp^3 . Ini menghasilkan filem yang berjurang tenaga lebih tinggi (2.8 eV) berbanding filem yang terhasil daripada campuran $\text{CH}_4:\text{N}_2$ dimana menunjukkan purata nilai jurang tenaga sebanyak 1.9 eV. Peningkatan ikatan CH_n ini juga menunjukkan bahawa filem ini mempunyai nilai kandungan H yang tinggi iaitu sebanyak 50 a.t%. Nilai ini mencadangkan bahawa filem yang terhasil adalah filem yang bersifat polimerik. Keamatan PL meningkat dengan ketara dengan peningkatan penglibatan N bagi kedua-dua set filem. Walaubagaimanapun, keamatan PL bagi filem yang dihasilkan daripada $\text{C}_2\text{H}_6:\text{N}_2$ secara amnya diperhatikan lebih tinggi berbanding $\text{CH}_4:\text{N}_2$. Daripada dapatan yang diperolehi, pemilihan campuran $\text{C}_2\text{H}_6:\text{N}_2$ adalah lebih baik dari segi keamatan PL yang tinggi dan keliangan filem yang lebih rendah berbanding filem yang dihasilkan daripada campuran $\text{CH}_4:\text{N}_2$. Namun yang demikian, kadar pertumbuhan dan penglibatan N yang terhasil daripada campuran $\text{C}_2\text{H}_6:\text{N}_2$ ini adalah lebih rendah. Dalam usaha menyelesaikan masalah dan memperbaiki sifat-sifat filem ini, gas hidrogen diperkenalkan ke dalam campuran $\text{C}_2\text{H}_6:\text{N}_2$ pada bahagian kedua kajian ini. Hasilnya, kadar pertumbuhan filem dan penglibatan N meningkat. Filem dengan kadar pertumbuhan dan penglibatan N yang tinggi disamping dapat mengekalkan filem yang berkeamatan PL tinggi dan berkeliangan rendah boleh diperolehi jika pencairan hidrogen adalah rendah. Pada campuran hidrogen yang tinggi, penglibatan N di dalam filem adalah tinggi tetapi mendorong kepada peningkatan keliangan filem dan penurunan keamatan PL. Walaupun kecekapan PL berkurangan, filem ini masih menunjukkan keamatan pancaran PL yang lebih tinggi berbanding filem yang terhasil daripada campuran $\text{CH}_4:\text{N}_2$. Kesimpulannya, campuran $\text{C}_2\text{H}_6:\text{N}_2:\text{H}_2$ dengan cairan gas hidrogen yang rendah adalah pilihan lebih baik berbanding campuran $\text{CH}_4:\text{N}_2$ yang biasa digunakan dalam pemendapan filem CN_x menggunakan rf PECVD untuk memperolehi keamatan PL dan penglibatan N yang tinggi dengan keliangan filem yang rendah.

ACKNOWLEDGEMENT

In the name of ALLAH, the Most Gracious, the Most Merciful.....

Alhamdulillah, all praises to Allah for the strengths and His blessing in completing this thesis. First and foremost, I would like to express my deepest gratitude to my supervisors, Professor Datin Dr. Saadah Abdul Rahman and Associate Professor Dr. Siti Meriam Ab. Gani for their guidance, support and patience during this research work. Thanks for believing in me and giving me the chance to do this research in my own way with your guidance. Thanks for your kindness in giving useful advice to me, not only in the field of research but in all circumstances.

My gratitude also goes to our science officers, Pn. Zurina Marzuki and Pn. Aida Hani and our assistants' science officers, En. Mohamad Aruf and Pn. Norlela for assistance in technical works. I am greatly indebted to my senior, Dr. Richard Ritikos for his endless support and assistance throughout my experimental work and thesis write-up. Not forgetting Dr. Goh Boon Tong for his kindness during my master work especially when problem occurred during the experiments. I would also like to thank my teammates, Ijah and Mai, and my entire laboratory mate especially to Kak Nor Khairiah, Sukong, Kee Wah, Ragib, Hajar, Saipul, Gan, Kak Toong and others for their support and assistance since my first day as a postgraduate student until now. Sincere thanks also goes to my juniors, Syed and Linda. Thanks a lot guys.

I would like to take this opportunity to express my gratitude to University of Malaya for awarding the SBUM scholarship to pursue this MSc. I would also like to acknowledge Ministry of Science, Technology and Innovation (MOSTI), Malaysia for the grants including Fundamental Research Grant Scheme FP016/2008C, FP052/2010B and University of Malaya (Grants PS313/2009B and RG064/09AFR) for financial support of my master work.

My deepest gratitude goes to my beloved parents, Hj. Othman bin Mohd Dom and Hjh. Julia Abdul Jalil, my brother, Mohd Hafiz, and my two sisters, Munirah and Mardhiah for their unconditional love and prayers. I would like to extent my thanks to my beloved future husband, Muhammad Aiman Basri for his constant support and encouragement. Thanks for lending me your ears, heart and time, each time I fall. Last but not least, I would like to express my sincere thanks to all those who have indirectly contributed to the completion of this thesis.

TABLE OF CONTENTS

| | |
|---|-------------|
| Original Literary Work Declaration..... | ii |
| Abstract..... | iii |
| Abstrak..... | iv |
| Acknowledgement | v |
| Table of Contents | vi |
| List of Figures..... | viii |
| List of Tables | xi |
| List of Abbreviation..... | xii |
| List of Publications | xiii |
| Chapter 1 Introduction..... | 1 |
| 1.1 Introduction of Carbon Films..... | 1 |
| 1.2 Nitrogen Incorporation into Carbon Films | 3 |
| 1.3 Research Objectives | 5 |
| 1.4 Outline of Thesis | 5 |
| Chapter 2 Literature Review | 7 |
| 2.1. Introduction..... | 7 |
| 2.2. Classification of Amorphous Carbon Nitride Films | 7 |
| 2.3. Deposition Gases | 9 |
| 2.3.1. <i>Hydrocarbon gas</i> | 9 |
| 2.3.2. <i>Nitrogen incorporation</i> | 10 |
| 2.3.3. <i>Hydrogen dilution</i> | 11 |
| 2.4. Analytical Studies | 12 |
| 2.4.1. <i>Raman spectroscopy</i> | 12 |
| 2.4.2. <i>Fourier Transform Infrared</i> | 22 |
| 2.4.3. <i>Optical</i> | 24 |
| 2.4.4. <i>Photoluminescence</i> | 27 |
| Chapter 3 Experimental Details | 28 |
| 3.1. Introduction..... | 28 |
| 3.2. Deposition System | 28 |
| 3.2.1. <i>Radio frequency plasma enhanced chemical vapour deposition</i> <i>(rf PECVD) system.</i> | 28 |
| 3.2.2. <i>The reaction chamber</i> | 32 |
| 3.3. Preparation Procedures for Films Substrate..... | 34 |

| | |
|--|------------|
| 3.4. Substrate Cleaning Procedure | 34 |
| 3.5. Deposition Procedure | 35 |
| 3.5.1. <i>Pre-deposition process</i> | 35 |
| 3.5.2. <i>Deposition process</i> | 37 |
| 3.5.3. <i>Post-deposition process</i> | 38 |
| 3.6. Characterization Techniques | 39 |
| 3.6.1. <i>Surface profilometry</i> | 39 |
| 3.6.2. <i>Auger electron spectroscopy</i> | 41 |
| 3.6.3. <i>Fourier transforms infrared spectroscopy</i> | 43 |
| 3.6.4. <i>Ultra-violet visible near infra-red spectroscopy</i> | 44 |
| 3.6.5. <i>Raman spectrometry</i> | 49 |
| 3.6.6. <i>Photoluminescence spectroscopy</i> | 53 |
| Chapter 4 Results And Discussion..... | 55 |
| 4.1. Introduction | 55 |
| 4.2. Effects of Nitrogen Incorporation on the Carbon Nitride Films Using Different Precursors. | 57 |
| 4.2.1. <i>Growth Rate</i> | 57 |
| 4.2.2. <i>Auger Electron Spectroscopy</i> | 59 |
| 4.2.3. <i>Fourier Transformation Infrared</i> | 62 |
| 4.2.4. <i>Raman Spectroscopy</i> | 70 |
| 4.2.5. <i>Ultra-violet Visible Near Infra-red Spectroscopy</i> | 82 |
| 4.2.6. <i>Photoluminescence</i> | 84 |
| 4.3. Effects of Hydrogen Dilution on the Properties of Amorphous Carbon Nitride Films..... | 91 |
| 4.3.1. <i>Growth Rate</i> | 91 |
| 4.3.2. <i>Auger Electron Spectroscopy</i> | 95 |
| 4.3.3. <i>Fourier Transform Infrared</i> | 98 |
| 4.3.4. <i>Raman Spectroscopy</i> | 101 |
| 4.3.5. <i>Optical</i> | 107 |
| 4.3.6. <i>Photoluminescence</i> | 109 |
| Chapter 5 Conclusions And Future Works | 114 |
| 5.1. Conclusions | 114 |
| 5.2. Future Work | 117 |
| References | 118 |

LIST OF FIGURES

CHAPTER 1

| | | |
|------------|--|---|
| Figure 1.1 | The sp^3 , sp^2 and sp^1 hybridized bonding..... | 2 |
|------------|--|---|

CHAPTER 2

| | | |
|-------------|---|----|
| Figure 2.1 | Carbon motions in the (a) E_{2g} G mode and (b) A_{1g} D modes..... | 13 |
| Figure 2.2 | A schematic variation of the G peak position and I_D/I_G ratio as a function of amorphization trajectory at three different stages. | 14 |
| Figure 2.3 | Variation in sp^2 configuration in the ‘three stage model’..... | 16 |
| Figure 2.4 | Amorphization trajectory, showing the schematic variation of (a) G position and (b) I_D/I_G for multi-wavelength. | 17 |
| Figure 2.5 | Schematic diagram of variation on the Raman spectra. A dotted arrow marks the indirect influence of the sp^3 content on increasing G position.. | 18 |
| Figure 2.6 | Variation in G peak position and I_D/I_G in UV excitation..... | 19 |
| Figure 2.7 | Photoluminescence background of Raman spectrum..... | 20 |
| Figure 2.8 | Raman spectra of different type of amorphous carbon with various H content at excitation wavelength of (a) 514.5 nm and (b) 244 nm | 21 |
| Figure 2.9 | FTIR spectra of various types of CN_x films separated into three different bands. | 24 |
| Figure 2.10 | Variation in optical gap as a function of nitrogen content of carbon nitride films using various techniques. | 26 |

CHAPTER 3

| | | |
|-------------|--|----|
| Figure 3.1 | Photograph of (a) PECVD deposition system and enlarged picture of (b) mass flow controller (c) pressure meter (d) reaction chamber (e) rf regulator and temperature controller (f) Rotary and diffusion pump. | 30 |
| Figure 3.2 | Schematic diagram of PECVD deposition system | 31 |
| Figure 3.3 | Schematic diagram of the home-built reaction chamber for the rf PECVD system..... | 33 |
| Figure 3.4 | Stainless steel substrate holder (top view)..... | 34 |
| Figure 3.5 | KLA-Tencor P-6 surface profiler system | 40 |
| Figure 3.6 | Example of profilometer scan of deposited film. | 40 |
| Figure 3.7 | The schematic diagram of the Auger process..... | 41 |
| Figure 3.8 | Picture of JEOL JAMP-9500F field emission Auger microprobe | 42 |
| Figure 3.9 | The list of quantitative data of the relative concentration taken from AES machine. | 42 |
| Figure 3.10 | The FTIR spectroscopy block diagram | 43 |
| Figure 3.11 | The transmittance of FTIR spectrum..... | 44 |

| | | |
|-------------|--|----|
| Figure 3.12 | A picture of Jasco V-570 Ultra-violet visible near infra-red (UV Vis NIR) spectroscopy | 45 |
| Figure 3.13 | Block diagram of typical spectrometer setup | 46 |
| Figure 3.14 | Schematic diagram of Czerny-Turner grating monochromator. | 46 |
| Figure 3.15 | Transmittance, T% and reflectance, R% spectrum of CN _x films. | 48 |
| Figure 3.16 | Values of E _g taken from the intersection of energy axis | 48 |
| Figure 3.17 | The Jablonski energy diagram for Raman scattering. | 49 |
| Figure 3.18 | A picture of Horiba Jobin Yvon 800 UV Micro-Raman Spectrometer..... | 50 |
| Figure 3.19 | Schematic diagram of Raman principle. | 51 |
| Figure 3.20 | Examples of typical Raman scattering spectra with (a) raw data showing baseline fitting and (b) spectra with base line correction showing Gaussian fitting to obtain D and G bands. | 52 |

CHAPTER 4

| | | |
|-------------|--|----|
| Figure 4.1 | Flow chart shows the preparations steps studies of CN _x films. | 56 |
| Figure 4.2 | Variation in growth rate using CH ₄ :N ₂ or C ₂ H ₆ :N ₂ mixture as a function of N ₂ flow rate. Line is as guide to the eye. | 58 |
| Figure 4.3 | Variation in nitrogen to carbon, N/C ratio for films deposited as a function of N ₂ flow rate. Line is as guide to the eye..... | 60 |
| Figure 4.4 | FTIR absorbance spectra as a function of N ₂ flow rate using (a) CH ₄ and (b) C ₂ H ₆ in the range of 1000-4000 cm ⁻¹ | 64 |
| Figure 4.5 | Fourier transform infrared spectra of CN _x films prepared from CH ₄ :N ₂ as a function of N ₂ flow rate separated into three different spectra range of (a) 1000-2000 cm ⁻¹ , (b) 2000-2400 cm ⁻¹ and (c) 2600-4000 cm ⁻¹ | 66 |
| Figure 4.6 | Fourier transform infrared spectra of CN _x films prepared from C ₂ H ₆ :N ₂ as a function of N ₂ flow rate separated into three different spectra range of (a) 1000-2000 cm ⁻¹ , (b) 2700-3100 cm ⁻¹ and (c) 3100-4000 cm ⁻¹ | 67 |
| Figure 4.7 | Variation in FTIR peaks of CN _x films prepared from C ₂ H ₆ :N ₂ with (a) highest absorbance intensities of C=N, C=C and CH _n ; and (b) the ratio of C=N/CH _n . Lines are as guide to the eye. | 68 |
| Figure 4.8 | Variation in Raman spectra as a function of N ₂ flow rate for films prepared from CH ₄ :N ₂ . m refers to the baseline slope of the PL background..... | 72 |
| Figure 4.9 | Variation in Raman spectra as a function of N ₂ flow rate for films prepared from C ₂ H ₆ :N ₂ . m refers to the baseline slope of the PL background..... | 73 |
| Figure 4.10 | Variation in deconvoluted Raman spectra as a function of N ₂ flow rate using (a) CH ₄ and (b) C ₂ H ₆ | 74 |
| Figure 4.11 | Variation in Raman G peak position and I _D /I _G as a function of nitrogen flow rate for film deposited from CH ₄ :N ₂ | 76 |
| Figure 4.12 | A schematic variation of the G peak position and I _D /I _G ratio as a function of amorphization trajectory at three different stages | 77 |

| | | |
|-------------|---|-----|
| Figure 4.13 | Variation in Raman G peak position and I_D/I_G as a function of N_2 flow rate for films deposited from $C_2H_6:N_2$. | 78 |
| Figure 4.14 | Variation in H content as a function of N_2 flow rate. | 81 |
| Figure 4.15 | Variation in energy gap as a function of N_2 flow rate. | 82 |
| Figure 4.16 | Variation on PL spectra as a function of N_2 flow rate. | 85 |
| Figure 4.17 | Gaussian fitting of PL spectra as a function of N_2 flow rate for a) CH_4 and b) C_2H_6 . The black line shows the cumulative fitting curve due to the best fit. | 88 |
| Figure 4.18 | Variation in integrated PL intensities as a function of N_2 flow rate. Line is drawn as guide for eye. | 89 |
| Figure 4.19 | Variation in integrated PL intensities as a function of N_2 flow rate. Line is drawn as guide for eye. | 90 |
| Figure 4.20 | Variation in growth rate with H_2 flow rate. Line is as guide to the eye. | 92 |
| Figure 4.21 | Variation of deposition rate with different flow rate of N_2 without inclusion of H_2 using CH_4 or C_2H_6 , and deposition rate of CN_x with different flow rate of H_2 gas with a mixture of C_2H_6 and N_2 . Line is as guide to the eye. | 94 |
| Figure 4.22 | Variation of nitrogen to carbon N/C ratio as a function of H_2 flow rate. Line is as guide to the eye. | 95 |
| Figure 4.23 | Variation in N/C ratio for films deposited as function of flow rate. | 97 |
| Figure 4.24 | Variation in FTIR spectra for $C_2H_6:N_2:H_2$ as a function of H_2 flow rate. The height of the spectrum for film deposited at H_2 flow rate of 0 sccm is adjusted for clarification. | 98 |
| Figure 4.25 | Fourier transform infrared spectra of CN_x films prepared from $C_2H_6:N_2:H_2$ as a function of H_2 flow rate separated into three different spectra range of (a) $1000-1800\text{ cm}^{-1}$, (b) $1800-2800\text{ cm}^{-1}$ and (c) $2600-4000\text{ cm}^{-1}$. | 100 |
| Figure 4.26 | Variation in Raman spectra as a function of H_2 flow rate. The height of the spectrum for film deposited at H_2 flow rate of 125 sccm adjusted for classification. | 102 |
| Figure 4.27 | Variation in original Raman spectra as a function of H_2 flow rate. | 103 |
| Figure 4.28 | Variation in G peak position and I_D/I_G as a function of H_2 flow rate. | 105 |
| Figure 4.29 | Variation in hydrogen content as a function of H_2 flow rate. | 106 |
| Figure 4.30 | Variation in E_g as a function of H_2 flow rate. | 107 |
| Figure 4.31 | Variation in E_g as a function of N_2 and/or H_2 flow rate. | 108 |
| Figure 4.32 | Variation in PL spectra as a function of H_2 flow rate. | 110 |
| Figure 4.33 | The PL intensity and peak position of CN_x films depending on H_2 flow rate. | 111 |
| Figure 4.34 | Variation in PL intensity as a function of N_2 flow rate for films produced from $CH_4:N_2$ and $C_2H_6:N_2$ together with the variation in PL intensity as a function of H_2 flow rate for the films produced from $C_2H_6:N_2:H_2$. | 112 |
| Figure 4.35 | Variation in PL intensity and H content as a function of H_2 flow rate. | 113 |

LIST OF TABLES**Chapter 2**

| | |
|--|----|
| Table 2.1 List of bonding assignments, wavenumber regions and corresponding references | 23 |
|--|----|

Chapter 3

| | |
|--|----|
| Table 3.1 Deposition parameters for the study of the effects of nitrogen and hydrogen flow rate on the structural properties of $\text{CN}_x\text{:H}$ thin films..... | 38 |
|--|----|

LIST OF ABBREVIATIONS

| | |
|------------------------|--|
| $a\text{-C:H}$ | Hydrogenated amorphous carbon |
| $a\text{-CN}_x$ | Amorphous carbon nitride |
| a.t % | Atomic percent |
| CH_4 | Methane |
| C_2H_6 | Ethane |
| DLC | Diamond like carbon |
| E_g | Energy gap |
| FWHM | Full width half maximum |
| H_2 | Hydrogen |
| MFC | Mass flow controller |
| N_2 | Nitrogen |
| PECVD | Plasma enhanced chemical vapour deposition |
| PL | Photoluminescence |
| rf | Radio frequency |
| sccm | Standard cubic centimeter per minute |
| $ta\text{-C}$ | Tetrahedral amorphous carbon |
| $ta\text{-C:H}$ | Hydrogenated tetrahedral amorphous carbon |

LIST OF PUBLICATIONS

1. Effect of N₂ flow rate on the properties of CN_x thin films prepared by radio frequency plasma enhanced chemical vapor deposition from ethane and nitrogen

Othman. M., Ritikos. R., Khanis. N. H., Rashid. N.M.A., Gani. S.M.A., Rahman. S.A.

Thin Solid Films, Article in press DOI: 10.1016/j.tsf.2012.03.090

Other related publications

2. Effects of rf power on the structural properties of carbon nitride thin films prepared by plasma enhanced chemical vapour deposition

Othman. M., Ritikos. R., Khanis. N. H., Rashid. N. M. A., Rahman. S. A., Gani. S. M. A., Muhamad. M. R.

Thin Solid Films, Volume 519, Issue 15, 31 May 2011, Pages 4981-4986

3. Effect of substrate bias on the optical, bonding and electrical properties of a-CN_x deposited by rf PECVD

M. Othman, R. Ritikos , S. M .A. Gani, S. A. Rahman and M. R. Muhamad

Solid State Science and Technology, Vol. 18, No 2 (2010) 99-104 ISSN 0128-7389

4. Effect of pre-deposited carbon layer on the formation of carbon nitride nanostructures prepared by radio-frequency plasma enhanced chemical vapour deposition

Khanis. N.H. , Ritikos. R. , Othman. M., Rashid. N.M.A., Gani. S.M.A., Muhamad. M.R., Rahman. S.A.

Materials Chemistry and Physics, Volume 130, Issues 1–2, 17 October 2011, Pages 218-222

CHAPTER 1 INTRODUCTION

1.1 Introduction of Carbon Films

Carbon forms a variety of crystalline and disordered structures due to its ability to exist in sp^3 , sp^2 and sp^1 hybridizations. However, the versatility of carbon material develops from the strong dependence of their physical properties on the ratio of sp^2 (graphitic-like) to sp^3 (diamond-like) bonds. In general, an amorphous carbon can have any mixture of sp^3 , sp^2 and even sp^1 sites. The hybridizations bonding of the sp^3 , sp^2 and sp^1 are shown in Figure 1.1. There has been a lot of interest on amorphous and nanocrystalline carbon films due to their beneficial chemical and physical properties such as high chemical inertness, diamond-like properties (Beghi et al., 2002; Elinson et al., 1999; Mehta & Ogryzlo, 1994; Wang, Shen, Ning, Ye, & Zhu, 1997) and favorable tribological properties suitable for industrial use (Bull, 1995). The material usually comprises of a hybrid of graphite and diamond microstructure and thus possesses properties that lie between them. Amorphous and nanocrystalline carbon films form in different matrices and mostly doped with high amount of hydrogen thereby making these films more diverse (Zhang, Tay, Sun, & Lau, 2002). The hydrogen usually plays an important role in the films properties. In a related study, it was found that a considerable amount of hydrogen can change the films properties by widening the optical band gap and can exhibit special optical absorption, intense photoluminescence and electron affinity. Thus, the tunable properties and thermal stability of these films have aroused enormous research interest due to their potential applications (Godet, Heitz, Bourée, Dré villon, & Clerc, 1998; Kumar, Dixit, Sarangi, & Bhattacharyya, 1996; Pappas et al., 1992; Sattel, Robertson, & Ehrhardt, 1997; Tsai & Bogoy, 1987).

Amorphous carbon films with low hydrogen concentration and high percentage of sp^3 carbon are referred to as hydrogenated tetrahedral amorphous carbon ($ta-C:H$). Carbon films with low hydrogen concentration are often called graphite-like $a-C:H$ (GLCH) due to its hardness but a considerable amount of sp^2 site in addition to sp^3 carbon sites. Films with moderate hydrogen concentration are referred to as hydrogenated amorphous carbon ($a-C:H$) films. Films with high hydrogen concentration are usually called hydrogenated polymeric-like carbon (PLCH) films. Most of the sp^3 bonds are hydrogen terminated and this material is soft and has low density (Robertson, 2002).

The role of hydrogen in $a-C:H$ films are different compared to amorphous silicon films. The hydrogen plays an important role in determining the properties of this $a-C:H$ films. In $a-Si:H$ films, the hydrogen mainly passivates the dangling bonds. However, in $a-C:H$ films, the hydrogen not only passivates the dangling bonds to reduce the number of defect states near mid gap, but also promotes the sp^3 bonding which gives higher films band gap (Robertson, 1997). High hydrogen concentration decreases the mass density and hardness of films.

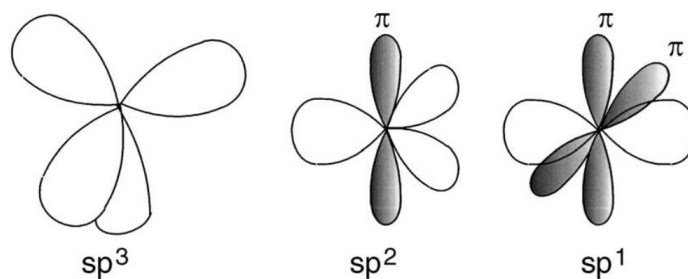


Figure 1.1 The sp^3 , sp^2 and sp^1 hybridized bonding (Robertson, 2002).

1.2 Nitrogen Incorporation into Carbon Films

Over the years, considerable efforts have been put into incorporating N into C film structure since the prediction by Liu and Cohen of the hypothetical super hard β - C_3N_4 phase (Liu & Cohen, 1990). The simulation work states that this crystalline C_3N_4 phase would exhibit a bulk modulus, hardness and optical gap similar to diamond. However, most follow-up experiments produce amorphous carbon nitride films ($a-CN_x$) which was found to be interesting in their own right (Badzian, Badzian, Roy, & Drawl, 1999; Muhl & Méndez, 1999). The synthesis of amorphous carbon nitride films has generated a great deal of interest due to their potential applications as hard coatings, protective overcoats for magnetic storage disks, gas sensor and others (Cutiongco, Li, Chung, & Bhatia, 1996; Hellgren, Johansson, Broitman, Hultman, & Sundgren, 1999; Yeh, Lin, Sivertsen, & Judy, 1991).

In general, the properties of the CN_x films are dependent on the nitrogen content and types of bonding between carbon-carbon and carbon-nitrogen atoms. It is therefore important to understand and identify the carbon-nitrogen bonding of the films as a function of the nitrogen content since non-nitrogenated carbon films has been extensively studied and good correlation between films properties have been obtained. It is also helpful to study the effect of deposition parameters on the films properties as this will enable construct able and tailoring of their properties. Furthermore most of the efforts in the research of CN_x have been carried out to obtain crystalline super-hard phase. However work on its structural and bonding characteristics are limited and there is no clear correlation between the films properties and these characteristics.

Methane is the most common gas used as a hydrocarbon source in the growth of CN_x films since this gas is by far the safest gas amongst hydrocarbons. Other popular gasses used are acetylene and ethylene. However, these gasses are extremely dangerous since they are normally classified as explosive and are highly volatile. There are very few comparative studies on the effects of using different hydrocarbon precursors on the properties of these CN_x films. Similarly, the deviation from using methane is not so common. In particular, the use of ethane in the growth of CN_x film is scarcely investigated. The higher ratio of C to H atoms in this gas compared to CH_4 is expected to produce interesting effects on the film properties. Examples of work done using ethane as the gas precursors are limited to the fabrication of multi wall carbon nanotube (MWCNT) films. Ethane gas is used as a cheap non-toxic carbon source (Gulino et al., 2005). They found that with higher ethane and hydrogen flow ratio result in enhanced carbon deposit with amorphous-phase inclusions which represent the best compromise between yield and quality of reaction products (Donato et al., 2007).

Among the different properties of α - CN_x films, photoluminescence (PL) are both of fundamental and practical interest (Demichelis, Schreiter, & Tagliaferro, 1995; Y. Liu, Demichelis, & Tagliaferro, 1996). The amount of nitrogen concentration always influences the PL properties (Demichelis, Liu, Rong, Schreiter, & Tagliaferro, 1995; Mendoza, Aguilar-Hernández, & Contreras-Puente, 1992; Mutsukura & Akita, 1999). CN_x films have possible application in electroluminescence devices (Iwasaki et al., 1999; M. Zhang, Nakayama, & Kume, 1999). The analysis of the various PL features signal also provides valuable information on the nature of electronic state (Fanchini, Ray, Tagliaferro, & Laurenti, 2002) and the mechanism of carrier recombination.

1.3 Research Objectives

This research work focuses on the structural, bonding and optical properties of carbon nitride (CN_x) films. In this study, methane and ethane were used as the hydrocarbon precursor to study and make a comparison between these two hydrocarbon gases on the properties of CN_x films. Ethane was chosen in view of having more C atom in its molecular configuration compared to methane gas. Besides that, this gas is safe to use and easily obtainable. There are four main objectives of this research work as stated below:

- (1) To investigate the different effects of using two different hydrocarbon gases to the structural and optical properties of the resulting CN_x films.
- (2) To investigate the effects of nitrogen dilution into these different hydrocarbon gases on the properties of the thin films.
- (3) To investigate the effects of hydrogen dilution into the mixture of ethane and nitrogen gases mixture on the properties of carbon nitride thin films.
- (4) To determine the different advantages of using either CH_4 or C_2H_6 and to tailor the mixture combination to obtain a desired film.

1.4 Outline of thesis

The first chapter of this thesis introduces this work. In the following chapter (Chapter 2) a literature review of other related works are presented. This chapter consists of three major parts. The first part contains a discussion on the different types of amorphous carbon nitride films. A brief discussion on the deposition techniques used to obtain these films is also included. The second part was focused on the review of

different hydrocarbon gases normally used in producing CN_x films. A brief discussion on the analytical method related to this work is presented in the last part of this chapter. These include Raman spectroscopy, Fourier transform infrared analysis, photoluminescence and optical characteristic.

The experimental and analytical methods are discussed in Chapter 3. This chapter is divided into two parts. The first part describes the sample preparation including description of the deposition system and process. The second part of this chapter discusses basic operation of the analytical apparatus used in this study. Besides that, the calculations used to analyze their data are also included.

Chapter 4 presents the experimental results and discussion. This chapter is divided into two parts. In the first part of the study, two sets of films prepared from either methane or ethane as a function of nitrogen flow rate are presented. This first part fulfills two of this work's objectives. Firstly, the effects of nitrogen flow rate and the nitrogen incorporation are determined. Secondly, the use of different hydrocarbon gas mixture is studied. The second part studies the effect of H_2 dilution in the formation of these CN_x films and its properties.

This thesis is concluded with Chapter 5 which presents the summary of the findings. Suggestion for future works is also included in this chapter.

CHAPTER 2 LITERATURE REVIEW

2.1 Introduction

This chapter presents the literature review which emphasises on the formation of different types of carbon nitride (CN_x) films. The initial part of this chapter focuses on the classification of various CN_x structures including a review on deposition techniques usually employed in the fabrication of these films. This is followed by the choices of the typical gases used in the synthesis of these films. A review on various analytical methods used is also presented. This is deemed necessary since the interpretation of the measured data is an essential part in the characterization of the films.

2.2 Classification of Amorphous Carbon Nitride Films

It is possible to classify carbon nitride (CN_x) films into different structural groups. These groups are analogous to those of their corresponding N-free films. There are four main groups of C films which are determined from the relative content of sp^2 -C bonds in the films. These include amorphous carbon ($a\text{-C}$), tetrahedral amorphous carbon ($ta\text{-C}$), hydrogenated amorphous carbon ($a\text{-C:H}$) and hydrogenated tetrahedral amorphous carbon ($ta\text{-C:H}$). Different types of CN_x films are produced from different deposition techniques and parameters. Brief descriptions on these groups and corresponding deposition techniques are described below.

The first type is amorphous carbon nitride ($a\text{-CN}_x$) films. Essentially, amorphous carbon films exhibit high sp^2 bonded fraction. Nitrogen was introduced to increase the carbon sp^3 bonding (Hellgren, Johansson, Broitman, Hultman, & Sundgren, 1999) in these films. Moreover, N incorporation causes cross-linking between graphitic

planes. Strong cross-linking increases its mechanical hardness and elastic recovery (Hellgren, et al., 1999; Sjöström et al., 1996; Sjöström, Stafström, Boman, & Sundgren, 1995). These films are usually produced using d.c, r.f or magnetron sputtering and low energy laser ablation.

Hydrogenated amorphous carbon nitride ($a\text{-CN:H}$) is similar to that of $a\text{-CN}_x$ film. The difference is seen in the presence of hydrogen in $a\text{-CN}_x$ film which varies its fraction of sp^2 and sp^3 bonds. $a\text{-C:H:N}$ films can be categorized into two different groups which are polymeric and diamond-like films. Among these two, polymeric CN_x film exhibit higher H content. In contrast to $a\text{-C:N}$, the hardness of films becomes lower with higher N due to the formation of more terminating groups such as NH_2 and nitrile groups. Usually, these films were grown by conventional plasma enhanced chemical vapour deposition (PECVD) technique (Hammer, Victoria, & Alvarez, 1998; Schwan, Batori, Ulrich, Ehrhardt, & Silva, 1998; Silva et al., 1997).

The third type is tetrahedral amorphous carbon nitride ($ta\text{-CN}_x$) films. Its analogous $ta\text{-C}$ is mainly made up of sp^3 bonded C and its film exhibits high hardness. The addition of nitrogen into this $ta\text{-C}$ increases the sp^2 bonds in the film while still retaining its hardness. However, due to the increase in sp^2 content, the resistivity and optical energy gap decrease compared to those of pure $ta\text{-C}$ film. These $ta\text{-CN}_x$ films have been produced using mass selected ion beam deposition (MSIBD), pulsed laser deposition (PLD) or filtered cathodic vacuum arc (FCVA). (Polo, Andújar, Hart, Robertson, & Milne, 2000; Spaeth, Kühn, Kreissig, & Richter, 1997; Veerasamy et al., 1993).

The fourth type is hydrogenated tetrahedral amorphous carbon nitride ($ta\text{-C:H:N}$). $ta\text{-C:H}$ film has highest sp^3 content with low H content. The incorporation of nitrogen into $ta\text{-C:H}$ up to ~20 %, induces clustering of the sp^2 phase and thus gives corresponding increase in conductivity and decrease in optical energy gap. The increase in sp^2 lowers the sp^3 fraction and softens the films. These films are prepared using high-density plasma source such as electron wave resonance (ECWR), ECR or helicon sources.

2.3 Deposition Gases

2.3.1 Hydrocarbon Gas

Methane has been the most widely used hydrocarbon gas for the synthesis of carbon based thin films using chemical vapour deposition (CVD) (Erdemir, Fenske, Terry, & Wilbur, 1997; Lacerda, Marques, & Freire, 1999). Though methane has shown to be very reliable and able to produce various types of CN_x structure, researchers have endeavored to find an alternative precursor which would give enhancement both to its production and its characteristics. One of the popular choices is acetylene. Under the same deposition condition, acetylene give higher film growth rate compared to those deposited from methane (Kim & Grotjohn, 2000). Besides that, while films deposited from methane exhibits dominant sp^3 sites, those of acetylene shows higher sp^2 content which gives film with increase in conductivity and decrease in optical energy gap. Due to this advantage, numerous studies have adopted this gas (Hassan, Pramanik, & Hatta, 2006; Shinohara et al.). However, though acetylene is widely used in producing carbon films, this gas is undoubtedly extremely dangerous since they are explosive and are highly volatile. The same could be said for other gases used in the fabrication of CN_x films such as ethylene (Santos, Silvestre, & Conde, 2002; Suzuki, Manita, Yamazaki,

Wada, & Noma, 1995), benzene (Lee, Baik, Eun, & Han, 1994; M. Tamor, J. Haire, C. Wu, & K. Hass, 1989), polystyrene (Widawski, Rawiso, & François, 1994) and polyethylene (Couderc & Catherine, 1987; J. Wang et al., 2004). Therefore the use of methane still gives an advantage in term of safety. Besides that, the need for cost efficiency and versatility in application makes methane the most favorable gas source among academic and industrial researches.

2.3.2 Nitrogen Incorporation

Nitrogen incorporation significantly modifies the properties of CN_x films (Fanchini et al., 2002b; Robertson & O'reilly, 1987; Silva, et al., 1997). It was found that N incorporation favors the formation of sp^2 units (Wang, Yang, & Zhang, 2008). The amount and organization of the sp^2 phase control the density of state in the gap and thus influence the optical and electronic properties.

A number of works has studied α -CN:H films especially through chemical bonding infrared (IR) absorption analysis (Camero, Gago, Gómez-Aleixandre, & Albella, 2003; Wood, Wydeven, & Tsuji, 1995). With the increase in nitrogen content, amino (NH_n) groups gradually replaces the CH_n groups (Rodil, Ferrari, Robertson, & Milne, 2001; Wood, et al., 1995). This group would exhibit a narrow stretching peak at approximately 3400 cm^{-1} and sharp bending and rocking-waging peaks at ~ 1600 and 1210 cm^{-1} in their IR spectra. However, the peak located at approximately 3400 cm^{-1} is also assigned to hydroxyl (OH) group which normally appear after its exposure to atmospheric water vapour. Thus, the increase in nitrogen incorporation and a corresponding increase in these IR peaks is an indication of the increase in porosity of the films.

Many attempts on doping diamond like carbon (DLC) films with nitrogen to produce n-type material (Hayashi, Kamio, Soga, Kaneko, & Jimbo, 2005) or phosphorus (Kuo, May, Gunn, Ashfold, & Wild, 2000) and boron for p-type (Hayashi, Ishikawa, Soga, Umeno, & Jimbo, 2003) have been made by other researchers. The resulting films have unique electrical properties ranging from insulating diamond to metallic graphite. Anita et al. found that nitrogen incorporation reduces the electrical resistivity of DLC films obtained from different precursors (Anita et al., 2004). Hayashi et al. has also studied the incorporation of nitrogen ion for n-type doping of *a*-C films and also doped *a*-C: H films for its potential in solar cell application (Hayashi, et al., 2003).

2.3.3 *Hydrogen Dilution*

Hydrogen dilution is an important aspect for device quality in film deposition for many types of films including microcrystalline and polycrystalline silicon, silicon carbon alloys and silicon nitride alloys (Swain, 2006; Swain, Gundu Rao, Roy, Gupta, & Dusane, 2006) and has been studied extensively for such material. For C based film, some investigation made so far in this regard that atomic hydrogen is catalytic for C_3N_4 deposition in HWCD process. At high substrate temperature and under high pressure, hydrogen acts as erosion and nitrogen removal agent (Muhl & Méndez, 1999).

It was initially important that there might be high fraction of non-bonded hydrogen in some hydrogenated amorphous carbon. This was based on the results on its most part where hydrogenated amorphous carbon (*a*-C:H) films, the fraction of non-bonded hydrogen could reach 50% (Grill & Patel, 1992). However, it is now generally accepted that the most part of hydrogen is bonded in hydrocarbon (CH_n) groups,

preferentially with sp^3 carbon sites and the fraction of unbounded hydrogen is low for these C films (Donnet et al., 1999; Popescu, Verney, Davis, Paret, & Brunet-Bruneau, 2000; Ristein, Stief, Ley, & Beyer, 1998). In contrast, for hydrogenated amorphous silicon (a-Si:H) films generally accepted that a relevant H fraction is non-bonded. The difference can be justified that Si-H bonds are weaker than C-H bonds (Robertson, 2002).

Another interesting study is the investigation on the structural changes induced by hydrogen in the amorphous CN_x network. The presence of hydrogen generates terminating N-H and C-H bonds favouring a polymeric-like structure of material (P. Hammer, N. Victoria, & F. Alvarez, 1998; Souto & Alvarez, 1997). These terminating bonds induce a strong decrease in density and internal stress of the films. The hydrogen incorporation also decreases the density of defects and improves the connectivity of the films network. Besides that, the increase in hydrogen also leads to the increase in sp^3 sites and broaden the optical energy gap. (Casiraghi, Ferrari, & Robertson, 2005; Xu et al., 2004). Furthermore, changes in IR band which is associated with aliphatic and nitrile structure are also observed.

2.4 Analytical Studies

2.4.1 Raman Spectroscopy

(i) Raman Analysis

Raman spectroscopy is a widely used nondestructive tool to determine the C-C bonding in carbon films and whether their structures are crystalline, nanocrystalline, or amorphous. (Nemanich & Solin, 1979; M. A. Tamor, J. A. Haire, C. H. Wu, & K. C. Hass, 1989; Tuinstra & Koenig, 1970). The visible Raman spectrum depends

fundamentally on the ordering of sp^2 sites and indirectly on the fraction of sp^3 sites. This is because Raman is more sensitive to sp^2 since Raman scattering of π bonding is 50 to 230 times stronger than those for σ bonds (Rodil, et al., 2001). Generally, two main peaks are identified from the Raman spectra which include the D and G peaks, which lie at approximately 1360 and 1500 to 1630 cm^{-1} , respectively (Carey & Silva, 2004; Chowdhury, Cameron, & Hashmi, 1998). The D peak is assigned to K –point phonons of A_{1g} symmetry while G peak usually assigned to zone center phonons of E_{2g} symmetry.

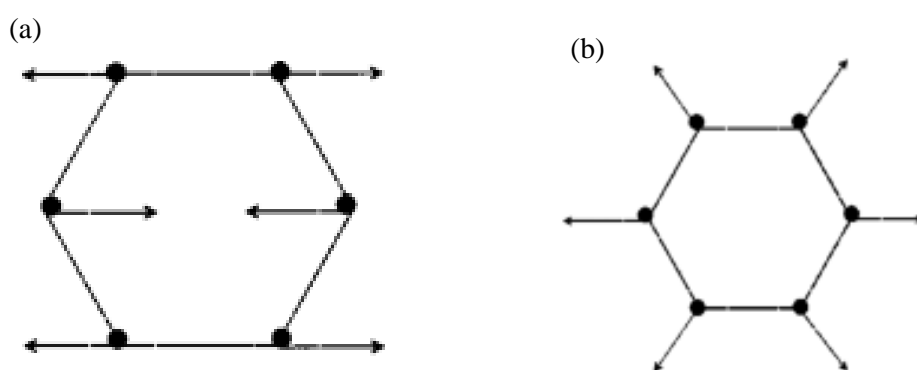


Figure 2.1 Carbon motions in the (a) E_{2g} G mode and (b) A_{1g} D modes (Ferrari & Robertson, 2000).

G mode of graphite with its eigenvector of E_{2g} symmetry involves the in-plane bond stretching motion of pairs of C sp^2 atoms as shown in Figure 2.1 (a). This mode occurs for all sp^2 sites including aromatic and olefinic molecules (LIN, Colthup, Fateley, & Grasselli, 1991). D peak is attributed to A_{1g} breathing modes of sp^2 atom in rings due to out of plane displacements (Chowdhury, et al., 1998; Mapelli, Castiglioni, Zerbi, & Müllen, 1999; Piscanec, Lazzeri, Mauri, Ferrari, & Robertson, 2004). This mode is forbidden in perfect graphite but is activated in the presence of disordered. Moreover, the intensity of D peak is strictly correlated to the presence of six-fold

aromatic ring (Ferrari & Robertson, 2000). Raman analysis is normally centred on the changes in the G peak position and the ratio of both peak intensities, I_D/I_G . A well-established model introduced by Ferrari called ‘Three stage model’ is widely used in interpreting Raman scattering of C bonded films (Ferrari & Robertson, 2000). This model explains the Raman parameter for three different structures. These three stages is grouped in an *amorphization trajectory* which ranges from graphite to tetrahedral amorphous carbon (*ta-C*) as shown in Figure 2.2.

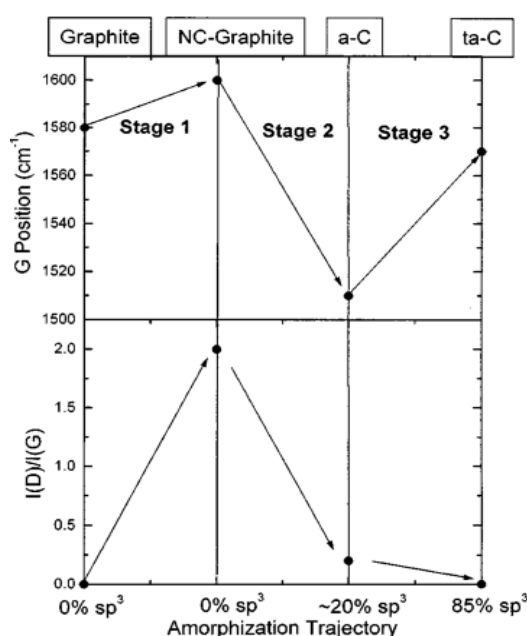


Figure 2.2 A schematic variation of the G peak position and I_D/I_G ratio as a function of amorphization trajectory at three different stages (Ferrari & Robertson, 2000).

The division of the amorphous trajectory is as listed below:

Stage 1: Graphite to nanocrystalline graphite (*nc-G*)

Stage 2: Nanocrystalline graphite to amorphous carbon (*a-C*)

Stage 3: Amorphous carbon to tetrahedral amorphous carbon (*ta-C*)

As can be seen in Figure 2.2, different stages give different effects in the evolution of the Raman spectrum. Due to the different films structures, the reason for the changes might differ for each transition phase. At the first stage, the G peak moves from 1581 to approximately 1600 cm^{-1} with no dispersion of the G mode. The evolution in the D peak indicates an increase in the disorder in the graphite network as the D mode is related to the presence of disorder and thus results in an increased in the I_D/I_G . At this stage, the graphitic nature of the film starts to undergo distortion and this change the film to *nc-G*.

In the second stage, the films start to change from *nc-G* to amorphous films where defects are progressively introduced into the graphite layer. The G peak decreases from 1600 to approximately 1510 cm^{-1} . The dispersion of G peak increased and its I_D/I_G approached zero. As the G peak is related to the relative motion of sp^2 atoms, the I_D decrease with respect to I_G . Thus, in this region, the previous relationships in I_D/I_G no longer hold. The D mode is now proportional to the probability of finding a sixfold ring in the cluster. Thus, for amorphous films, the development of a D peak indicates ordering which is totally opposite from the case of graphite. Towards the end of stage 2, the structures consist predominantly of sp^2 sites which are completely disordered and made up of puckered six-fold rings. There are only a few if any sp^3 sites making up the branches chain-like structure. The presence of non-six-fold rings increase the bond-angle and bond-bending disorder which softens the vibrational density of state (VDOS) (Beeman, Silverman, Lynds, & Anderson, 1984; Kresse, Furthmüller, & Hafner, 1995).

With the transition from *a-C* to *ta-C* in the third stage, the G peak increases from approximately 1510 to about 1570 cm^{-1} and dispersion of G peaks occurs with very low

or approximate zero value in I_D/I_G . At this stage, the sp^3 content rises from approximately 20% to 85%, while the sp^2 sites change gradually from rings to chain as shown in Figure 2.3. The π states is increasingly localized in the olefinic sp^2 chains, and eventually, the transition lead to the formation of sp^2 dimers embedded in the sp^3 matrix (Drabold, Fedders, & Stumm, 1994; Gilkes, Sands, Batchelder, Robertson, & Milne, 1997; Köhler, Frauenheim, & Jungnickel, 1995). The increase in G peak position with sp^3 is due to the change in sp^2 configuration from ring to olefinic groups which are shorter than aromatic bonds with higher vibrational frequency. However, these three stage model was established for UV laser excitations. Nonetheless, Ferrari and Robertson have also studied different types of amorphous carbon using multi-wavelength Raman response (Ferrari & Robertson, 2001). The response in Raman at different laser excitation especially in G peak position and I_D/I_G based on a similar ‘three stage model’ is shown in Figure 2.4.

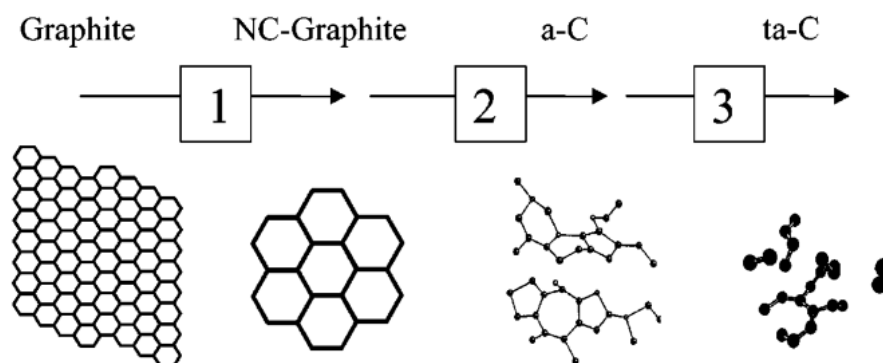


Figure 2.3 Variation in sp^2 configuration in the ‘three stage model’ (Ferrari, 2008).

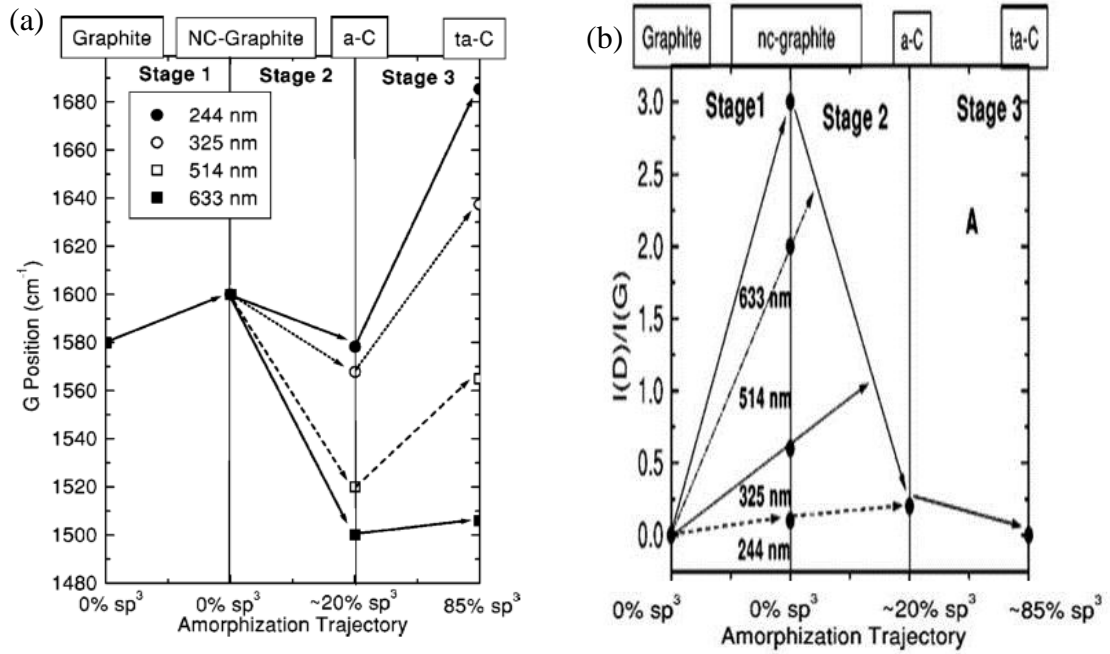


Figure 2.4 Amorphization trajectory, showing the schematic variation of (a) G position and (b) I_D/I_G for multi-wavelength (Ferrari & Robertson, 2001).

As a summary, the Raman spectrum is considered to depend on these factors (Ferrari & Robertson, 2000):

- (1) Clustering of the sp² phase
- (2) Bond disorder
- (3) Presence of sp² rings or chains
- (4) The sp²/sp³ ratio

These factors can influence the profile of the Raman spectra. The changes in the profile can be summarized as shown schematically in Figure 2.5.

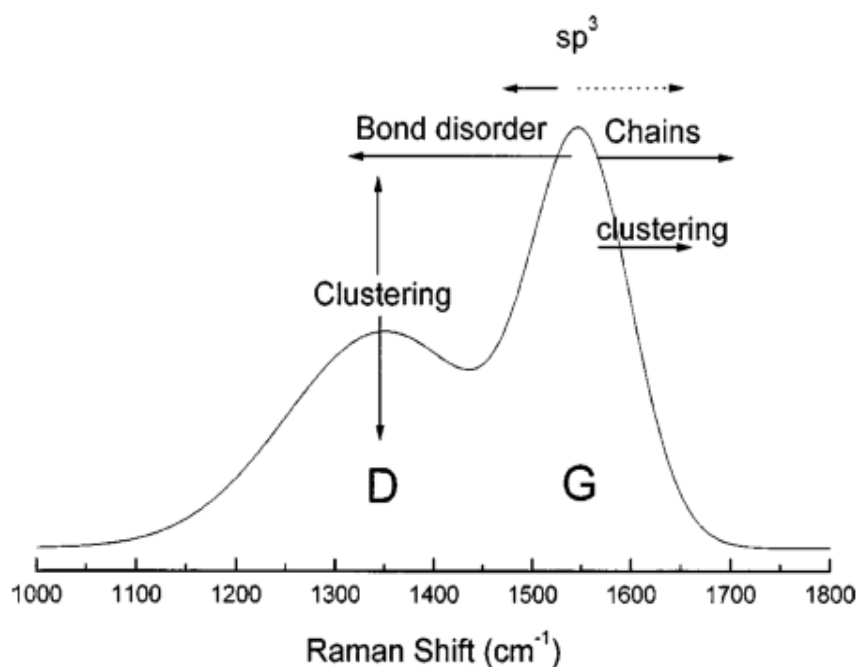


Figure 2.5 Schematic diagram of variation on the Raman spectra. Dotted arrow marks the indirect influence of the sp^3 content on increasing G position (Ferrari & Robertson, 2000).

(ii) The Hysteresis Cycle

In some cases, films can also undergo the opposite direction in the amorphization trajectory. This reversion in the direction trajectory is called hysteresis where the film follows an ordering trajectory from ta-C to graphite as shown in Figure 2.6. These situations favor clustering of sp^2 sites into the ordered aromatic rings. Two fundamental processes may occur, either the sp^3 sites convert to sp^2 or sp^2 cluster size increases, and sp^2 eventually re-orders in rings. However there are no unique relationship between I_D/I_G or G position and sp^3 fraction for this hysteresis effect.

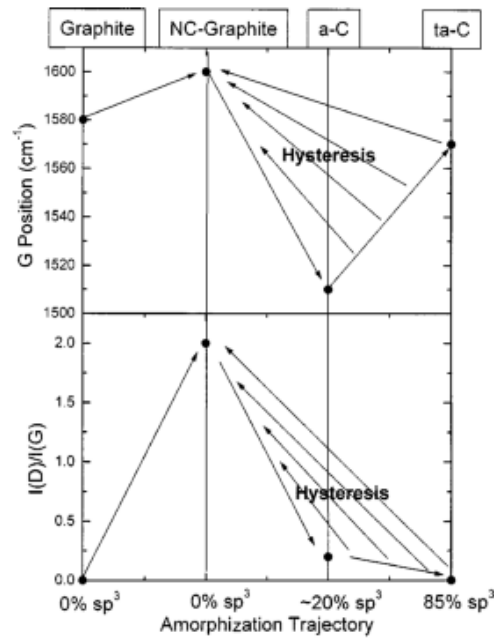


Figure 2.6 Variation in G peak position and I_D/I_G in UV excitation (Ferrari & Robertson, 2000).

(iii) Other Peaks

The existence of other features apart from D and G modes would be observed in Raman spectra especially when these films are incorporated with nitrogen. These other bands may appear at approximately 700, 1060, 2000 and 2200 cm^{-1} and are correlated to L peak, T peak, ordering and/or C-C sp^3 , and C-N sp^1 , respectively. The T peak becomes visible only for UV excitation and is observed due to the vibration of C-C sp^3 bonds (Ferrari & Robertson, 2000; Ferrari & Robertson, 2001). The other three peaks appears with the presence of nitrogen bonds (Rodil, et al., 2001a).

(iv) Hydrogen Content

The raw Raman spectrum with oblique position as shown in Figure 2.7 is always related to hydrogenated amorphous films. The slanting or slope in the baseline is caused by photoluminescence backgrounds (Casiraghi, et al., 2005b). A good correlation has been reported of the slope of the PL background and the amount of hydrogen in the

films. This allows estimation of H content in the films from the slope. The hydrogen content effects the band gap and determines the types of films produced. Figure 2.8 shows the Raman results of different types of C films reported by Casiraghi. The rise in PL background correlates to the increase in hydrogen content in the films due to hydrogen saturation of non-recombination centers within sp^2 bonded clusters in a sp^3 bonded amorphous matrix (Casiraghi, et al., 2005b; Robertson, 1996a). The ratio between slope, m of the fitted linear background and the intensity of G peak, $m/I_{(G)}$, can be empirically used to calculate the H content according to the equation proposed by A. Ferrari (Ferrari & Robertson, 2000):

$$H [\text{a.t \%}] = 21.7 + 16.6 \log \left\{ \frac{m}{I_{(G)}} [\mu\text{m}] \right\} \quad (2.1)$$

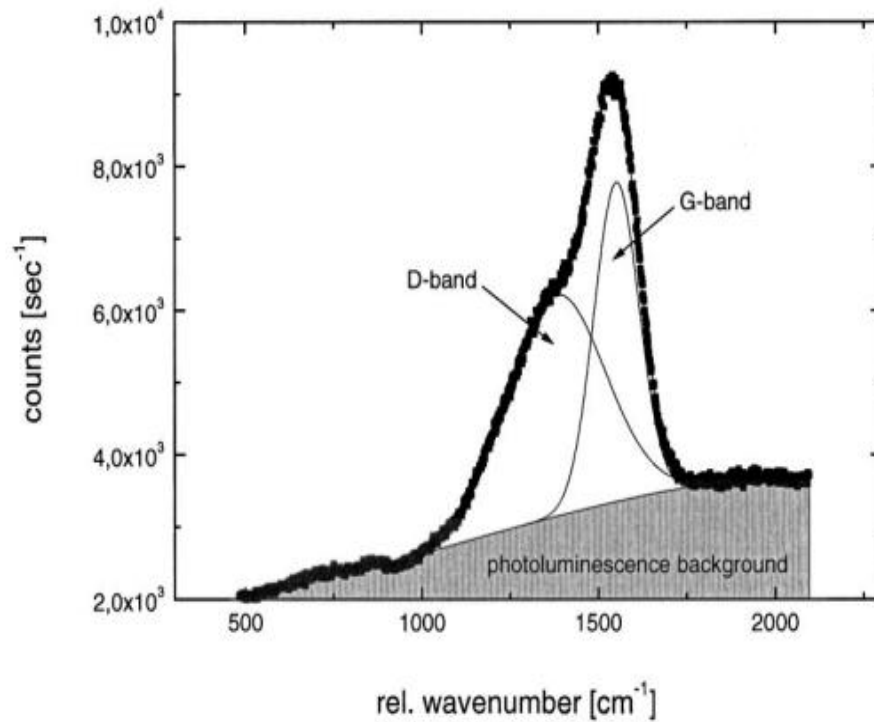


Figure 2.7 Photoluminescence background of Raman spectrum (Neuhaeuser, Hilgers, Joeris, White, & Windeln, 2000).

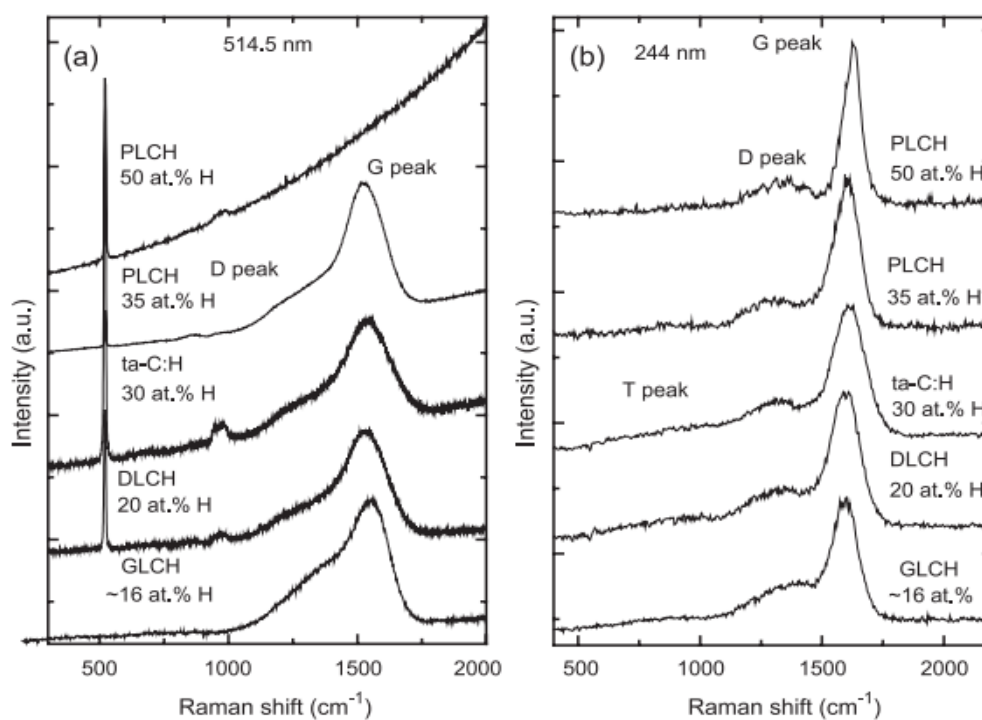


Figure 2.8 Raman spectra of different type of amorphous carbon with various H content at excitation wavelength of (a) 514.5 nm and (b) 244 nm (Casiraghi, et al., 2005b).

2.4.2 Fourier Transform Infrared

Information regarding chemical bonding was obtained from the IR absorption analysis. Different types of carbon nitride films obtained from various techniques and parameter used gives different IR spectra. The assignment of various chemical bonding for CN_x obtained from literature is listed in Table 2.1.

The FTIR spectra for CN_x films can be grouped into four absorption regions. The first region in the range of 1000 to 1700 cm^{-1} is dominated by nitrogen related absorption peaks. For the second region, absorption peaks observed around 2000 cm^{-1} are assigned to various vibrations of $\text{sp}^1 \text{C}\equiv\text{N}$ bonds. These $\text{C}\equiv\text{N}$ bonds can be separated into nitrile and/or isonitrile bonds. At higher wavelength, the band located at approximately 2800 to 3000 cm^{-1} is associated to C-H group. The absorption broad band between 3000 and 3800 cm^{-1} is related to the O-H and/or N-H vibrational modes. The list of functional groups taken from references is listed in Table 2.1.

Numerous studies have been carried out on IR absorption of CN_x films (Hammer, Lacerda, Droppa Jr, & Alvarez, 2000). One of the noteworthy works is by Rodil. In his work, the IR spectra of CN_x were categorized into different types of CN_x films. The groups were divided into two subgroups which are the amorphous carbon nitride (*a*-CN) and tetrahedral amorphous carbon nitride (*ta*-CN). The *a*-CN is then classified into two sub-groups consisting of hydrogenated carbon nitride films with high H content and hydrogen free CN_x films. Similarly, *ta*-CN is also divided into two groups which are the hydrogenated films and non-hydrogenated films.

Table 2.1 List of bonding assignments, wavenumber regions and corresponding references.

| Range (cm ⁻¹) | Wavenumber (cm ⁻¹) | Assignment | References |
|---------------------------|--------------------------------|--|--|
| 1000 to 1700 | 1020-1150 | C-N (aliphatic) , N-H | (Lazar et al., 2005; Motta & Pereyra, 2004) |
| | 1220-1265 | C-N (in C ₃ N ₄), C≡N | |
| | 1300-1350 | C-N, C=N | |
| | 1360-1380 | Raman D, C=N | |
| | 1500-1510 | C-N, C=N, C=C | |
| | 1550 - 1570 | Raman G, C=N | |
| | ~1600 | C=N, C=C | |
| | 1620 - 1650 | C=C, C=N, NH _x | |
| 2000 to 2400 | 2050-2200 | -N≡C ⁺ (isonitrile group) | (Mutsukura, 2001; Nobuki Mutsukura & Akita, 1999) |
| | 2200-2300 | -C≡N (nitrile group) | |
| 2800 to 3000 | 2850-2855 | sp ³ CH ₂ (symmetrical) | (Fanchini et al., 2005; Lazar, et al., 2005) |
| | 2865-2875 | sp ³ CH ₃ (symmetrical) | |
| | 2915-2920 | sp ³ CH | |
| | 2920-2925 | sp ³ CH ₂ (asymmetrical) | |
| | 2960-2970 | sp ³ CH ₃ (asymmetrical) | |
| | 3000 | sp ² CH (olefinic) | |
| | 3020 | sp ² CH ₂ (olefinic) | |
| 3000 to 3800 | 3100-3500 | N-H | (Pereira, Géraud-Grenier, Massereau-Guilbaud, & Plain, 2005) |
| | 3200-3650 | O-H | |

These four types of structure cover clearly all of the different IR profile for CN_x films seen in literature (Rodil & Muhl, 2004). Figure 2.9 show the different spectra for each of the four groups. These bands are similar to carbon films but lack the bonding of C-H group which are normally seen at the 2800 cm⁻¹ region. For *ta*-CN films formed at high energetic pressure, the NH and OH bands at 3000 to 3300 cm⁻¹ are absent, as shown in the figure.

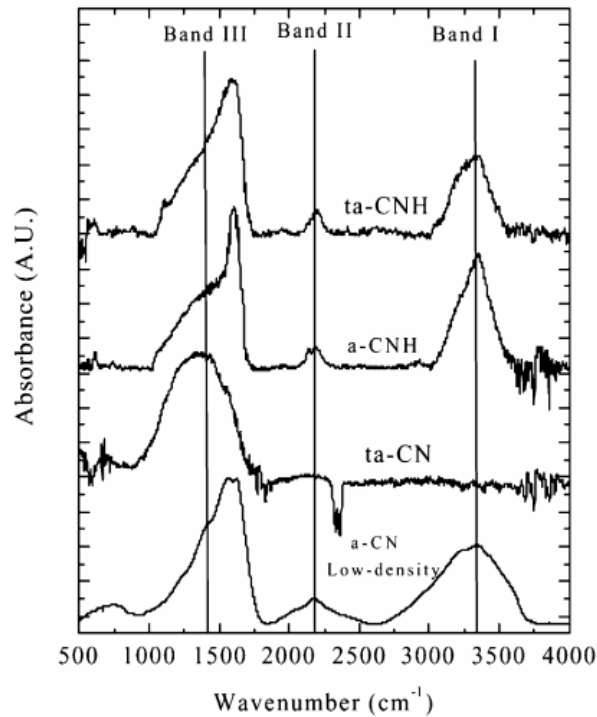


Figure 2.9 : FTIR spectra of various types of CN_x films separated into three different bands (Rodil & Muhl, 2004).

2.4.3 Optical

The optical energy gap (E_g) is mainly determined by the size and distribution of sp^2 bonded cluster in the films. This optical band gap is deduced from Tauc plot based on the optical spectra measured in a UV-Vis Nir spectroscopy. It was reported, for all type of $a\text{-C:H}$ and $a\text{-C:N:H}$ films, the optical band gap varies almost linearly with the sp^2 content (Ferrari & Robertson, 2000; Rodil, Muhl, Maca, & Ferrari, 2003). However, with the introduction of nitrogen, a small decrease in E_g is observed for hydrogenated carbon nitride films ($a\text{-CN:H}$) (Amir & Kalish, 1991; Schwan, Dworschak, Jung, & Ehrhardt, 1994; Zhang, Nakayama, Miyazaki, & Kume, 1999). The decrease is related to the increase in size of sp^2 cluster since the nitrogen acts as a bridging atom between clusters (Mariotto, Freire Jr, & Achete, 1994).

Different types of carbon nitride films give different trends in E_g . For non-hydrogenated carbon nitride films (*a*-CN), it is not directly correlated to the sp^2 fraction (S. E. Rodil, Milne, Robertson, & Brown, 2001) or N content. E_g decreases as the nitrogen increases (Lee et al., 1997; S. E. Rodil, et al., 2001b) but above a certain nitrogen concentration the optical gap widens (Bousetta, Lu, & Bensaoula, 1995; Iwasaki et al., 1999; Takada, Arai, Nitta, & Nonomura, 1997; Weber & Oechsner, 1999; Zhao et al., 1995). This behavior was observed from numerous studies reported by researchers as shown in Figure 2.10. Interestingly, highly polymeric a-C: N: H films deposited at low ion energies exhibit wide E_g (>2 eV).

Rodil has come out with two possible explanations of the differences in optical gap at different conditions (Rodil, et al., 2003) :

- (1) There is a localization of π electrons as nitrogen content increases due to the partial ionic characteristics of the CN bonding. The increase in sp^2 fraction influences the optical gap of the CN_x films which is different from the case of a-C films.
- (2) Higher nitrogen content increases the film's porosity which can be observed from the OH absorption signal due to strong water absorption. This porosity may modify the absorption spectra similar to that observed for porous silicon.

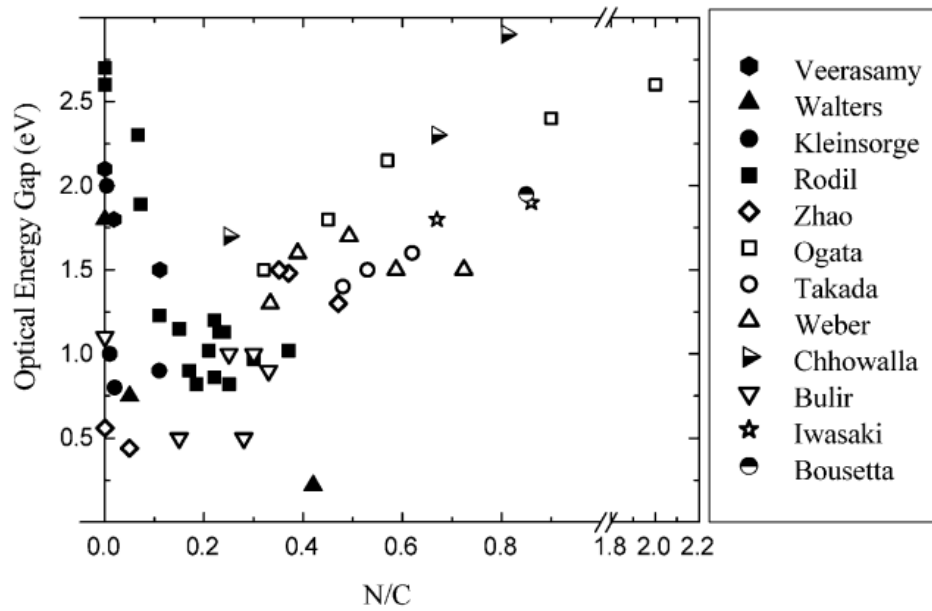


Figure 2.10 Variation in optical gap as a function of nitrogen content of carbon nitride films using various techniques (Rodil, et al., 2003).

2.4.4 Photoluminescence

The intensity of photoluminescence (PL) emission is always related to the recombination process of electrons and holes in a material. This recombination process is similar to the case in hydrogenated amorphous silicon (a-Si:H) films which uses band-tail model to describe this recombination process (Demichelis, Schreiter, & Tagliaferro, 1995; Robertson, 1996). This band-tail model propose that the electrons and holes recombine radiatively at the band-tail states associated to the π -bonded sp^2 hybridized sites (Robertson, 1996).

In α -CN_x films, PL intensity increases with the increase in nitrogen incorporation (Demichelis, Liu, Rong, Schreiter, & Tagliaferro, 1995; Mendoza, Aguilar-Hernández, & Contreras-Puente, 1992; Mutsukura & Akita, 1999). Nitrogen incorporation may promote the presence of lone pair which may contribute to the recombination centres (Fanchini, Ray, & Tagliaferro, 2003). When high amount of nitrogen is incorporated into the films, nitrile termination of the bond may occur. The presence of this nitrile group is accompanied by a strong reduction in the film's internal stress which results in an enhancement of its PL intensities. In contrast, the presence of lone pair, involved by nitrogen may act as non-radiative recombination centre which reduces the PL intensity. However, with the presence of significant amount of disorder in the films, these lone pair tends to form 'weak bonds'. The interaction of these bonds with surrounding ions, results in lone pair- π mixing where the electron-hole pairs can radiatively recombine (Fanchini, Ray, Tagliaferro, & Laurenti, 2002b).

CHAPTER 3 EXPERIMENTAL DETAILS

3.1 Introduction

Radio frequency plasma enhanced chemical vapour deposition (rf PECVD) technique is one of the common technique used in the fabrication of carbon nitride (CN_x) films. In this work, CN_x films were fabricated from a mixture of gases using a home-built PECVD system. This chapter will cover the experimental part of the deposition process and the analytical methods used to characterize the films. The experimental part described the deposition system and the sample preparation whereas the analytical method discussed the instruments and measurement technique used in this work. In addition, the calculation methods used to analyze the results of the measurements was also included in this chapter.

3.2 Deposition System

3.2.1 Radio Frequency Plasma Enhanced Chemical Vapour Deposition (rf PECVD) System

A home built radio frequency plasma enhanced chemical vapour deposition (rf PECVD) system was designed specifically according to the conventional characteristics appropriate for the production of hydrogenated amorphous carbon ($a\text{-C:H}$) based thin films. A photograph of the deposition system is shown in Figure 3.1. The deposition system consists of a reaction chamber, evacuation system, gas distribution subsystem and electrical subsystem as shown in a schematic diagram in Figure 3.2. A detail description of the system is discussed in the following sections.

A reaction chamber was designed to deposit the carbon nitride (CN_x) thin films. The chamber is attached to an evacuation system which consists of a rotary pump and a diffusion pump. Its function is to evacuate the chamber and also to maintain the pressure in the reaction chamber during deposition. The chamber needs to be pump down to minimum vacuum condition to decrease contamination during film deposition.

The gas distribution system consists of a series of gas tubes and mass flow controllers (MFC) connecting the chamber and the gas cylinders. The gas flow rate is controlled using the MFC. The electrical system consists of a rf power supply with a matching impedance network and temperature controller connected to a substrate heater and thermocouple. The rf power supply and temperature controller are respectively used to produce the plasma and regulate the substrate temperature.

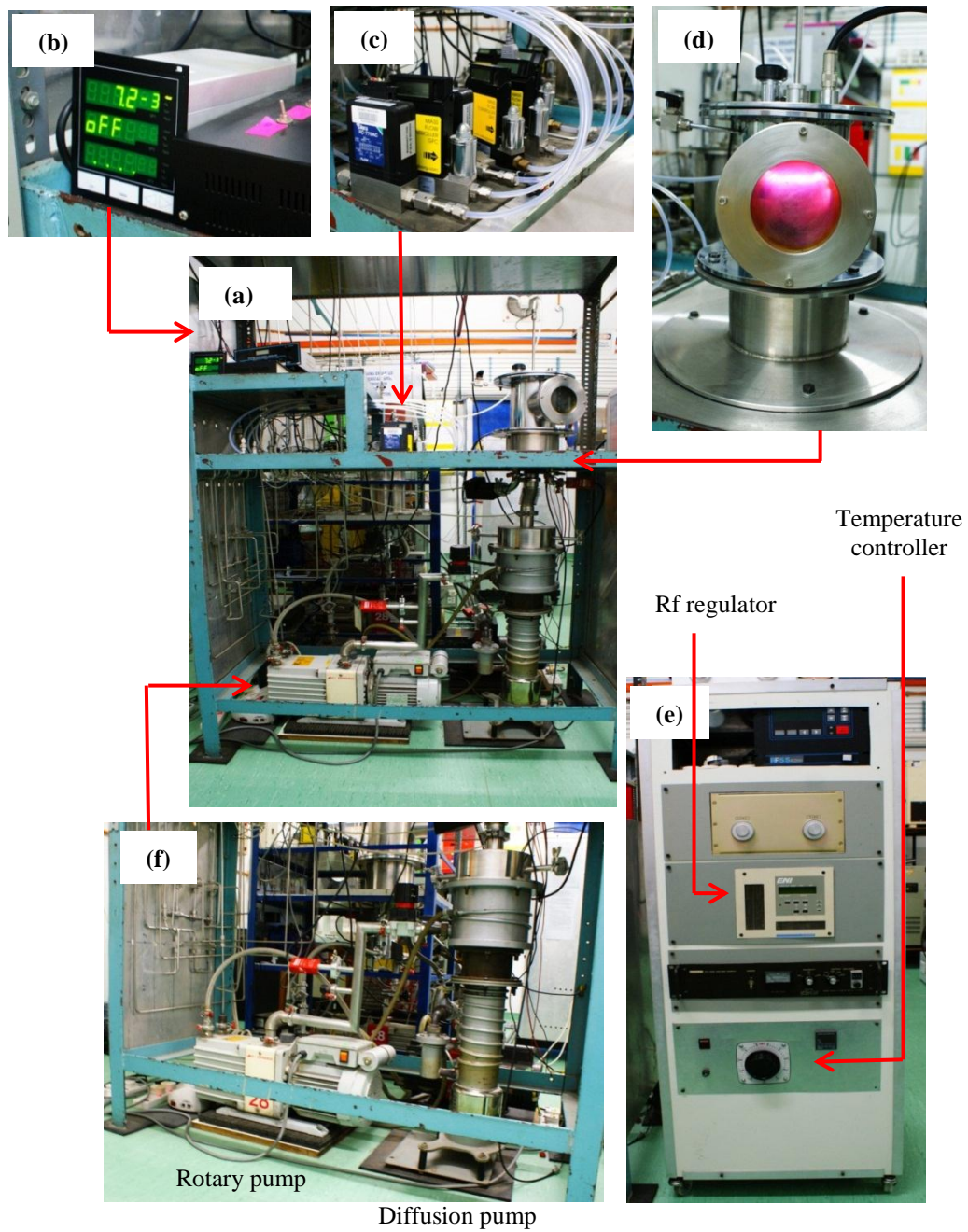


Figure 3.1 Photograph of (a) PECVD deposition system and enlarged picture of (b) mass flow controller (c) pressure meter (d) reaction chamber (e) rf regulator and temperature controller (f) rotary and diffusion pump.

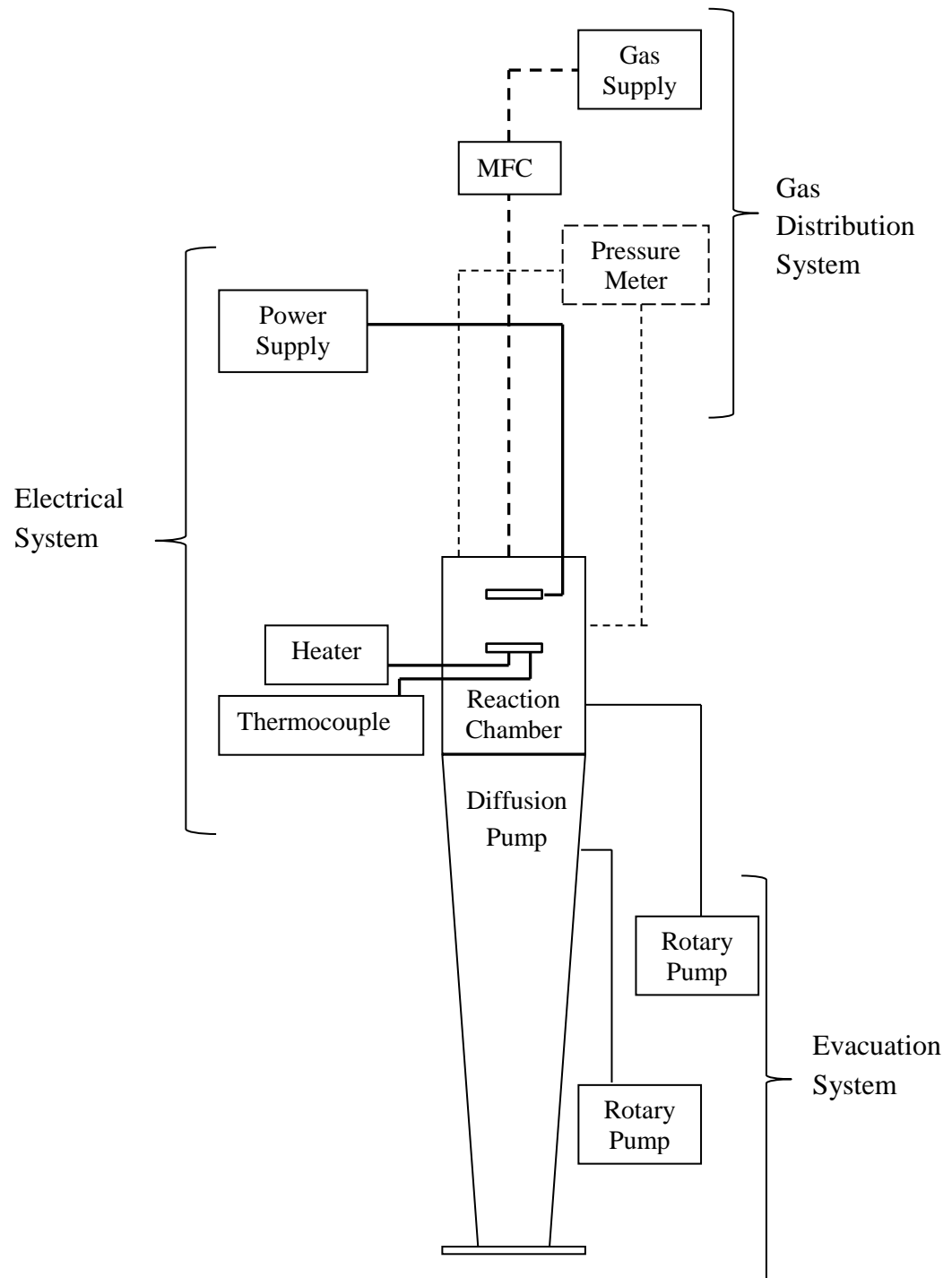


Figure 3.2 Schematic diagram of PECVD deposition system.

3.2.2 The Reaction Chamber

The reaction chamber consists of a top plate, body chamber and a base plate made of stainless steel to withstand high temperature as well as to maintain a good vacuum condition during the deposition process. Figure 3.3 shows the schematic diagram of the reaction chamber.

The top cover is a circular stainless steel plate, 25 cm in diameter and 0.5 cm thick. This circular plate has an air admittance valve, gas inlets and the rf power supply connector. The gas inlet is located in the middle of the chamber. A shower head is attached to the inlet on the inside of the chamber and isolated using a teflon block. The shower head also acts as the powered electrode being connected to the rf power supply. The rf power is supplied by a ENI power supply operating at 13.56 MHz.

The body of the chamber has internal diameter of 13 cm, 0.5 cm thick and 18.5 cm high. This chamber is equipped with a view port in order to monitor the deposition process. Inside the chamber, a substrate holder of 10 cm in diameter and 0.5 cm in thickness is positioned which also acts as a grounded electrode. A mask is used to position the substrate on the holder and keep the substrates stationary while also gives well-define film boundaries for easy films thickness measurements using a surface profilometer. The mask is designed identical to the substrate holder as shown in Figure 3.4. A heater and thermocouple are inserted carefully positioned holes in the substrate holder. A glass slide is clamped between the holder and teflon base. By clamping the thermocouple between the glass slide and teflon base such that its tip would be touching the glass slide, an approximation of the substrate temperature could be measured. The substrate distance which is the distance between the shower head and substrate holder could be adjusted by changing the height of the teflon base.

The chamber base is equipped with six pin electrical feed through which are meant for thermocouple, heater and ground wire. The lower plate is also attached to the diffusion pump.

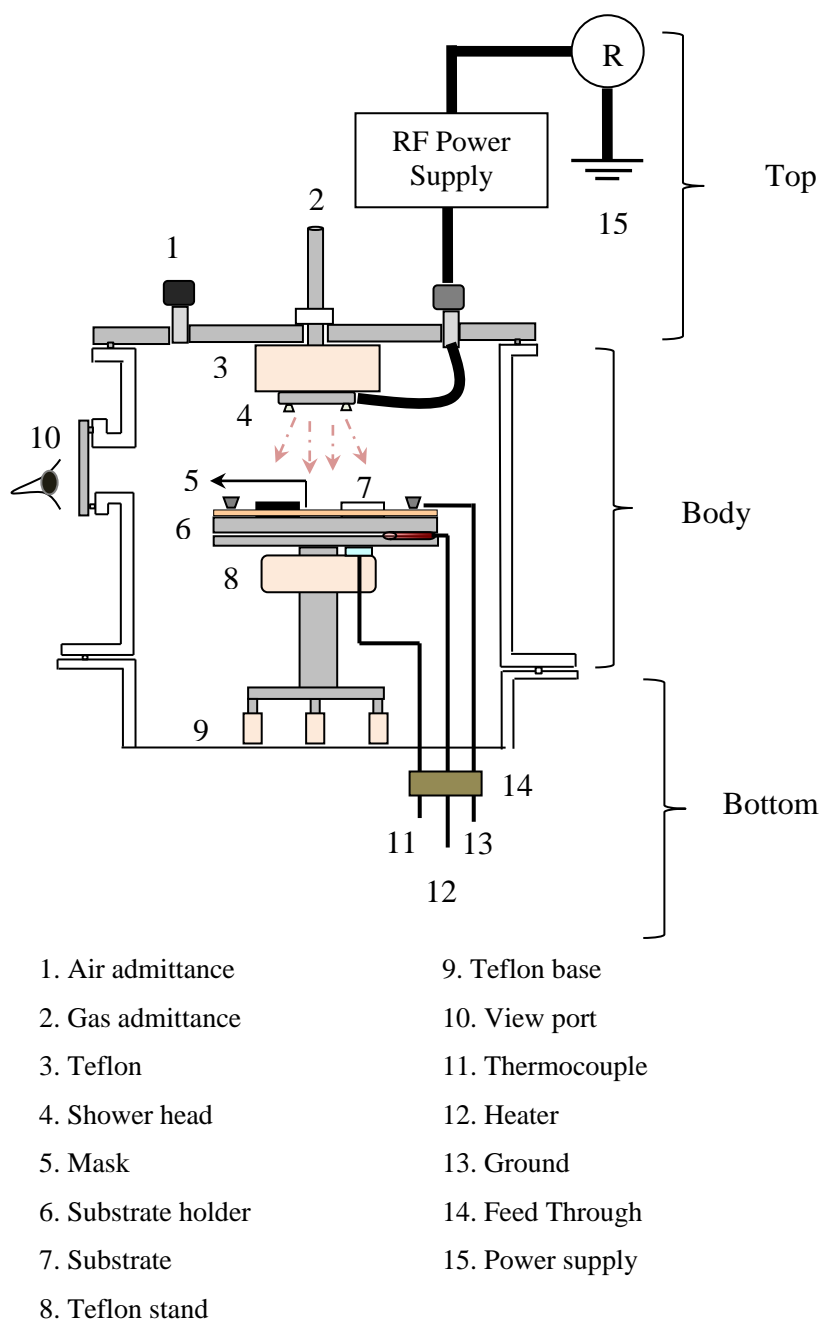


Figure 3.3 Schematic diagram of the home-built reaction chamber for the rf PECVD system.

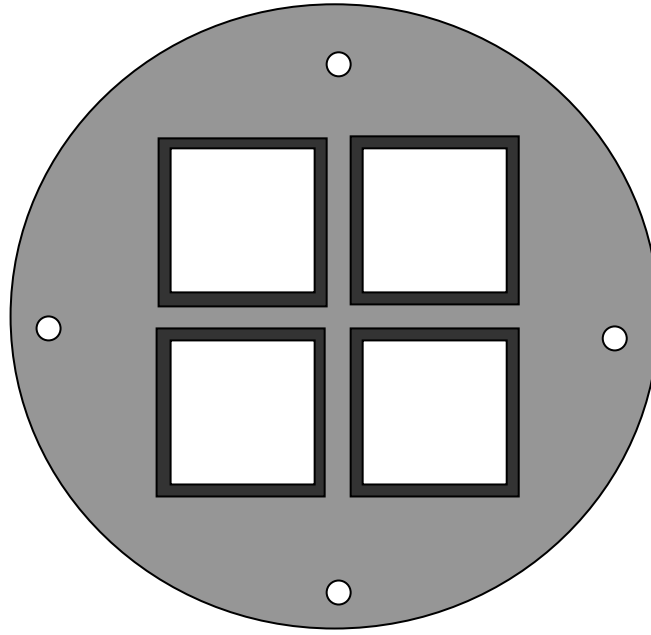


Figure 3.4 Stainless steel substrate holder (top view)

3.3 Preparation Procedures for Films Substrate

Carbon nitride thin films were deposited on silicon and quartz substrates. P-type $\langle 111 \rangle$ oriented crystal silicon (c-Si) with thickness of $625\mu\text{m}$ and quartz glass with thickness of 1.0 mm are used. Substrates were cleaved into rectangular shape with dimension of 2.5 cm by 2cm and cleaned thoroughly before being used in the deposition process. The cleaning procedure depends on the kind of substrate.

3.4 Substrate Cleaning Procedure

The cleaning process of the substrate is one of the essential steps in the deposition of the thin films. This process is necessary to eliminate contamination,

hydrogen termination and water on the substrate, to increase the adhesion of the film on the substrate.

For silicon substrate, firstly, the substrate was rinsed with deionized water to remove dust and particles on the surfaces. The silicon was then immersed in a hydrochloric acid solution of $\text{H}_2\text{O}:\text{H}_2\text{O}_2:\text{HCL}$ with ratio of 6:1:1 for 10 minutes. Then, the substrate was rinsed in deionized water and place in ultrasonic bath for about 10 seconds. This was repeated using ammonia solution with a $\text{H}_2\text{O}:\text{H}_2\text{O}_2:\text{NH}_4\text{OH}$ ratio of 5:1:1 and fluoric acid solution with a $\text{H}_2\text{O}:\text{HF}$ ratio of 10:1 sequentially for approximately 30 second. The silicon was then rinse in ethyl alcohol followed by acetone to prevent water marks. The substrate was dried in a flow of nitrogen.

The cleaning process for quartz substrate is simpler than for silicon substrate. The quartz was immersed in a beaker filled with soap water which was placed in an ultrasonic bath and sonicate for 15 minutes. Then they were rinse in deionized water. Afterwards the substrate was rinsed in ethyl alcohol followed by acetone. The substrate was then dried in a flow of nitrogen gas.

3.5 Deposition Procedure

3.5.1 Pre-deposition Process

Cleanliness is of utmost importance in carrying out good deposition process. This process is not only to obtain good samples but also to avoid problem occurring due to contamination. Firstly, the chamber was thoroughly cleaned using acetone as a degreasing agent to eliminate dirt and contamination. The chamber was wiped using tissue and left to dry. The electrical power supply, heater and thermocouple were then

connected to the substrate holder in the chamber. Clean substrates were placed on the substrate holder. The mask was then screwed into place to ensure that the substrates were stationary. Next, the chamber was screwed tightly before the chamber was pumped down.

The second step is the evacuation process where all the valves within the system are closed before the rotary pump was switched on. The rotary valve is then slowly opened to maximum, and pumping is carried out until the pressure reached about 10^{-3} mbar. Next, the gas line valve is opened to clear any residual gases inside the gas line. The diffusion pump is then warmed up for 20-30 minutes in preparation for the next pumping stage. The rotary valve needs to be closed just before the diffusion valve is fully opened. After the pressure of the chamber reached around 10^{-5} mbar, the diffusion pump valve is closed and the rotary valve is open fully. At this stage hydrogen (H_2) gas is immediately allowed into the system for the next phase which is the H_2 plasma treatment. Under this condition the substrate was heated to 100°C and the rf generator is warmed up. In this work, the H_2 gas flow was set at 50 sccm using the mass flow controller (MFC). H_2 treatment process was carried out for 10 minutes at rf power of 50 W to remove the contamination on the substrate surface and to activate the substrate surface. This will enhance the adhesion of films on the substrate. Once finished, the H_2 source is turned off and residual H_2 was pumped out.

3.5.2 Deposition Process

The actual CN_x film deposition begins by flowing in the precursor gases together into the chamber. The flows of these gases are adjusted using their MFCs. The source gases are flowed for at least 5 minutes before applying the rf power. The pressure is maintained by regulating the rotary valve. The substrates are then heated to 100 °C for all samples. The pressure, substrate temperature and the power are monitored and regulated during the deposition process. Once the pressure and temperature are stable, the rf power is applied and deposition begins. The heater and the gases supply from the tank are turned off shortly after the deposition is completed.

Three sets of samples were prepared in this work. The first two sets were prepared in the same deposition condition but using different hydrocarbon precursors gases. The CN_x films were deposited from a mixture of methane (CH_4) and nitrogen (N_2) whereas the other one was prepared from a mixture of ethane (C_2H_6) and N_2 gases. The effects of varying the N_2 flow rate were studied for these first two sets. Another set of sample was then prepared by adding hydrogen (H_2) into a mixture of ethane and nitrogen gases. The effects of hydrogen variation in the properties of CN_x films were studied. All the samples were prepared on quartz slides and polished p-type <111> silicon substrates. Other deposition parameters were kept constant and are summarized in Table 3.1 below.

Table 3.1 Deposition parameters for the study of the effects of nitrogen and hydrogen flow rate on the structural properties of $\text{CN}_x\text{:H}$ thin films.

| Parameter | Set Values | | |
|--|----------------------------|-------------------------------|-------------------------|
| | Set 1 | Set 2 | Set 3 |
| Methane (CH_4) mass flow rate | 25 sccm | - | - |
| Ethane (C_2H_6) mass flow rate | - | 25 sccm | 25 sccm |
| Nitrogen (N_2) mass flow rate | 0, 13, 20, 30, 50, 80 sccm | 0, 13, 25.0, 50, 75, 100 sccm | 100 sccm |
| Hydrogen (H_2) mass flow rate | - | - | 0, 25, 50, 75, 125 sccm |
| Rf power | 80 W | 80W | 80W |
| Electrode distance | 5 cm | 5 cm | 5 cm |
| Substrate temperature | 100° C | 100° C | 100° C |
| Deposition time | 90 minutes | 90 minutes | 90 minutes |

3.5.3 Post-deposition Process

After the deposition process was completed, the system needs to be cool down until the temperature reached below 50° C. During this time, the reaction chamber and the gas line were evacuated until all excess gases were pump out. Once the chamber is cooled the rotary valve is closed and the rotary pump is switch off. Finally, the air admittance valve is opened to allow the chamber to reach atmospheric pressure. The samples are removed and stored for characterization.

3.6 Characterization Techniques

The films were characterized by various techniques. The films growth rates were estimated by measuring their thickness using a surface profilometry. The Fourier transform infrared spectroscopy (FTIR) was needed to study the chemical bonding in the CN_x thin films. Ultra-violet visible near infra-red (UV Vis NIR) and photoluminescence (PL) spectroscopy were used to obtain the optical energy gap (E_g) and PL properties respectively. The structural properties of the films were studied using Raman spectroscopy.

3.6.1 Surface Profilometry

The deposition rate of the films was calculated from the films thickness. In this work, the thicknesses of the films were measured using a KLA-Tencor P-6 surface profiler system as shown in Figure 3.5. This unit is a contact profilometer which uses a diamond stylus that touches the surface to be profiled. As the stylus moves along the surface, its displacement is converted into a digital signal that is stored, analyzed, and displayed by the profilometer. The film was scanned from the edge to the center of the film from different location along the films. The average values of the measurement were obtained. Example of the cross section profile is shown in Figure 3.6.

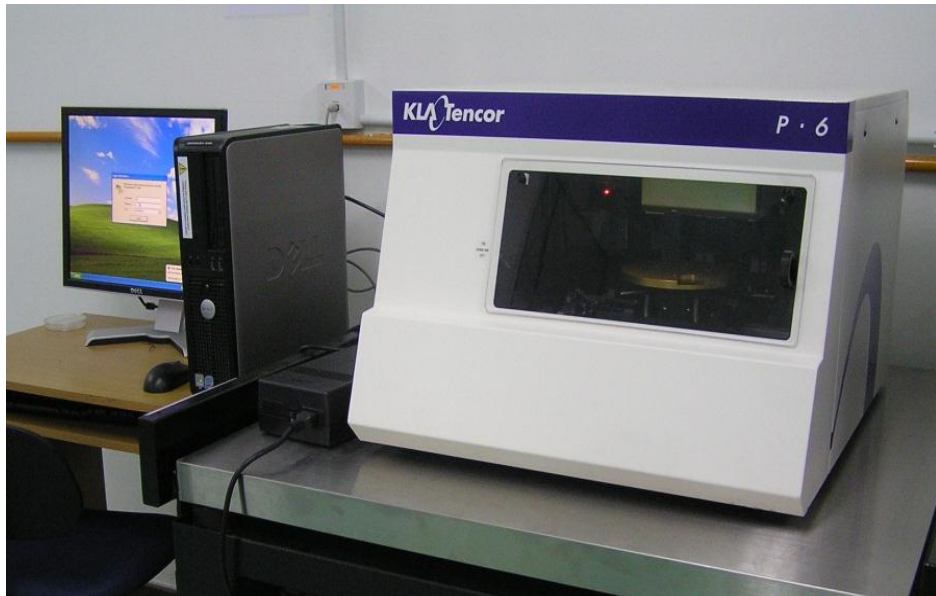


Figure 3.5 KLA-Tencor P-6 surface profiler system.

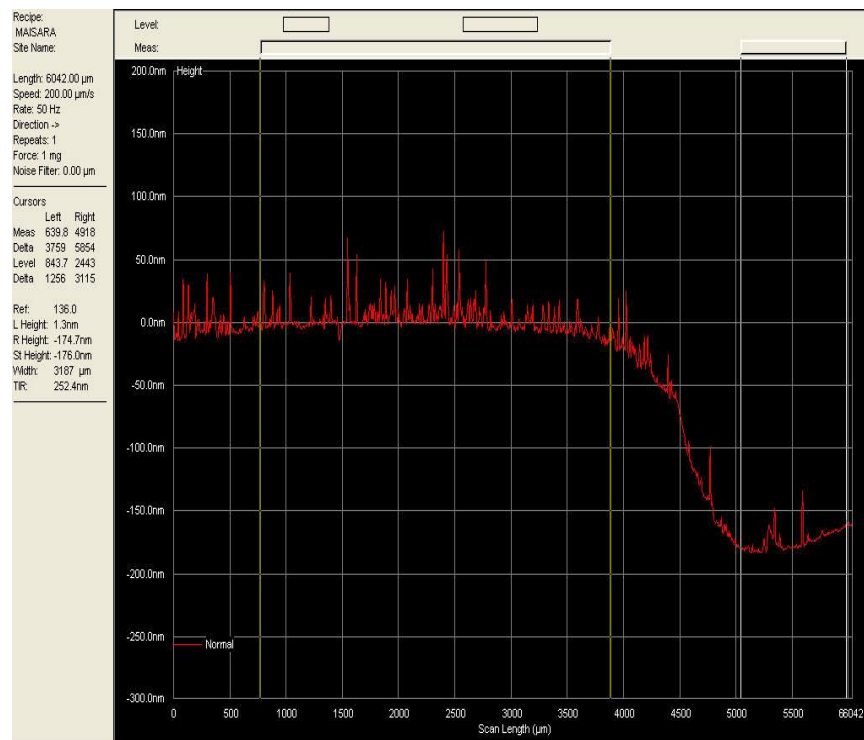


Figure 3.6 Example of profilometer scan of deposited film.

3.6.2 Auger Electron Spectroscopy

Auger electron spectroscopy (AES) is a technique for determining the composition of films. All the elements can be detected by AES except hydrogen. This analytical technique uses primary electron beam as a probe. Emitted secondary electrons are then analysed as a result of the Auger process and their kinetic energy is determined. Auger electrons are emitted at discrete energies that allow the atom it originates to be identified. Figure 3.7 shows the schematic diagram of the Auger process. The Auger process involves three steps:

- (1) Excitation of the atom causing emission of an electron
- (2) An electron relaxes to fill the vacancy created in step 1.
- (3) The energy released in step 2 causes the emission of an Auger electron

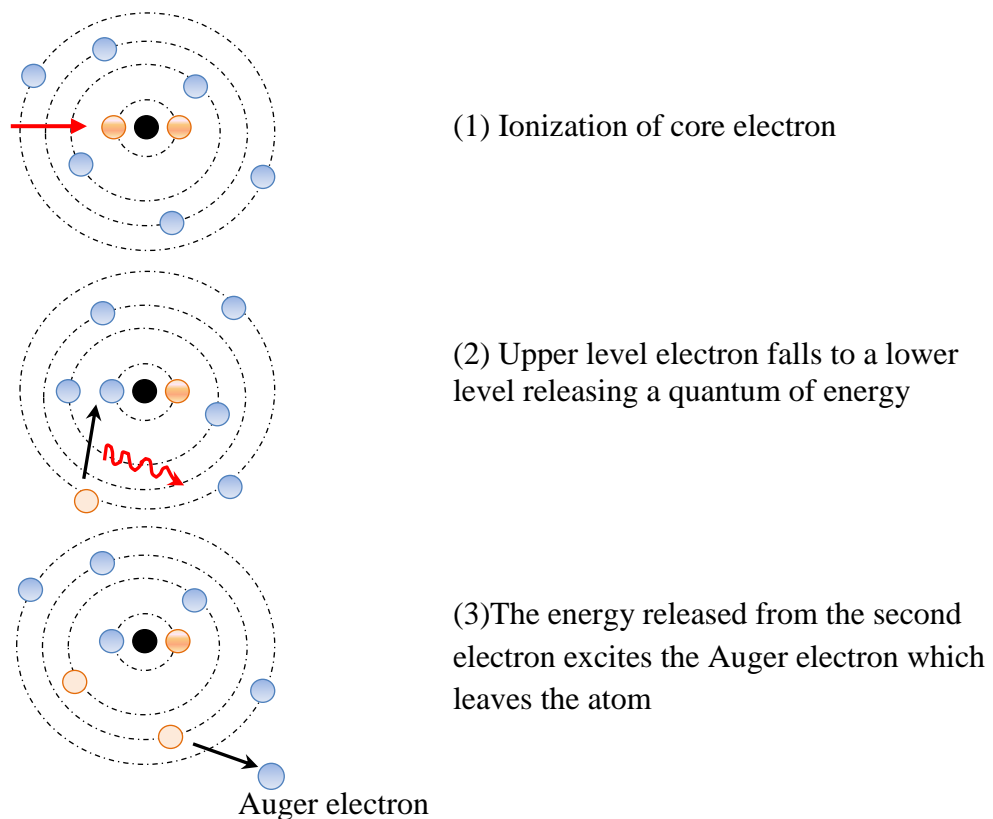


Figure 3.7 The schematic diagram of the Auger process.



Figure 3.8 Picture of JEOL JAMP-9500F field emission Auger microprobe.

In this study, the composition of the films were carried out using JEOL JAMP-9500F field emission Auger microprobe as shown in Figure 3.8. From the spectra, the relative concentrations of carbon and nitrogen atoms were taken straight from the data analysis of the AES as shown in Figure 3.9. These results were used to calculate the ratio of N to C (N/C) in the films.

| Result of Quantitative Analysis | | | | | | | |
|---------------------------------|-------|-------|-----------|-----------|-------|-----------|----------------------------|
| ROI Name | Start | Stop | Peak Min. | Peak Max. | RSF | Intensity | Relative [%] Concentration |
| C | 245.0 | 292.0 | 9258.0 | 10814.0 | 0.250 | 1556 | 59.4 |
| N | 353.0 | 396.0 | 10075.0 | 10593.0 | 0.122 | 518 | 40.6 |

Figure 3.9 The list of quantitative data of the relative concentration taken from AES machine.

3.6.3 Fourier Transforms Infrared Spectroscopy

Fourier transform infrared (FTIR) spectroscopy is an analytical technique that provides information about the chemical bonding or molecular structure of material. The FTIR spectrum was observed by passing a beam of infrared (IR) light through the sample using a monochromatic source. The measurement of the transmitted light reveals the total energy absorbed at each wavelength. Thus, the transmittance or absorbance spectrum can be examined and the peaks exhibited at the particular wavelength gives the details about the molecular structure of the sample. Figure 3.10 shows the block diagram of FTIR spectroscopy.

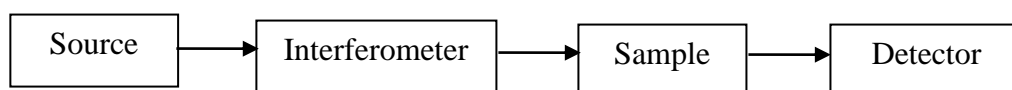


Figure 3.10 The FTIR spectroscopy block diagram.

The focus of study in this work is the assignment of CC_n , CN_n , CH_n , NH_n and OH in the carbon nitride films. The analysis was done using a Perkin Elmer System 2000 FTIR on crystal silicon, c-Si substrates. Bare silicon was used as background. The FTIR spectrum was carried out in a transmittance mode in a wavenumber range of 1000 to 4000 cm^{-1} .

An example of a typical FTIR spectrum is shown in Figure 3.11. From this transmittance spectrum, the absorption coefficient was obtained from equation:

$$\alpha = \ln \left[\frac{100 - T}{\text{thickness}} \right] \quad (3.1)$$

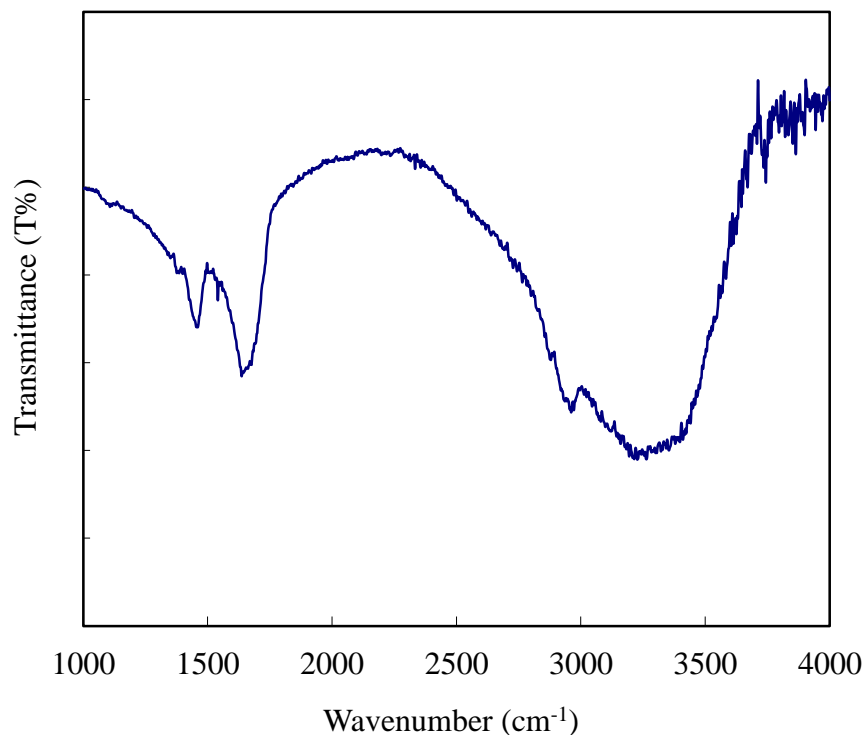


Figure 3.11 The transmittance of FTIR spectrum.

3.6.4 Ultra-violet Visible Near Infra-red Spectroscopy

The optical experiment provides a good way of examining the properties of semiconductor material, particularly in determining the absorption coefficient which gives information about the optical band gap, E_g of the material. This optical band gaps is extremely important for understanding the optical properties of a semiconductor material. The E_g is the difference between the highest occupied molecular orbital (HOMO) and the lowest unoccupied molecular orbital (LUMO). A Jasco V-570 Ultra-violet visible near infra-red (UV Vis NIR) spectroscopy was used to measure the optical properties of the films. The spectra were measured in transmission and reflectance mode in the wavenumber range of 190 to 2500 nm. These measurements were carried out on samples deposited on the quartz substrates. Figure 3.12 shows a picture of the Jasco V-570 UV Vis NIR spectrometer.



Figure 3.12 A picture of Jasco V-570 Ultra-violet visible near infra-red (UV Vis NIR) spectroscopy.

A schematic diagram of a typical spectrometer set-up is shown in Figure 3.13. Hydrogen lamp as the same of a wavelength range of 190 to 350 nm (ultra-violet region) and tungsten iodine lamp for the wavelength range of 350 to 2500 nm (visible to near infrared region) were used. The light source is converged before entering the monochromator. The light enters the monochromator through an entrance slit and collimated by collimating lenses. Then, the grating diffracts the beam into its component wavelength. The exit slit allows only a particular wavelength to pass thus giving a monochromatic light. The schematic diagram shown in Figure 3.14 summarizes this monochromatic effect. The light is then split into two by a sector mirror and passes through the sample and the reference sample, and then is incident on the detectors. The detectors is made up of a photomultiplier tube. The signal is then processed and displayed as optical spectrum.

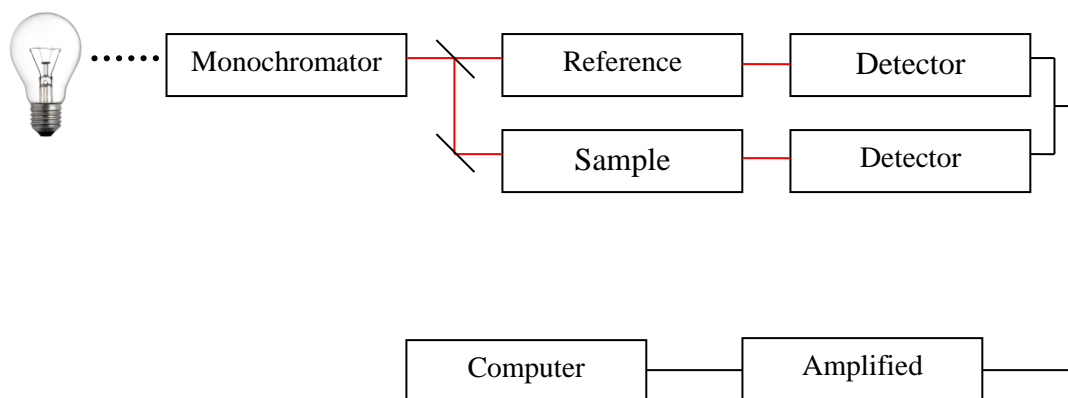


Figure 3.13 Block diagram of typical spectrometer setup.

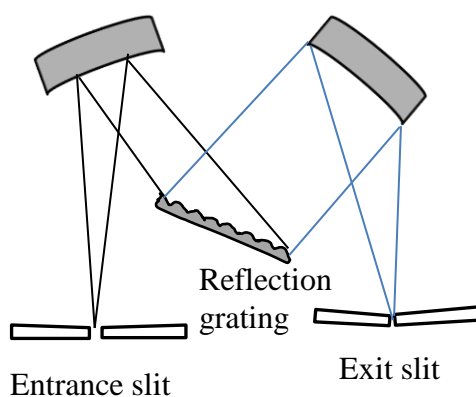


Figure 3.14 Schematic diagram of Czerny-Turner grating monochromator.

The optical measurement for all samples was carried out on the carbon nitride thin films deposited on the quartz substrate. The spectrometer measured the transmission and reflectance spectra. A bare quartz slide was used as a reference for the transmission measurement while a total reflection of an aluminum coated glass slide was used as reference for the reflectance measurement. The absorption coefficient is calculated from these transmission and reflectance spectra using the relation:

$$\alpha = \frac{1}{d} \ln \frac{(1-R)}{T} \quad (3.2)$$

where α is the absorption coefficient. d , T and R are the thickness of film, transmittance and reflectance of the spectra, respectively. The E_g of the film is determined from Tauc relation

$$\alpha E = B(E - E_G)^\varphi \quad (3.3)$$

where α is taken from equation 3.1, B is a constant, E is the photon energy, $\varphi = 1/2$ for a direct allowed transition and $\varphi = 2$ for an indirect allowed transition. For the CN_x thin film which is considered as an indirect semiconductor, the Tauc relation is taken as (Gharbi, Fathallah, Alzaied, Tresso, & Tagliaferro, 2008):

$$(\alpha E)^{1/2} = B^{1/2}(E - E_G) \quad (3.4)$$

Example of the transmittance and reflectance spectra was taken directly from this measurement as shown in Figure 3.15. The corresponding graph of $(\alpha E)^{1/2}$ against photon energy, E is shown in Figure 3.16. E_g was obtained from the intersection of the linear part of the curve extrapolated to intercept the energy axis.

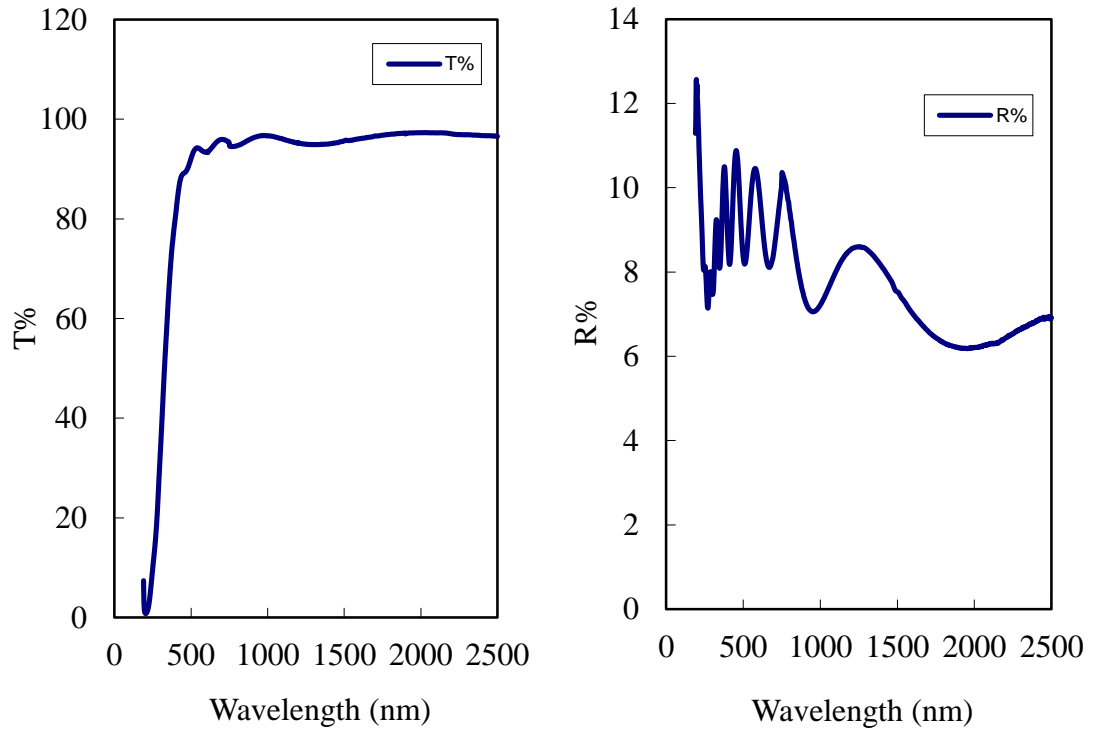


Figure 3.15 Transmittance, T% and reflectance, R% spectrum of CN_x films.

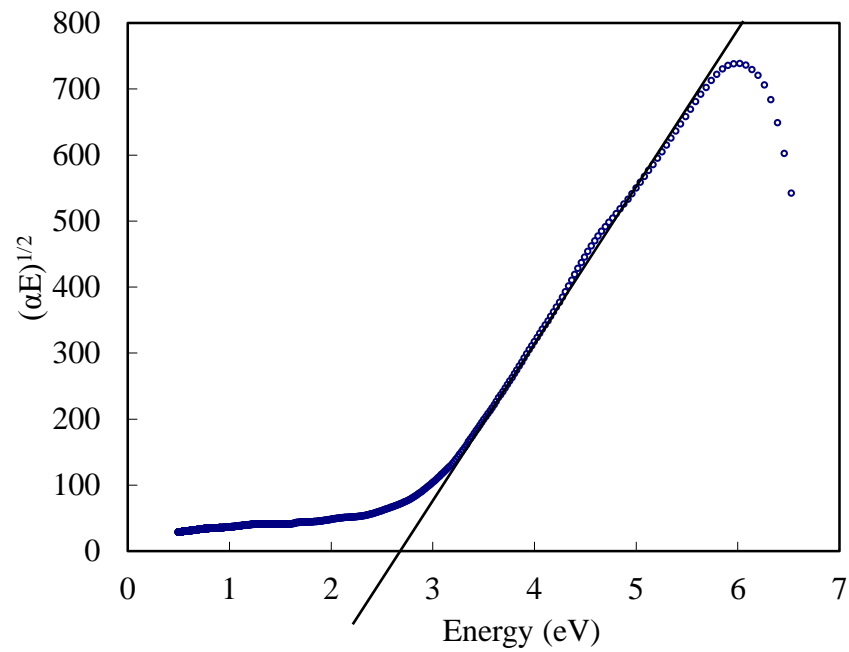


Figure 3.16 Values of E_g taken from the intersection of energy axis.

3.6.5 Raman Spectrometry

In Raman spectroscopy a photon of light interacts with a sample to produce radiation scattering. Normally, a laser is used as a photon source as it is a powerful monochromatic source. The laser interacts with the sample and only the scattered photons were measured during the Raman process. The interaction between photon and molecules is an elastic scattering most commonly called Rayleigh scattering. In Rayleigh scattering, the photons have the same wavelength as the incident light. However, wavelength may shift either to lower (red shift) or higher (blue shifted) due to the photon and matter interaction called Raman scattering. The red shifted photons are subject to a "Stokes shift" where the photon has interacted with the electron cloud of the functional groups bonds, exciting an electron into a virtual state. The electrons are then relaxed into an excited vibrational or rotational state. This causes the photons to lose some of its energy and is detected as Stokes Raman scattering. This loss of energy is directly related to the functional group, the structure of the molecule to which it is attached, the types of atoms in that molecule and its environment. The Jablonski energy diagram for Raman scattering is shown in Figure 3.17.

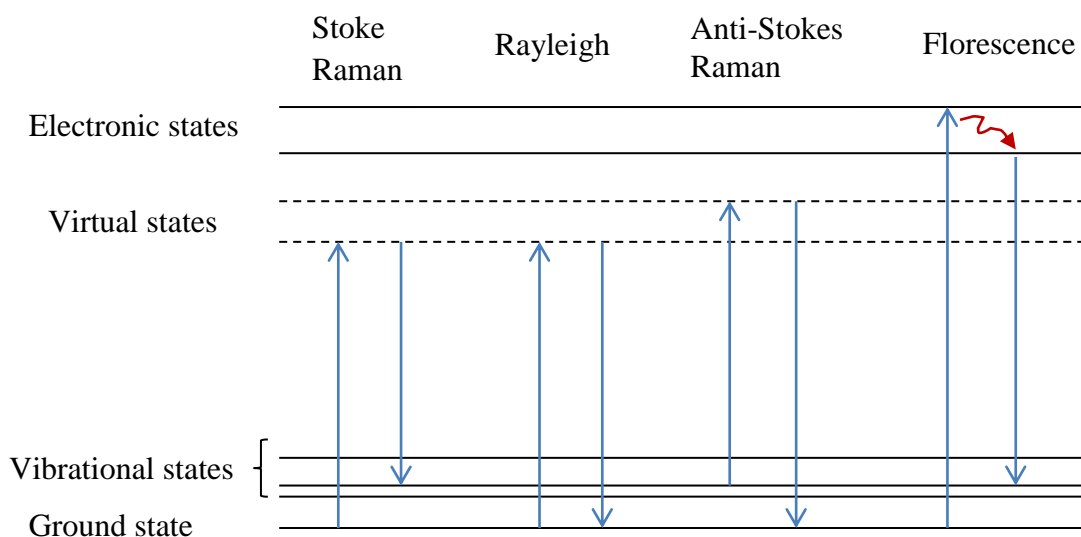


Figure 3.17 The Jablonski energy diagram for Raman scattering.

The most important use of Raman spectroscopy is to identify whether the material are amorphous, graphitic or diamond like films. In this work, a Renishaw Raman spectrometer employing an Ar^+ laser with excitation wavelength of 325 nm was used to analyze the CN_x films. The unit is shown in Figure 3.18. The Raman shift was measured in the wavenumber range of 1000 to 2000 cm^{-1} . A schematic of a typical micro-Raman spectrometer is shown in Figure 3.19. A sample is placed at the sample stage which is attached to a microscope. The scattered light is collected from the sample enters the device through the microscope objective and is then separated into its Stokes shifted frequency by a diffraction grating. This is focused onto a CCD array detector. The intensity of each frequency is measured by individual pixel on the array. The CCD is then read-off to a computer and the result is converted into a spectrum which displays the intensity of the inelastically scattered light in wavenumbers relative to the wavelength of the exciting laser.

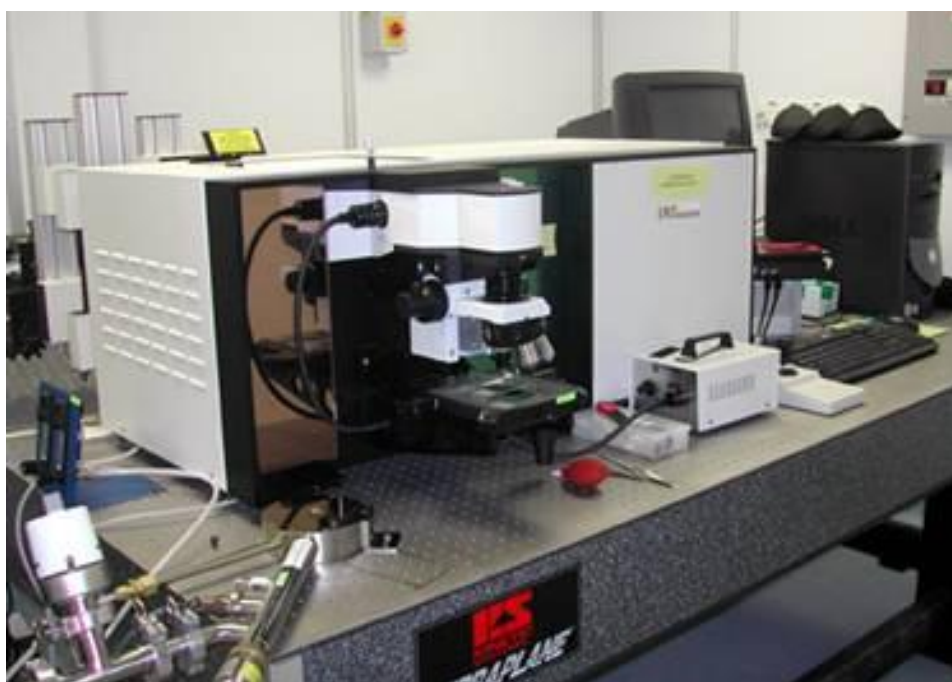


Figure 3.18 A picture of Horiba Jobin Yvon 800 UV Micro-Raman Spectrometer.

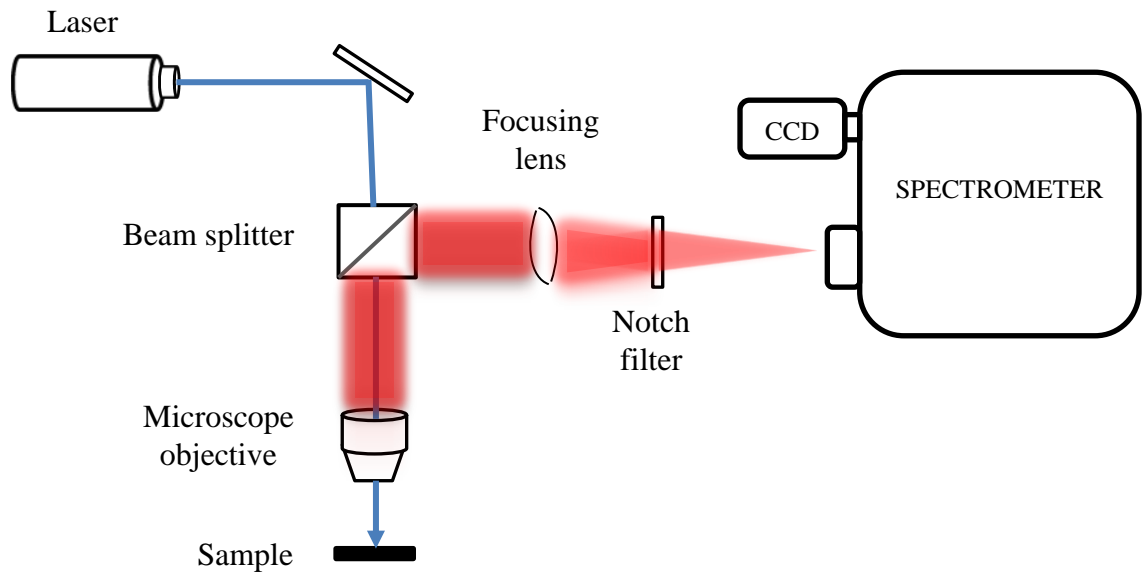


Figure 3.19 Schematic diagram of Raman principle.

An example of a raw Raman spectrum is shown in Figure 3.20 (a). This shape shows a descending baseline slope which is normally attributed to an overlapping PL emission background within the same measurement range. Thus, the baseline of the spectrum needs to be corrected using a straight line interpretation as shown in Figure 3.20 (a). The resulting Raman spectrum could be deconvoluted into 2 overlapping bands similar to those reported by other researchers (Chen et al., 1997; Xie, Jin, Wang, & He, 1998; Zhang et al., 2000). The deconvoluted peaks were obtained from Gaussian-Lorentzian fitting generated using OriginPro 8.1. Example of the fitting is shown in Figure 3.20 (b). The fitting provides the peak position (ω), width of the band calculated as the full width half maximum (FWHM) and peak intensity (I) for both the D and G bands.

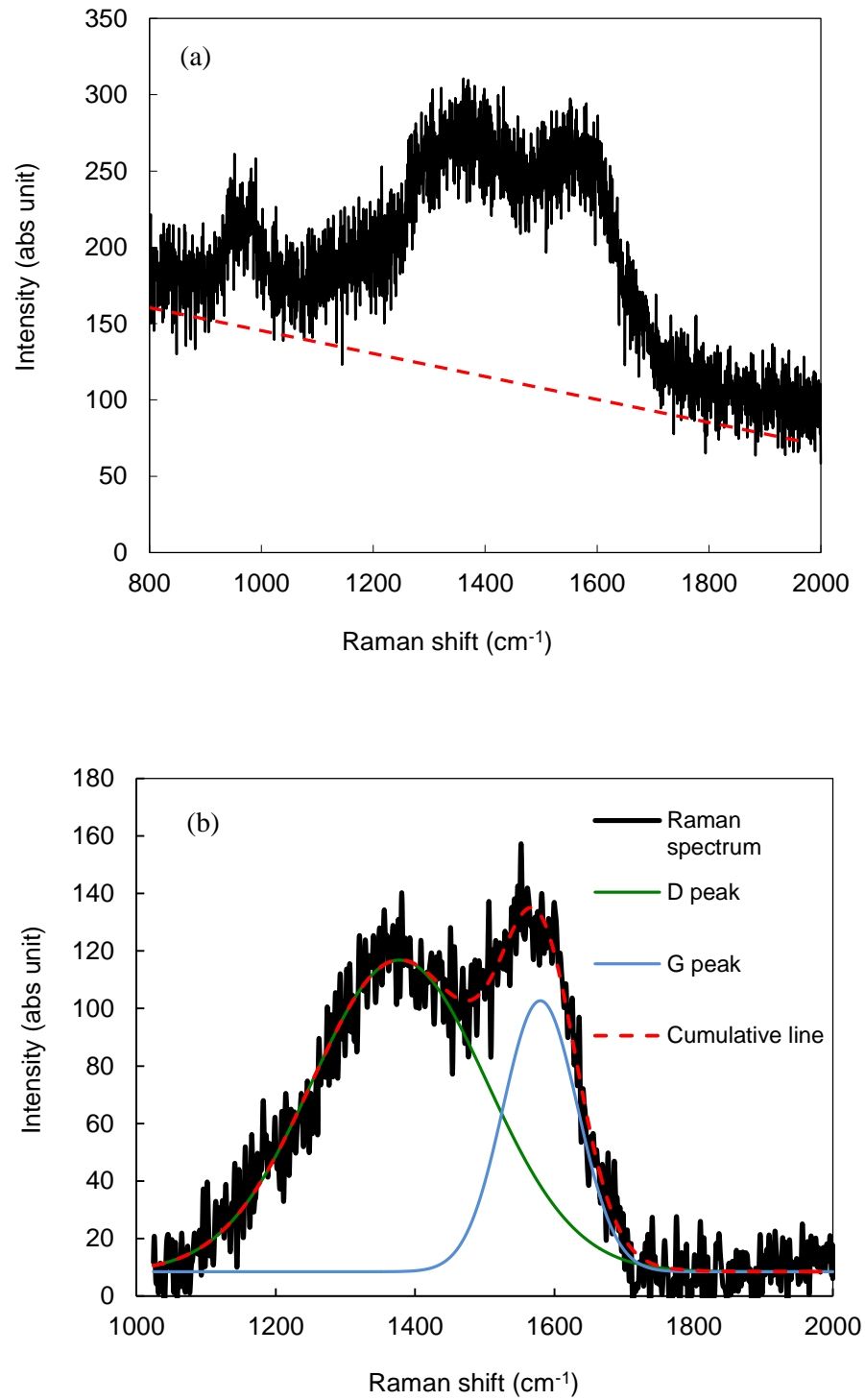


Figure 3.20 Examples of typical Raman scattering spectra with (a) raw data showing baseline fitting and (b) spectra with base line correction showing Gaussian fitting to obtain D and G bands.

The Raman spectra also provide information on the H content from the descending baseline slope of strong photoluminescence background as seen in Figure 3.20 (a). This background is due to the recombination of electron hole pairs within sp^2 bonded cluster embedded in sp^3 bonded amorphous matrix (Marchon, 1997). The H content is determine from the PL slope and the G peak's intensity using the relation (Casiraghi, Ferrari, & Robertson, 2005a) :

$$H [at\%] = 21.7 + 16.6 \log\left\{\frac{m}{I_{(G)}} [\mu m]\right\} \quad (3.5)$$

where m and $I_{(G)}$ are the slope and the intensity of the G peak, respectively.

3.6.6 Photoluminescence Spectroscopy

Photoluminescence occurs when the electronic states of films are excited to higher energy level and release its energy as a light. A particular energy of light source is required in able to make this to happen. By using the principle of Stroke law (seen in figure 3.17), the energy of the emitted light is generally equal to or less than the exciting light. The difference between these two in energy is due to the transformation of the exciting light. The exciting light could transform to greater or lesser extent or to non-radiative vibration energy of atom.

Photoluminescence characteristics of the films were also recorded using a Renishaw Raman spectrometer. A helium cadmium (HeCd) laser was used with excitation wavelength of 325 nm. In this PL spectroscopy, the HeCd laser is used as the photon energy source. Photon with energy greater than band gap of the material studied is directed onto the surface of the material. The incident monochromatic photon beam is

partially reflected, absorbed, and transmitted by the material being probed. The absorbed photons create electron-hole pairs in the material. The electrons are excited to the conduction band or to the energy states within the gap. Photon produced as a result of the recombination of electron and holes are emitted from the material surface and it is the resulting photon emission spectrum that is studied in PL. Different energy states that presence in the material are produced by different defects and impurities incorporated into the material. As a consequence, PL emission spectrum provides information concerning the point defect nature of material by determining not only the presence but also the types of vacancies and impurities in the lattice.

A direct conduction band to valence band recombination is rarely observed in PL spectra due to the strongly photon reabsorption of atom. Therefore, the recombination process is observed with emission energy less than the material band gap. These processes include excitonic recombination and direct transitions, which involve the trapping of electrons by the impurities.

CHAPTER 4 RESULTS AND DISCUSSION

4.1 Introduction

Two studies are presented in this work. The first part of the work focuses on the fabrication and comparison of carbon nitride (CN_x) films deposited using different hydrocarbon and nitrogen (N_2) mixtures. For this reason two sets of samples were prepared by using two different precursor gases. The first set was deposited from a mixture of methane (CH_4) and N_2 while the other one was prepared from a mixture of ethane (C_2H_6) and N_2 gases. The effects of varying the N_2 flow rate for both sets were studied. The objective is to compare the structural and optical properties of films produced from the discharge of different precursor gases. The structural and bonding characteristics of these films were determined from the FTIR and Raman analysis done on the films. The optical and photoluminescence spectra of the films were scrutinized and correlated to the opto-electronic properties.

The second part of the work were focused on studying the effects of hydrogen (H_2) dilution on the properties of the films deposited from the discharged of C_2H_6 and N_2 gas. The variations of H_2 flow rate on the properties of the films were analyzed. All the samples were prepared on quartz slides and polished p-type $\langle 111 \rangle$ silicon substrates. The flow chart in Figure 4.1 depicted the sequence of the work flow of the different sets of films deposited and characterized in this work.

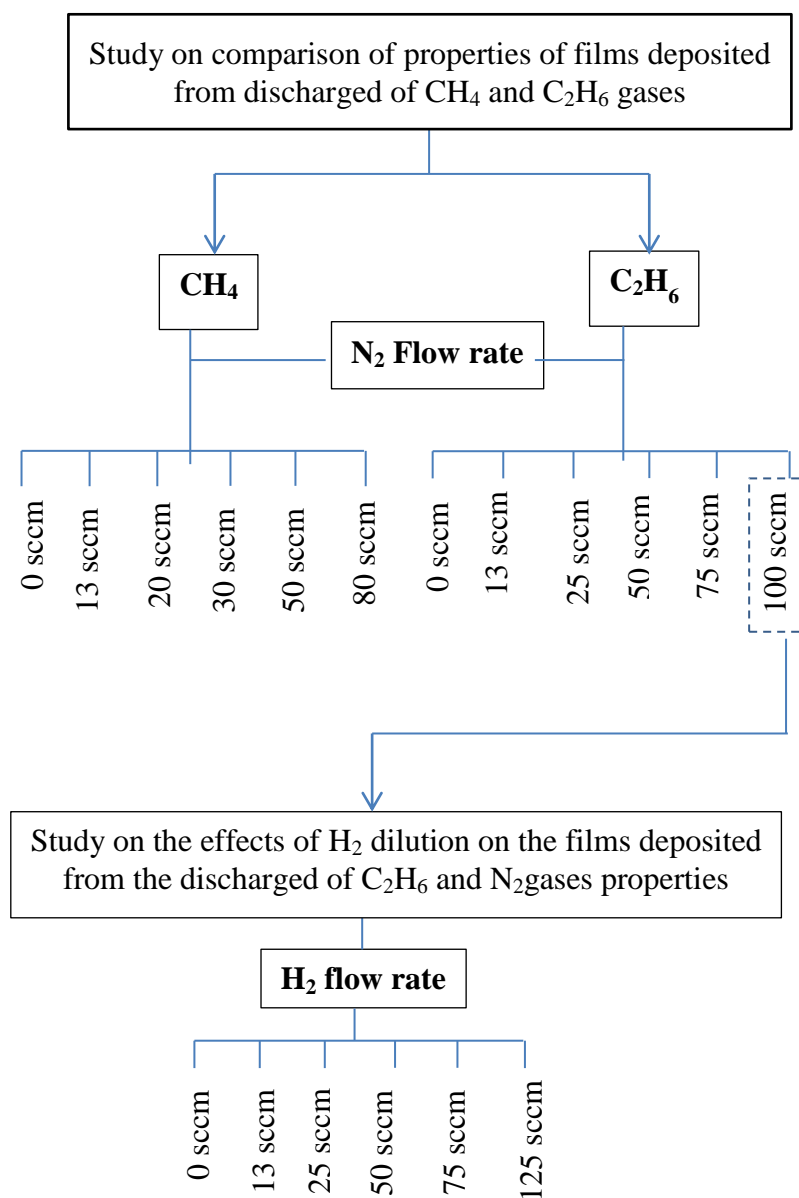


Figure 4.1 Flow chart shows the preparations steps studies of CN_x films.

4.2 Effects of Nitrogen Incorporation on the Carbon Nitride Films Using Different Precursors.

4.2.1 Growth Rate

Figure 4.2 shows the influence of N₂ flow rate on the deposition rate of the films produced using either CH₄ or C₂H₆. The combination of CH₄ and N₂ mixture is henceforth denoted as CH₄:N₂, while that of C₂H₆ and N₂ mixture is denoted as C₂H₆:N₂. Generally, from the results, the growth rate of films produced from CH₄:N₂ is higher than the films deposited from C₂H₆:N₂. Commonly, the growth mechanisms of PECVD films are strongly determined from the dissociation of the precursor gas, secondary gas phase reaction and the surface reaction. However, this work not focused on detail reaction mechanism of the films growth but focuses on the properties of films produced with respect to the parameters presented in Figure 4.1. The dissociation of CH₄ usually results in a formation of radicals of CH₄, CH₃ and CH₂ and these radicals are directly incorporated into the film and thus contribute to its growth. CH₃ is known to be the dominant growth radical which is formed mainly through secondary gas phase reactions in the plasma (Von Keudell, Meier, & Hopf, 2002).

Using the following reactions proposed by Legrand et. al (Legrand, Damiy, Hrach, & Hrachová, 1999) the role of N₂ towards the growth rate of the films as shown in Figure 4.2 is explained.



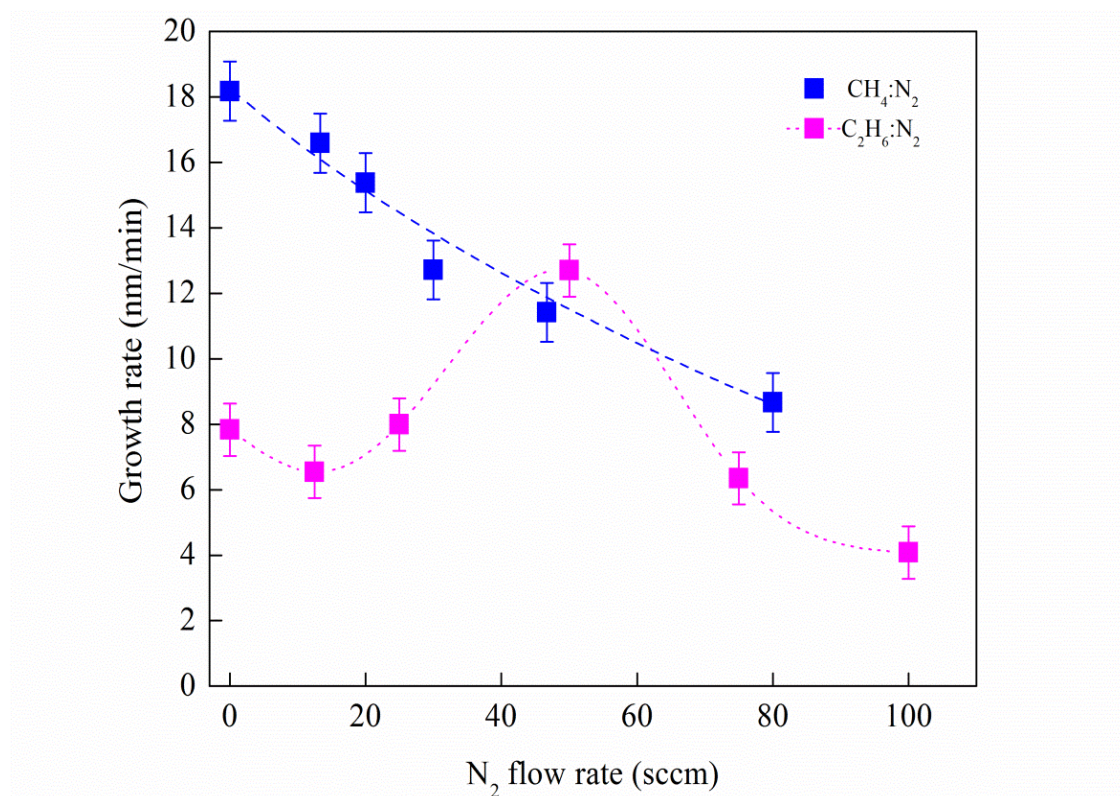


Figure 4.2 Variation in growth rate using CH₄:N₂ or C₂H₆:N₂ mixture as a function of N₂ flow rate. Line is as guide to the eye.

The reactions show that the dissociation of CH₄:N₂ permits a one step process to form the CH₃ precursors in comparison to C₂H₆:N₂ which have to undergo an additional step to form the CH₃ radical. The presence of N₂ induces the formation of CH₃ radicals at a faster rate during the dissociation gas of CH₄ compared to C₂H₆. This contributes to the higher growth rate of the films produced from CH₄:N₂ gas compared to C₂H₆:N₂ gas.

With respect to N₂ dilution, both films show remarkable differences in their growth rate. The films deposited using CH₄:N₂ show an almost linear decrease in growth rate with the increase in N₂ flow rate. While those deposited using C₂H₆:N₂ increase significantly up to the flow rate of 50 sccm and then decreases with further

increase in the N_2 flow rate. It is believed that the decrease in growth rate of the films at high N_2 flow rate is due to the decrease in the hydrocarbon partial pressure since the deposition pressure is maintained at a fixed value with the increase in N_2 dilution. This reduces the availability of CH_n radicals reaching the growth sites. This occurs for both hydrocarbon mixtures. This effect is related to the N incorporation in the films structure which will be analyzed in the following section of this chapter.

4.2.2 Auger Electron Spectroscopy

N incorporation is easily attained with N_2 dilution as seen in the N/C ratio in Figure 4.3. The N incorporation increased with the increase in N_2 flow rate for both hydrocarbon mixtures. For $CH_4:N_2$ the N/C increases almost linearly for N_2 flow rate up to 30 sccm then begin to saturate above N_2 flow rate of 50 sccm. For $C_2H_6:N_2$ the N/C ratio increases abruptly in the initial introduction of N_2 flow rate which then increases only slightly leading to an almost constant value above H_2 flow rate of 50 sccm. The incorporation of N into the films produced from $C_2H_6:N_2$ is much lower than those of $CH_4:N_2$. This result shows that the N atoms or ions in the plasma are not easily incorporated into the film structure.

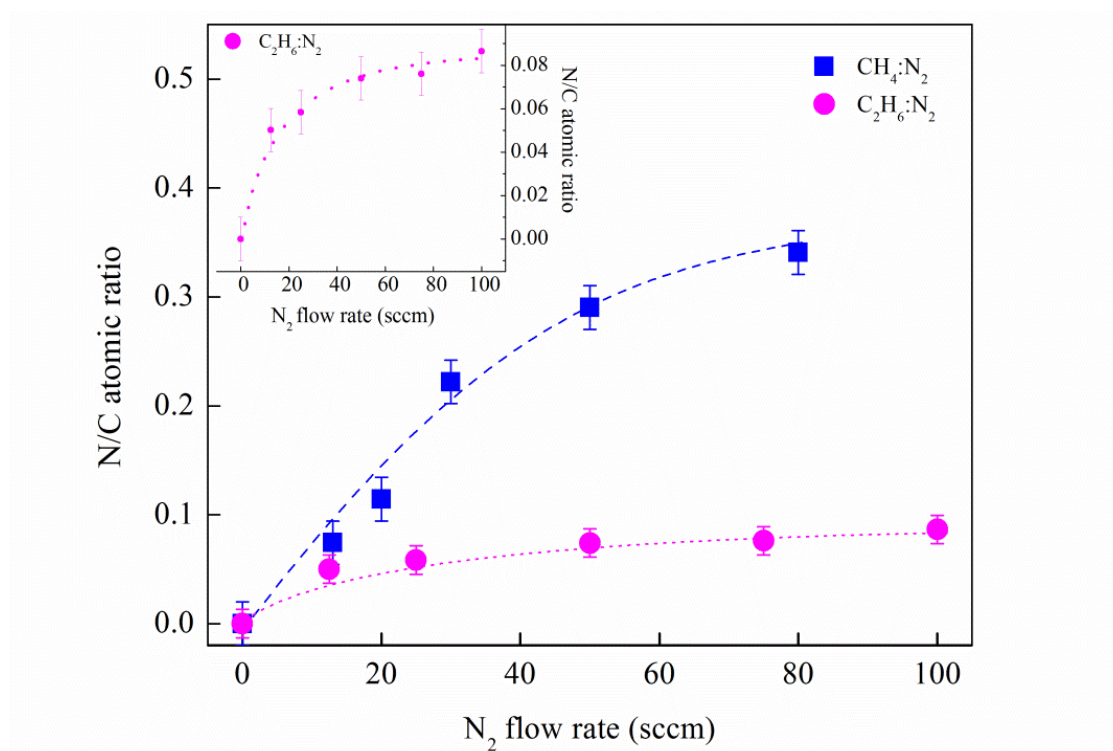


Figure 4.3 Variation in nitrogen to carbon, N/C ratio for films deposited as a function of N₂ flow rate. Line is as guide to the eye.

As mentioned earlier, there is a relationship between the N incorporation and the growth rate of the films. Thus, the variation in the N/C ratio with respect to N₂ flow rate will be used to explain the influence of N₂ flow rate on the growth rate presented in the previous section. The significant increase in N/C ratio with the increase in N₂ dilution for CH₄:N₂ coincides with the significant decrease in its film growth rates. This suggests that high N₂ partial pressure encourages N incorporation but suppresses the film growth. As for the films deposited from C₂H₆:N₂, lower N₂ flow rate up to 50 sccm increases the growth rate. Thus, at low N flow rate, the N atoms in the plasma promote the dissociation of the C₂H₆ precursor. Here the role of N atoms in the plasma may induce the growth of the films but very few get incorporated into the film structure. Thus N does not get incorporated much in the film, while the film itself grows at a rate that is almost linear with the increase in N₂ flow rate. However, with further increase in N₂ flow rate above 50 sccm the reduction in C₂H₆ partial pressure may be significant

enough to result in the suppression of the film growth but the N incorporation continues to increase very slowly.

Consequently for the films deposited from $C_2H_6:N_2$, below the flow rate of 50sccm, the slight increment in N incorporation (N/C) appears to increase the growth rate but above this flow rate, the incorporation of N atoms shows no increment resulting in decrease in growth rate. From Equation 4.2, the N_2 promotes the dissociation of C_2H_6 to C_2H_5 , and further reactions with H atom promote the formation of CH_3 radicals which is the main growth precursor for DLC or *a*-C: H films. At low N_2 flow rate, the partial pressure of C_2H_6 is enough to promote films growth, however at higher growth rate above 50 sccm the partial pressure of C_2H_6 is reduced resulting in lower concentration of H atom in the plasma. This retards the formation of CH_3 radicals thus reduce the growth rate.

4.2.3 Fourier Transformation Infrared

Fourier Transform Infrared is a useful technique for basic understanding of the bonding configuration in CN_x films. The effect of N incorporation on the bonding characteristics of these films was investigated by infrared absorption studies. The absorption spectra of the deposited films were recorded as a function of gas flow rate as shown in Figure 4.4. The spectra for both sets of films show the expected functional groups for CN_x films. These include C-N, C=N and C \equiv N bonds within the wavenumber range of 1020-1280, 1600 and 2240 cm^{-1} , respectively (Mutsukura & Akita, 1999), together with C=C, C-H_n groups and OH bonds within the wavenumber region of 1300-1500, 2700-3100 and 3000-3500 cm^{-1} , respectively (Zhang, Nakayama, & Harada, 1999c).

The N free C film obtained from pure CH_4 shows a lone strong broad CH_n peak within the wavenumber region of 2700-3100 cm^{-1} . The expected peak normally associated with the content of sp^2 bonds in the films within the range of 1300-1500 cm^{-1} is absent for this film. Indeed this is similar to the FTIR studies by other researchers (Escobar-Alarcón, Arrieta, Camps, Romero, & Camacho-Lopez, 2005; Shinohara et al.; Smith et al., 2001). With the N_2 dilution and corresponding N incorporation, a significant change in the CN_x films FTIR spectra is seen. This includes a drastic decrease in CH_n peak intensities and appearance of a broad peak of the expected sp^2 bonds within the range of 1300-1500 cm^{-1} . The decrease in CH_n peak suggest the preferential formation of CN bonds including sp^3 C-N, sp^2 C=N and sp^1 C \equiv N in the films. Indeed the appearance of the sp^2 bonds could be attributed to sp^2 C=N bonds in the films. N incorporation breaks the symmetry of sp^2 C bonds allowing this band to be seen. The assignment of this peak to sp^2 C=N is supported by the FTIR results for the films deposited from $C_2H_6:N_2$. The N free C films obtained from pure C_2H_6 shows not

only a strong broad peak of the CH_n group but also two smaller distinctly sharp peaks centered at approximately 1375 and 1460 cm^{-1} , both assigned to sp^2 $\text{C}=\text{C}$ bonds. With the incorporation of N in the films produced from $\text{C}_2\text{H}_6:\text{N}_2$ a broad peak centered at 1630 cm^{-1} appears and its intensity increases with the increase in N_2 flow rate. From AES analysis discussed earlier the increase in N_2 flow rate also result in the increase in N/C ratio and its corresponding N incorporation. Thus this peak is assigned to the sp^2 $\text{C}=\text{N}$ bonds. It is also seen that at higher N_2 flow rate (above 25 sccm) distinct broad peaks centered at approximately 1020 cm^{-1} appears. These peaks are assigned to sp^3 C-N bonds (Gharbi, Fathallah, Alzaied, Tresso, & Tagliaferro, 2008; Szörényi, Fuchs, Fogarassy, Hommet, & Le Normand, 2000).

Drastic changes in FTIR spectra for C films would occur when there is structural transition which normally happens when N is incorporated into the films (Ferrari, Rodil, & Robertson, 2003; Heitz, Dré villon, Godet, & Bourée, 1998; Shiao & Hoffman, 1996). However, the results in this work show that the effect of N_2 dilution is dependent on whether CH_4 or C_2H_6 gas is used in the mixture. Apart from the efficiency of N incorporation and hence the bonded N content, the type of bonding plays a crucial roles. While N incorporation in films obtained from the $\text{CH}_4:\text{N}_2$ result in significant decrease in CH_n bonds and significant increase in $\text{C}=\text{N}$ bonds, films obtained from the $\text{C}_2\text{H}_6:\text{N}_2$ still showed dominant CH_n bonds with significantly lower content of the $\text{C}=\text{N}$ bonds. However the peaks obtained for the latter are sharp and easily identifiable.

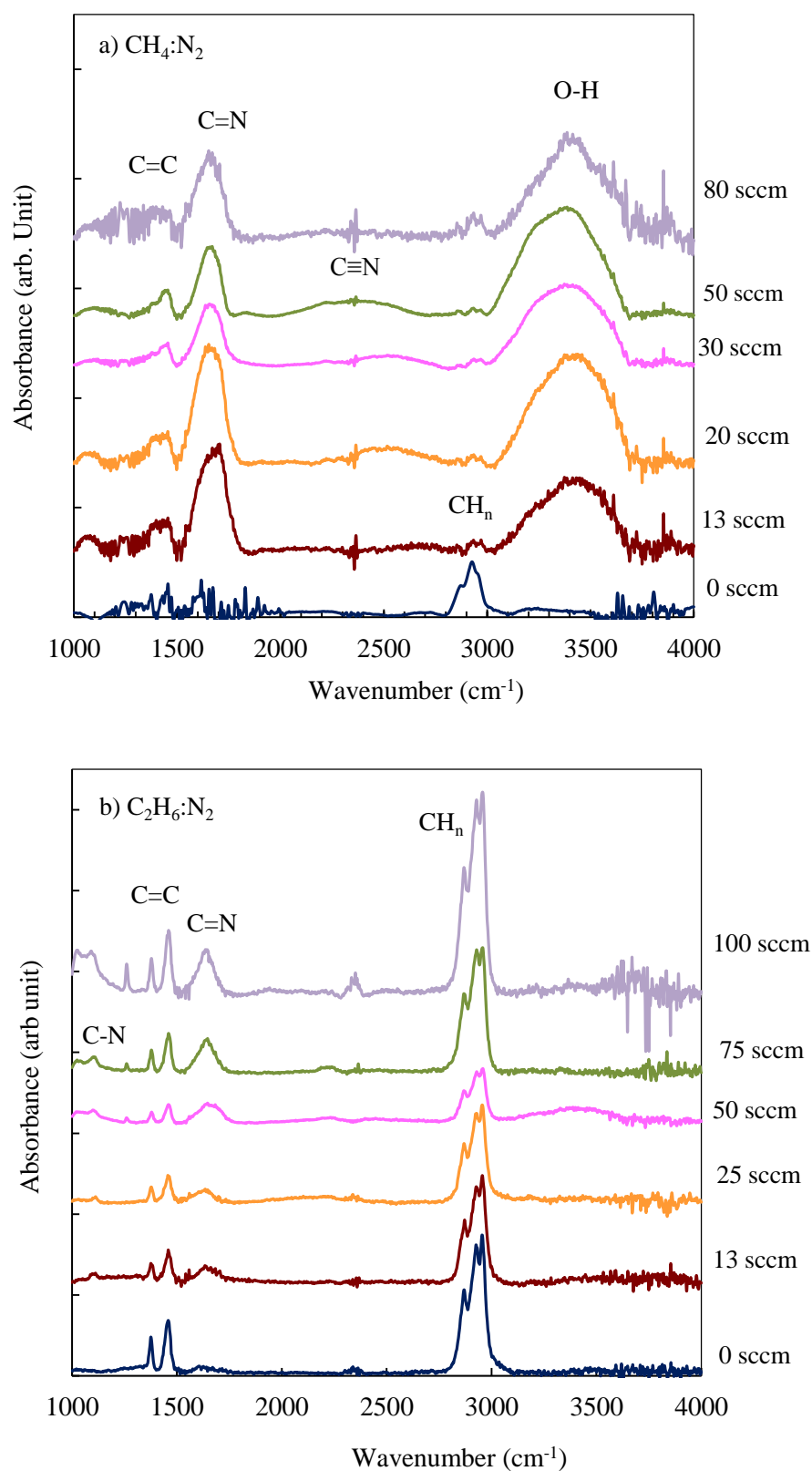


Figure 4.4 FTIR absorbance spectra as a function of N_2 flow rate using (a) CH_4 and (b) C_2H_6 in the range of 1000-4000 cm^{-1} .

The FTIR spectra for both sets of films show some interesting traits. Firstly, the spectra for films prepared from $\text{CH}_4:\text{N}_2$ shows an additional small peak centered at 2200 cm^{-1} shown in Figure 4.5 b. This peak is assigned to nitrile and/or isonitrile of $\text{C}\equiv\text{N}$ bonds. These bonds are terminating bonds and may influence the long range ordering in the films. The increase in $\text{C}\equiv\text{N}$ bonds would increase the disorder in the films. Thus, these CN_x films should show higher disorder than the N free C films.

The films prepared from $\text{C}_2\text{H}_6:\text{N}_2$ shows a certain trend in their bonding. These are shown in figure 4.7 which includes the variation in the highest intensities of the CH_n , $\text{C}=\text{C}$ and $\text{C}=\text{N}$ bonds together with the ratio of the intensities of $\text{C}=\text{N}$ to CH_n bonds ($\text{C}=\text{N}/\text{CH}_n$). With the initial increase in N_2 flow rate up to 50 sccm the intensities of the CH_n and $\text{C}=\text{C}$ bonds decreases but begin to increase with further increase in N_2 flow rate. In contrast, the intensities of the $\text{C}=\text{N}$ bonds increases in the whole range of the N_2 flow rate. The increase in this bond is in line with the increase in N incorporation with the increase in N_2 flow rate in these films. The ratio of $\text{C}=\text{N}/\text{CH}_n$ increases with the initial increase in N_2 flow rate up to 50 sccm and then decreases with further increase in N_2 flow rate. While the initial increase in this ratio is in line with the corresponding increase in $\text{C}=\text{N}$ bonds and decrease in CH_n bonds, the opposite is not necessary true for the decrease at higher N_2 flow rate. It is believed that this did not occur due to preferential formation of CH_n bonds but instead to a preferential formation of sp^3 C-N bonds compared to $\text{C}=\text{N}$ bonds. The C-N bonds centered at wavenumber of approximately 1020 cm^{-1} is clearly evident in Figure 4.6 a. The increase in these bonds occur above N_2 flow rate of 50 sccm in line with the decrease in the $\text{C}=\text{N}/\text{CH}_n$ ratio. This shows the different variations in bonding configuration of N as it is incorporated in the films produced from $\text{C}_2\text{H}_6:\text{N}_2$.

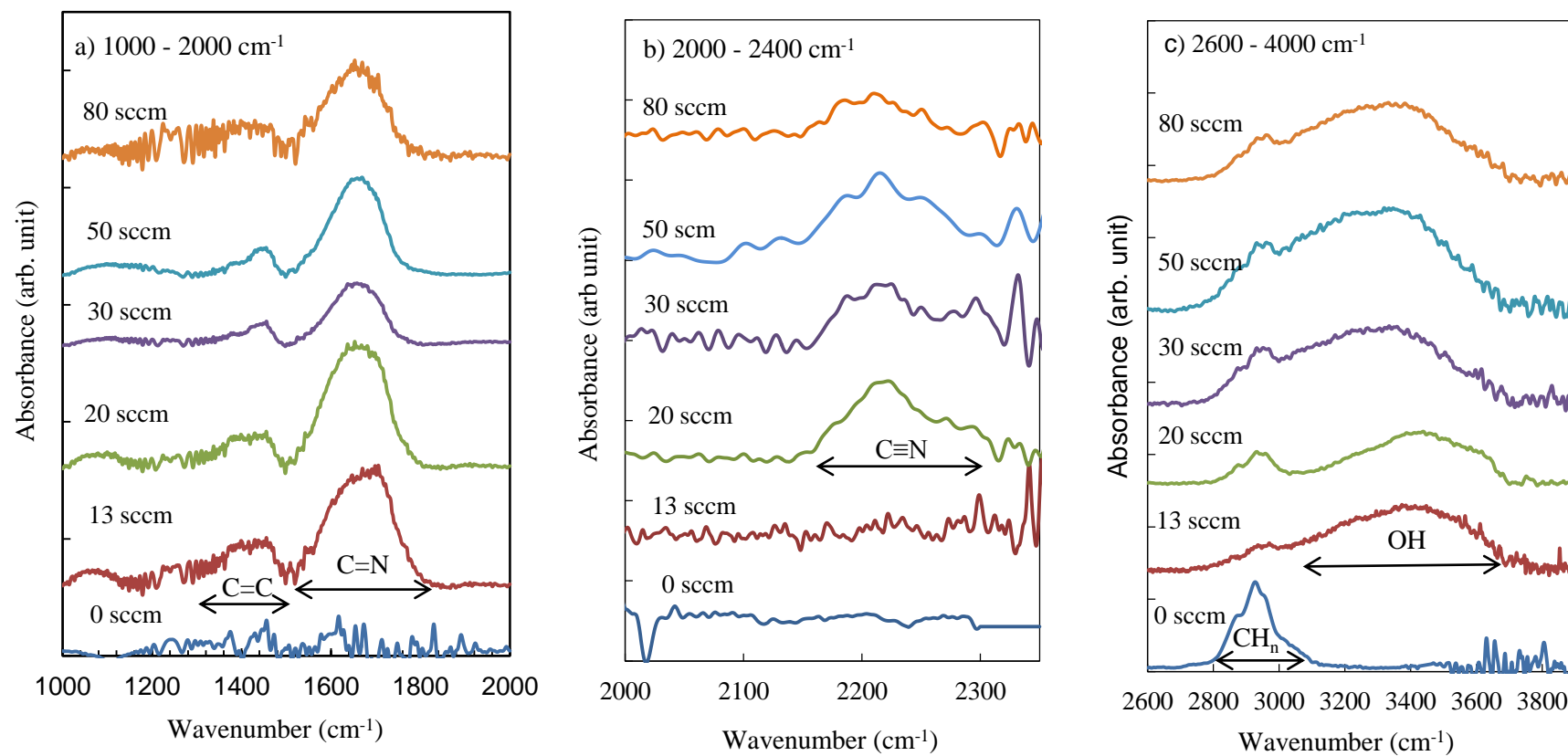


Figure 4.5 Fourier transform infrared spectra of CN_x films prepared from $\text{CH}_4:\text{N}_2$ as a function of N_2 flow rate separated into three different spectra range of (a) 1000-2000 cm^{-1} , (b) 2000-2400 cm^{-1} and (c) 2600-4000 cm^{-1} .

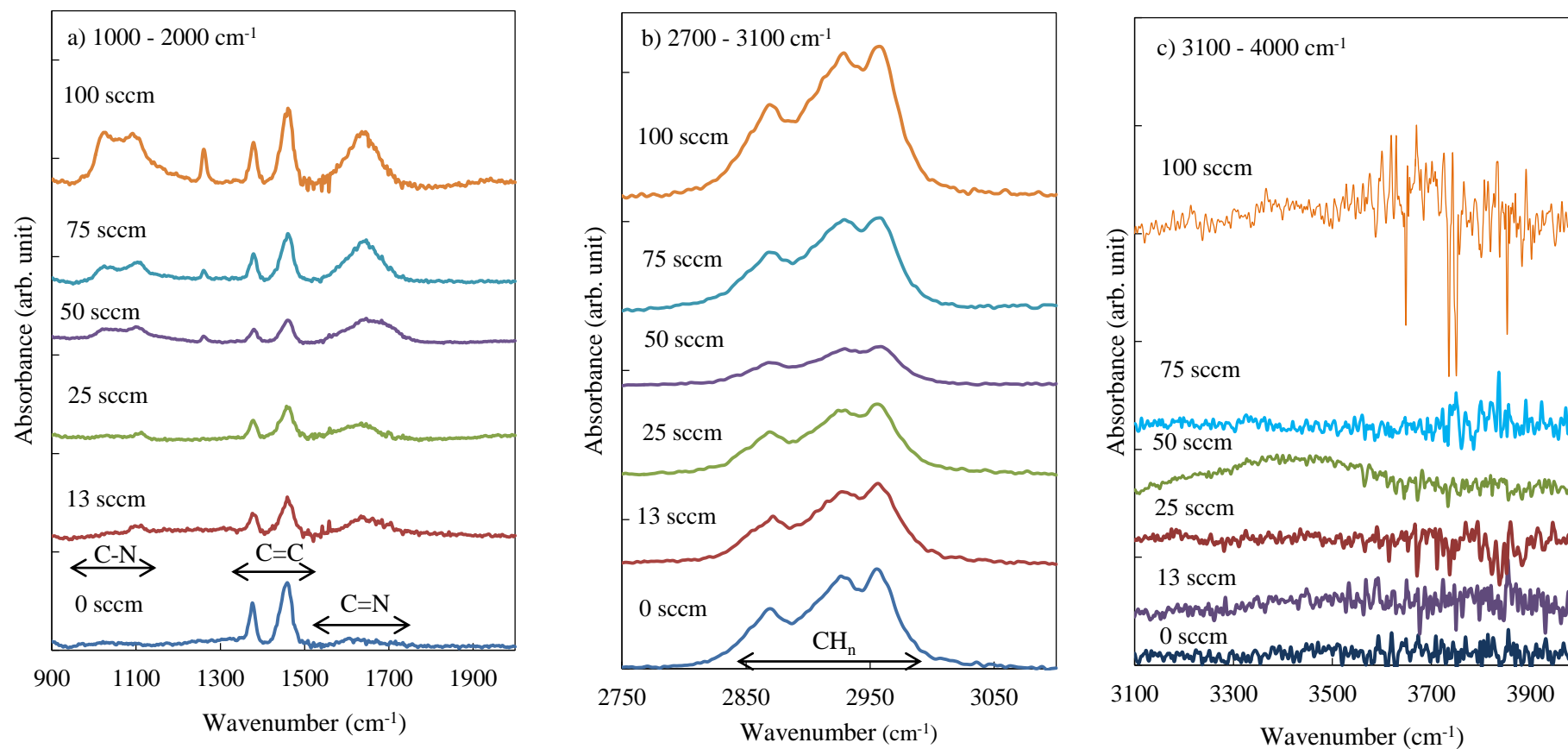


Figure 4.6 Fourier transform infrared spectra of CN_x films prepared from $\text{C}_2\text{H}_6:\text{N}_2$ as a function of N_2 flow rate separated into three different spectra range of (a) 1000-2000 cm^{-1} , (b) 2700-3100 cm^{-1} and (c) 3100-4000 cm^{-1} .

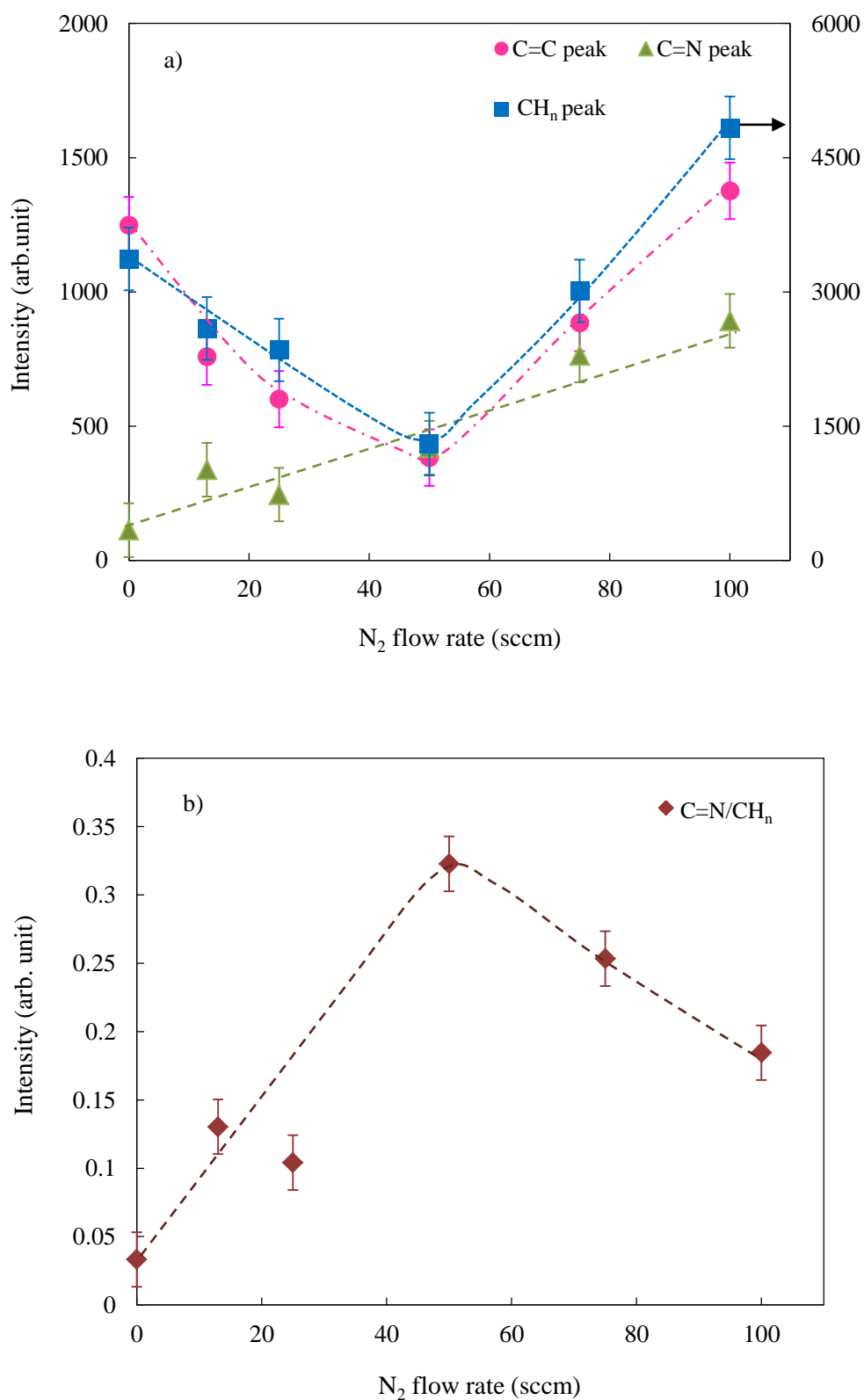


Figure 4.7 Variation in FTIR peaks of CN_x films prepared from $C_2H_6:N_2$ with (a) highest absorbance intensities of C=N, C=C and CH_n ; and (b) the ratio of C=N/ CH_n . Lines are as guide to the eye.

In addition to all the bonds mentioned earlier, another noteworthy aspect of the spectra is the presence of a broad strong peak observed at the wavenumber region of 3000 to 3500 cm^{-1} which is assigned to stretching vibration of O-H bond in the films. It is generally accepted that this O-H bond is attributed to post-deposition contamination of atmospheric water vapour (Ristein, Stief, Ley, & Beyer, 1998) that is absorbed due to porous nature of these films. The presence of O-H could be used as an indicator of the softness and the porosity of C and CN_x films (Muhl & Méndez, 1999). The higher the porosity the more water vapour is absorbed into the films and thus the O-H peak strengthens. It is seen that the FTIR spectra depicted in Figure 4.4 of the N free C films produced from both pure hydrocarbon gases do not show this O-H bond. This O-H bond becomes prominent with N_2 dilution for the films produced from $\text{CH}_4:\text{N}_2$. This indicates the N incorporation induced the porous nature of these films which could be related to the breaking of H bond in the films and increase in disorder as mentioned before. In contrast it is seen that even with N incorporation the films produced from $\text{C}_2\text{H}_6:\text{N}_2$ do not exhibit this O-H bond. This shows that the films produced from $\text{C}_2\text{H}_6:\text{N}_2$ do not exhibit the porous nature of the films produced from $\text{CH}_4:\text{N}_2$. The porous nature of this material is one of the major causes of the degradation of their films. Thus in aspect of sample stability due to the films porosity, the use of $\text{C}_2\text{H}_6:\text{N}_2$ appears to be favourable.

4.2.4 Raman Spectroscopy

The Raman spectra for both sets of materials obtained from either CH₄:N₂ or C₂H₆:N₂ as a function of N₂ flow rate are shown in Figure 4.8 and 4.9, respectively. These Raman spectra show high photoluminescence (PL) background which gives them overlapping baselines slopes. The slopes represented by *m* in the figures would be used latter to calculate and analyse the H content in the films. For now, these spectra will be corrected by eliminating the PL background and the resulting spectra were deconvoluted using Gaussian and Lorentzian line fittings as shown in Figure 4.10.

The spectra were seen to be significantly different and are dependent on the hydrocarbon precursor used. Two common broad bands correspond to D and G peaks located at approximately 1350 and 1570-1600 cm⁻¹ respectively, were observed for both sets of samples. Those obtained from C₂H₆:N₂, also show another broad strong peak at approximately 2000 cm⁻¹. This peak is rarely reported. Some researchers have associated it to high N incorporation into CN_x films (Rodil, Ferrari, Robertson, & Milne, 2001). However this not only contradicts the low N/C seen from the AES results of the films produced from C₂H₆:N₂ but was also present for the N free C films shown in Figure 4.10 (b). A possible alternative explanation could be given. This peak could be a second order band related to the combination of peaks located at 700 and 1300 cm⁻¹ which are assigned to L and D band respectively, that are associated with the presence of sixfold rings (Rodil, et al., 2001). The increase in these peaks with nitrogen would indicate more rings in these films and higher ordered films are produced with the increase in N incorporation.

It was also observed that while the relative intensities of the D and G bands for films obtained from CH₄:N₂ are almost equivalent, the films produced from C₂H₆:N₂ shows a significantly stronger G peak than the D peak. The intensity, peak position and width of these two peaks are generally used to analyse the films structure. Consequently, the deconvolution of these peaks enables the calculation of the I_D/I_G and peak position for both sets of films.

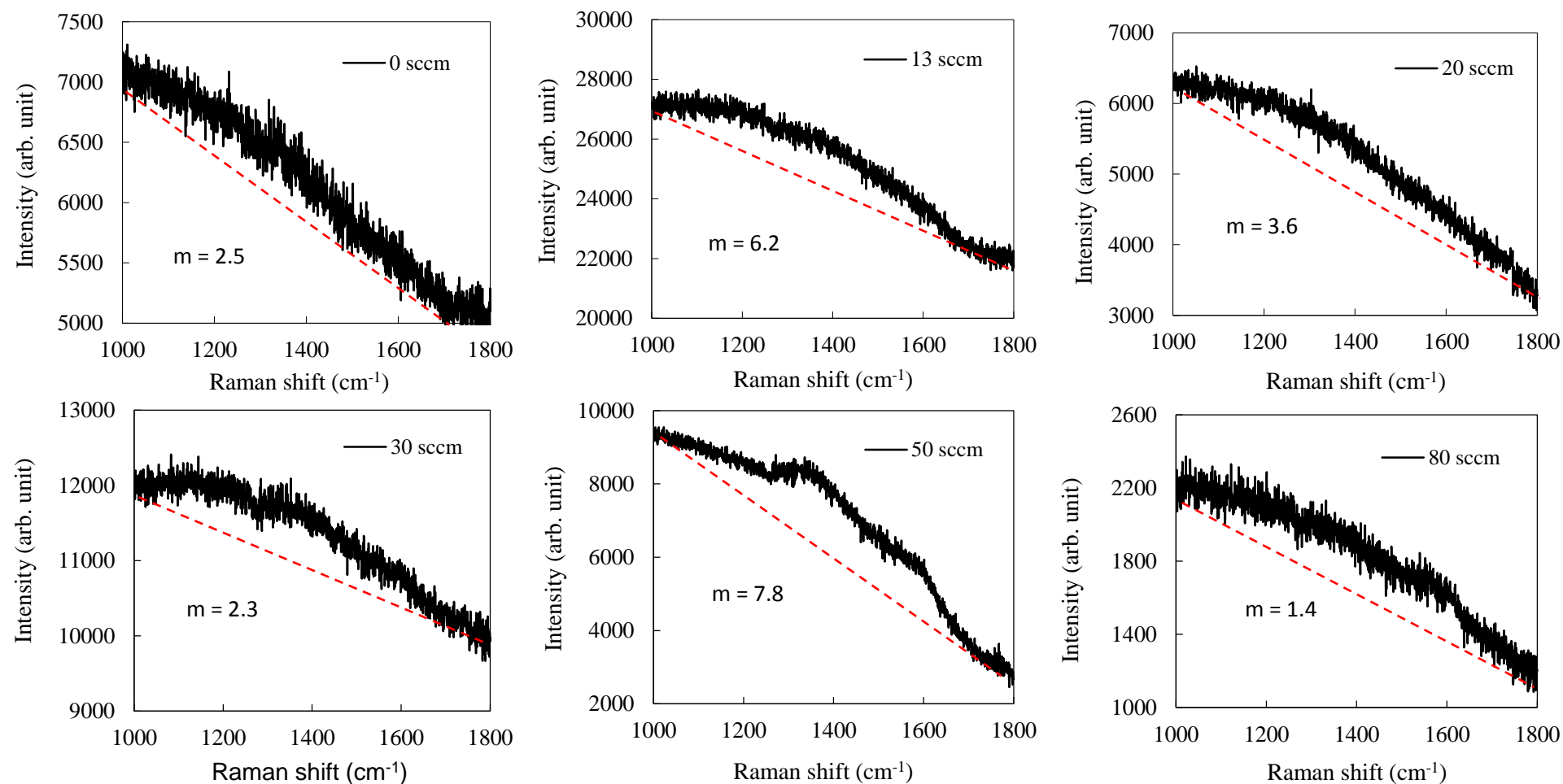


Figure 4.8 Variation in Raman spectra as a function of N_2 flow rate for films prepared from $CH_4:N_2$. m refers to the baseline slope of the PL background.

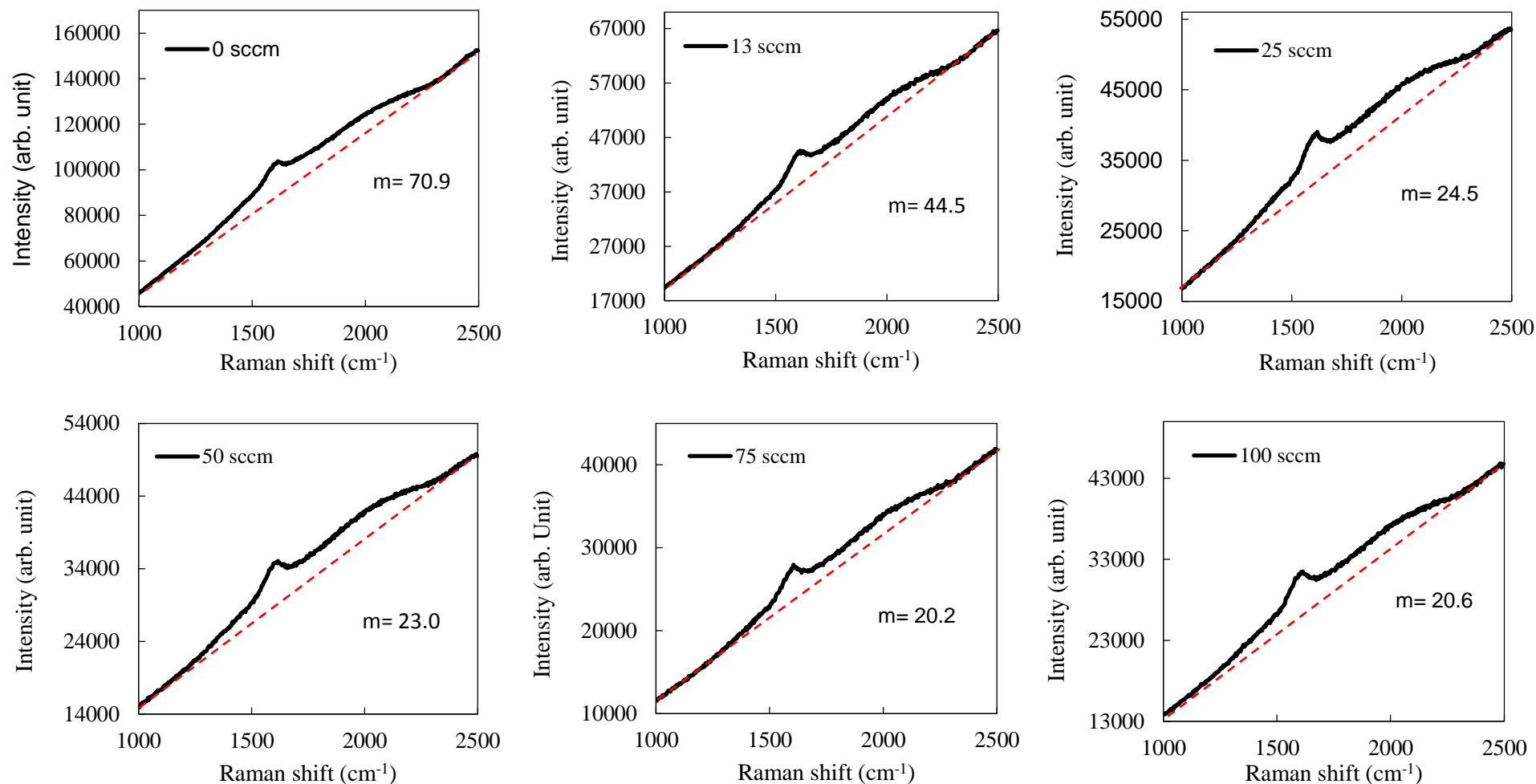


Figure 4.9 Variation in Raman spectra as a function of N_2 flow rate for films prepared from $C_2H_6:N_2$. m refers to the baseline slope of the PL background.

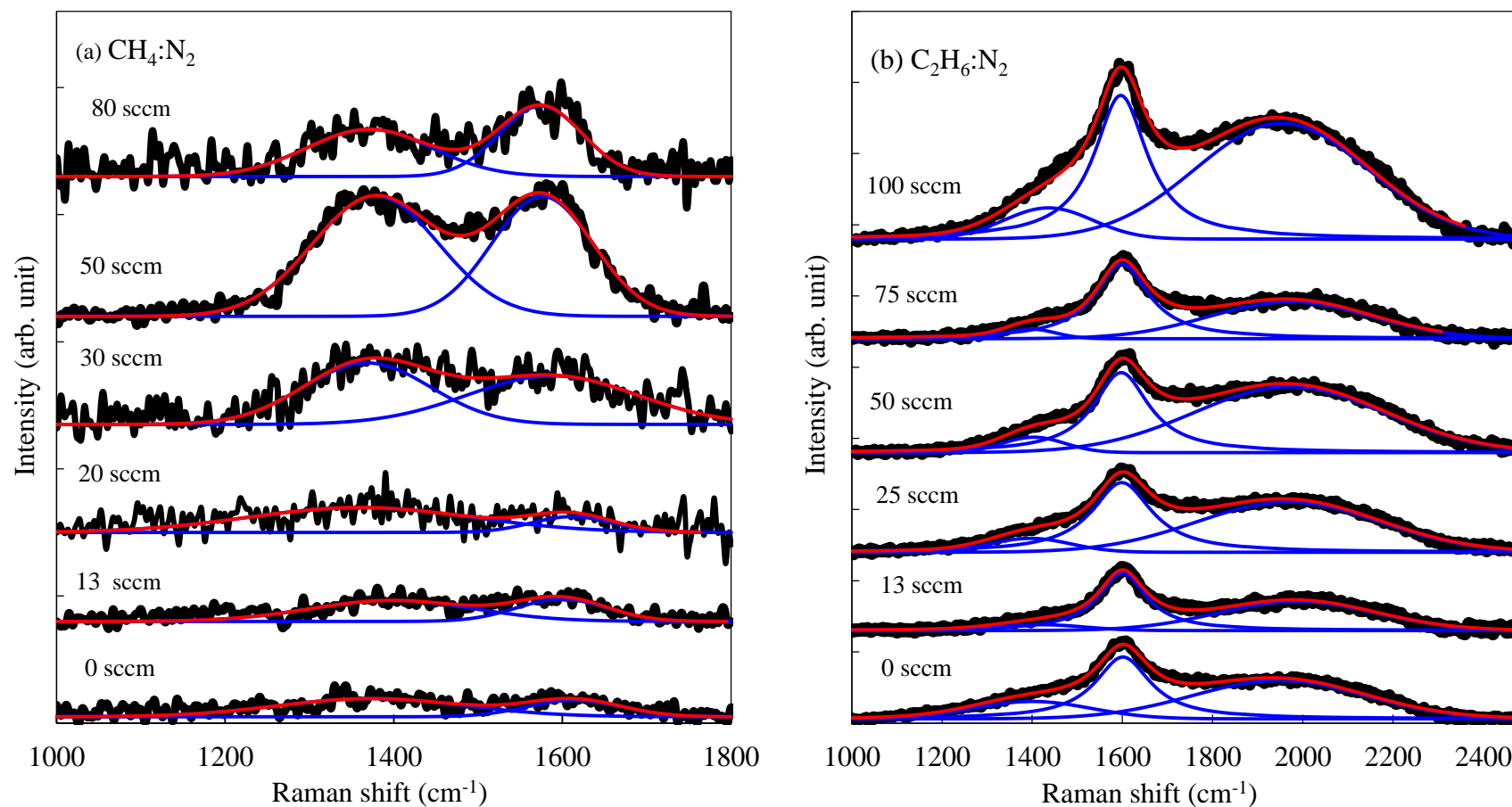


Figure 4.10 Variation in deconvoluted Raman spectra as a function of N_2 flow rate using (a) CH_4 and (b) C_2H_6

The variation in the I_D/I_G and G peak position for films deposited using $\text{CH}_4:\text{N}_2$ and $\text{C}_2\text{H}_6:\text{N}_2$ are presented in Figure 4.11 and 4.13, respectively. Using the deconvolution method, the uncertainty in the value of peak positions from the fitting procedure was smaller than 1 cm^{-1} (Neuhaeuser, Hilgers, Joeris, White, & Windeln, 2000). While D peak indicates the structure order of films, the G peak is related exclusively to bond stretching of sp^2 pairs (Ferrari & Robertson, 2000). The G mode occurs at all sp^2 sites in aromatic and olefinic molecules, not only those in rings. The D peak becomes active in the presence of disordered but is prohibited in perfect graphite. With reference to the ‘three stage model’ described by Ferarri (Chapter 2), the variation and trend of the Raman parameter indicate that these films fall under the category of the second stage of the model which characterized these films as amorphous. Indeed the spectra obtained is similar to those reported by Chu and Li for amorphous and nanocrystalline carbon (*nc-C*) films (Chu & Li, 2006). The three stage model normally used to characterize C films could be adopted for CN_x films since there are no direct contributions of CN or NH vibration to Raman spectra (Escobar-Alarcón, Arrieta, Camps, Romero, & Camacho-Lopez, 2005; Rodil, Ferrari, Robertson, & Milne, 2001).

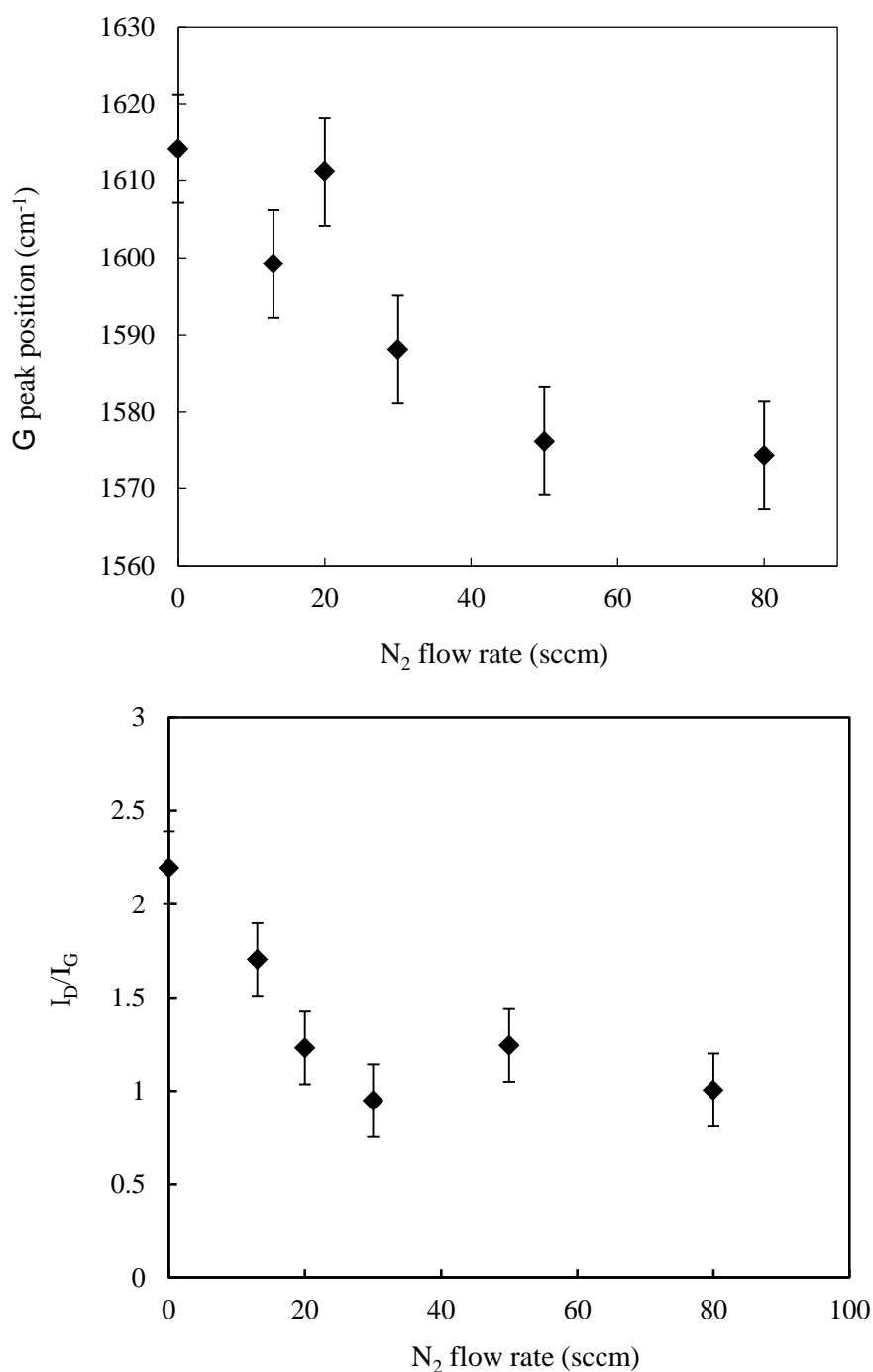


Figure 4.11 Variation in Raman G peak position and I_D/I_G as a function of nitrogen flow rate for film deposited from $CH_4:N_2$.

As seen in the Figure 4.11 for films deposited using $CH_4:N_2$, the G peak position was blue shifted from approximately 1610 to 1570 cm^{-1} with the increase in N content. Such decrease in the G peak position has also been observed by others (Beeman, Silverman, Lynds, & Anderson, 1984; Y. Wang, Alsmeyer, & McCreery, 1990; Wei,

Zhang, & Johnson, 1998). They attributed the shift to an increase in bond structure disorder and/or an increase of sp^3 content. The presence of sp^3 sites result from a distortion of sixfold rings in the carbon network (Beeman, et al., 1984). In this case, the D peak is closely related to the probability of finding ordered six-fold rings in the films (Ferrari & Robertson, 2000). The I_D/I_G also decreases with the increase in N_2 flow rates. This indicates a decrease in the number of ordered ring which leads to the formation of more disordered films with more sp^2 -C bonds making up distorted or rings of other orders (non-sixfold rings). However, it is important to stress that the values of I_D/I_G for these films are above 1.0. With reference to the three stage model, these films follow the amorphization trajectory (Figure 4.12) though at low N_2 flow rate the high I_D/I_G indicates characteristic which is close to that of nc-graphitic structure. It is seen that with the increase in N_2 flow rate that the amorphization of the films occurs.

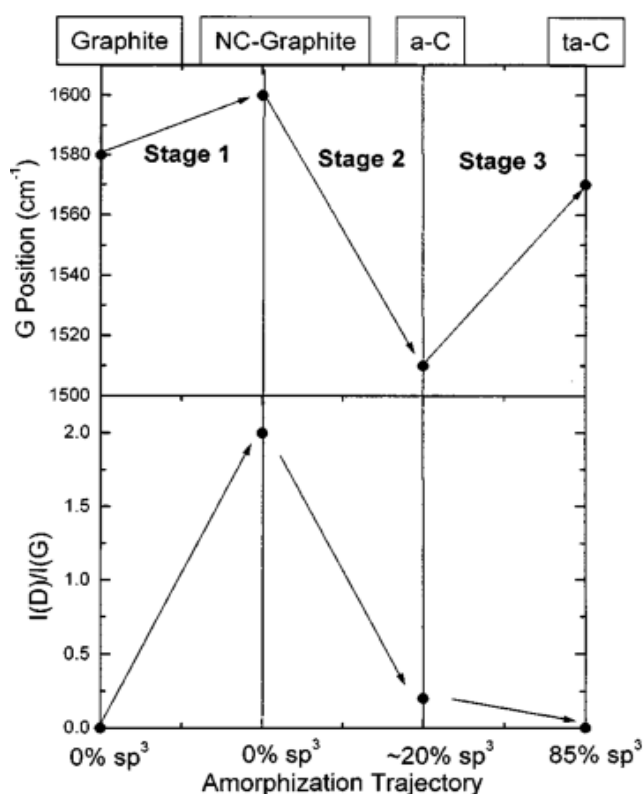


Figure 4.12 A schematic variation of the G peak position and I_D/I_G ratio as a function of amorphization trajectory at three different stages (Ferrari & Robertson, 2000).

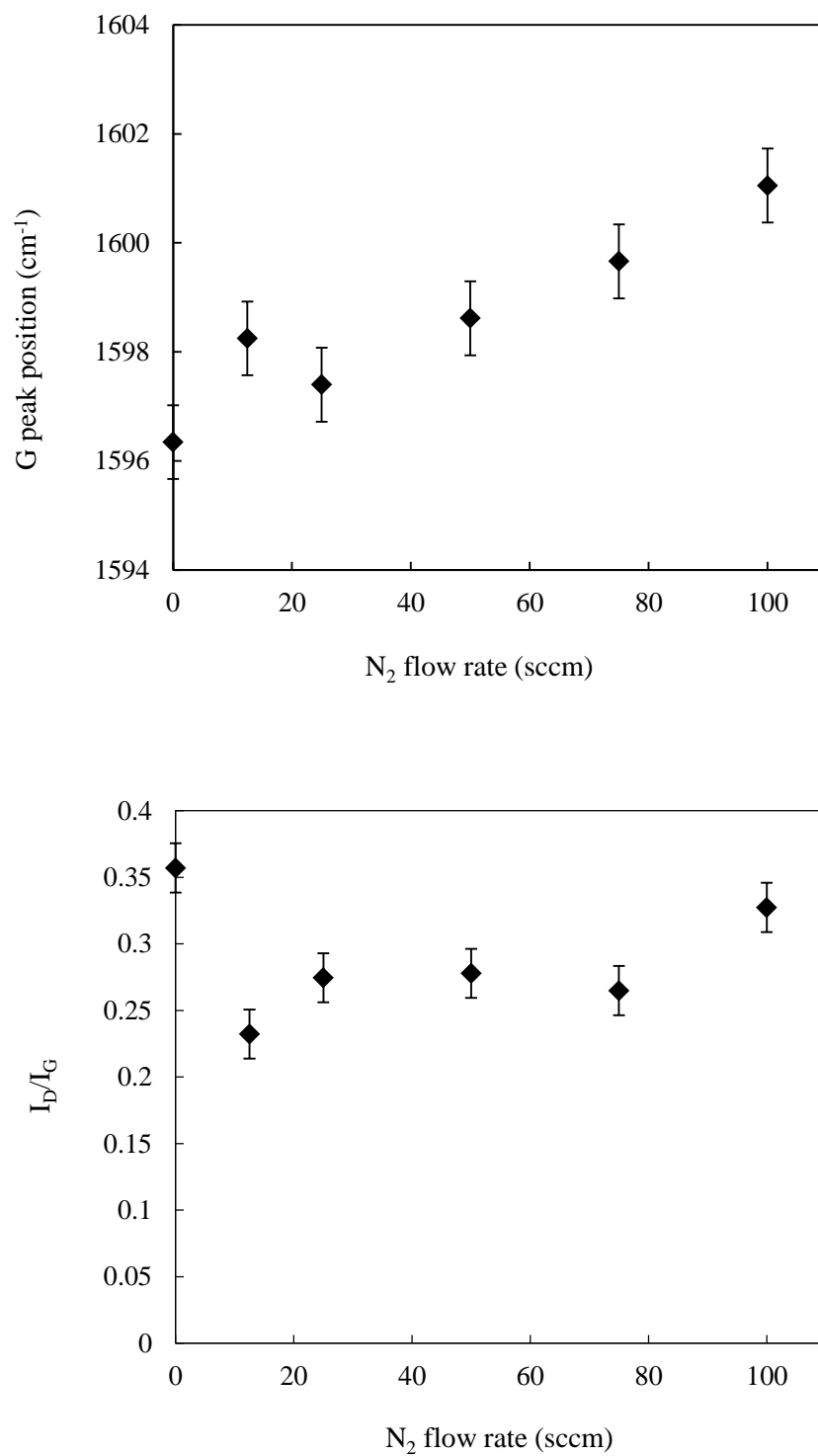


Figure 4.13 Variation in Raman G peak position and I_D/I_G as a function of N_2 flow rate for films deposited from $C_2H_6:N_2$.

In contrast to those of $\text{CH}_4:\text{N}_2$, the films deposited using $\text{C}_2\text{H}_6:\text{N}_2$ shows the opposite trend in the G peak position and I_D/I_G as can be seen in Figure 4.13. The G peak red shifted from wavenumber of approximately 1596 to 1601 cm^{-1} with the increase in N_2 flow rate. This indicates an increase in the presence of sixfold rings and decrease in the bond bending disorder (Ferrari & Robertson, 2000). The increase in I_D/I_G also reflects the formation of more ordered films. The differences between the Raman results for films deposited from $\text{CH}_4:\text{N}_2$ and $\text{C}_2\text{H}_6:\text{N}_2$ indicate changes in the trajectory's direction. While those of $\text{CH}_4:\text{N}_2$ follows the amorphization trajectory, with the increase in N_2 flow rate the films produced from $\text{C}_2\text{H}_6:\text{N}_2$ follows the opposite direction in what is called ordering trajectory. The difference is attributed to the preferential clustering of sp^2 sites into fairly ordered aromatic rings in films produce from $\text{C}_2\text{H}_6:\text{N}_2$ with the incorporation of N. At this point, it is well known that N incorporation strongly influence the ordering of the films structures and with the use of $\text{C}_2\text{H}_6:\text{N}_2$ films with ordered aromatic rings are preferred.

As mentioned earlier, the PL background in visible Raman spectra is related to H bonds in the films. A good correlation is obtained between the amount of H and the slope of the photoluminescence (PL) background is seen for these spectra. Figures 4.8 and 4.9 show the variation of slopes calculated from the PL background at different N_2 flow rate for films deposited from $\text{CH}_4:\text{N}_2$ and $\text{C}_2\text{H}_6:\text{N}_2$ respectively. The relationship between H bonding and PL emission results from H saturation of non-radiative recombination centres (Casiraghi, Piazza, Ferrari, Grambole, & Robertson, 2005; Robertson, 1996) in the films. Thus, with the increase in H content and hence the radiative recombination centres, the PL emission also increases resulting in the increase in the slope of the baseline of the Raman spectra. The H bonded content in unit of a.t%, was measured from the fraction of the slope (m) of the fitted linear background and the

intensity of the G peak (I_G), m/I_G as proposed by Ferrari (Casiraghi, Ferrari, & Robertson, 2005; Ferrari & Robertson, 2000). Note that the formula indicates that H content is not only dependent on the slope but also the value of I_G .

In term of the slopes, the spectra for the films produced from $\text{CH}_4:\text{N}_2$ shows values which are more erratic than those of $\text{C}_2\text{H}_6:\text{N}_2$. For $\text{C}_2\text{H}_6:\text{N}_2$, the slopes decreases with the increase in N_2 flow rate but in general is much higher than for films deposited from $\text{CH}_4:\text{N}_2$. Thus, the H content is also believed to be higher in the films formed from $\text{C}_2\text{H}_6:\text{N}_2$ than those of $\text{CH}_4:\text{N}_2$. These H atoms are believed to be bonded as C-H bonds which from FTIR was seen to be significantly higher in films produced from $\text{C}_2\text{H}_6:\text{N}_2$. Furthermore, since N was seen from AES incorporate better in films produced from $\text{CH}_4:\text{N}_2$, its lower H content is expected.

This is supported by the H content calculated from m/I_G . Figure 4.14 shows the variation in H content as a function of N_2 flow rate. For the films produced from $\text{CH}_4:\text{N}_2$, the H content decreased with the increase in N_2 flow rate up to 30 sccm and then remains almost constant with further increase in flow rate. A similar trend is seen for the films prepared from $\text{C}_2\text{H}_6:\text{N}_2$. However, in line with the previous argument these films show a much higher percentage of H content as compared to those $\text{CH}_4:\text{N}_2$ films. The reduction in H content with the increased in N_2 flow rate is due to the replacement of the H atom with N in the films with the N enrichment (Rodil, et al., 2001; C. Wang, Yang, & Zhang, 2008). The decrease in H bonds also leads to the loss of sp^3 sites due to structural rearrangement in the films with N incorporation. Indeed, N incorporation would induce the formation of sp^2 clustering in such films. However, with regard to the H values both films shows relatively high content which still categorized them as amorphous.

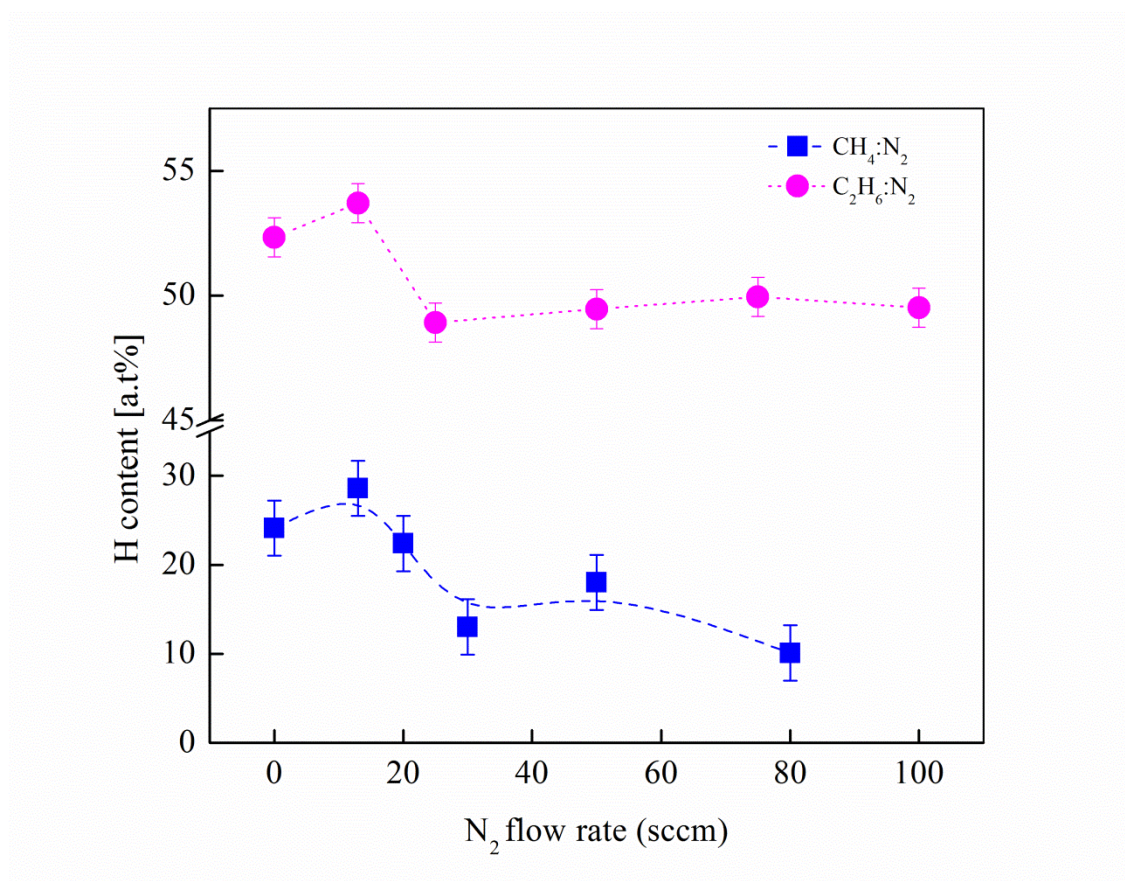


Figure 4.14 Variation in H content as a function of N₂ flow rate.

4.2.5 Ultra-violet Visible Near Infra-red Spectroscopy

The optical absorption coefficients were calculated from the optical transmittance and reflectance spectra of the films. Figure 4.15 shows the variation in energy gap (E_g) as a function of N dilution. For the films produced using $\text{CH}_4:\text{N}_2$, the E_g decreases from approximately 2.2 to 1.7 eV when the N dilution increases up to 50 sccm. The E_g is then shows significant increase up to 2.4 eV with further increase in dilution. The decrease E_g with the increase in N_2 flow rates coincides with the increase in N incorporation as shown by AES results. This relationship is also reported by other researchers (Kleinsorge et al., 2000; Veerasamy et al., 1993; Walters, Kühn, Spaeth, Dooryhee, & Newport, 1998) and they attributed this to the presence of N inclusions that act as bridging atoms between sp^2 clusters (Mariotto, Freire Jr, & Achete, 1994). This in turn increases the size of these clusters, broadening the associating π and π^* states (Ilie et al., 2000; Robertson & Davis, 1995) and decreases the E_g .

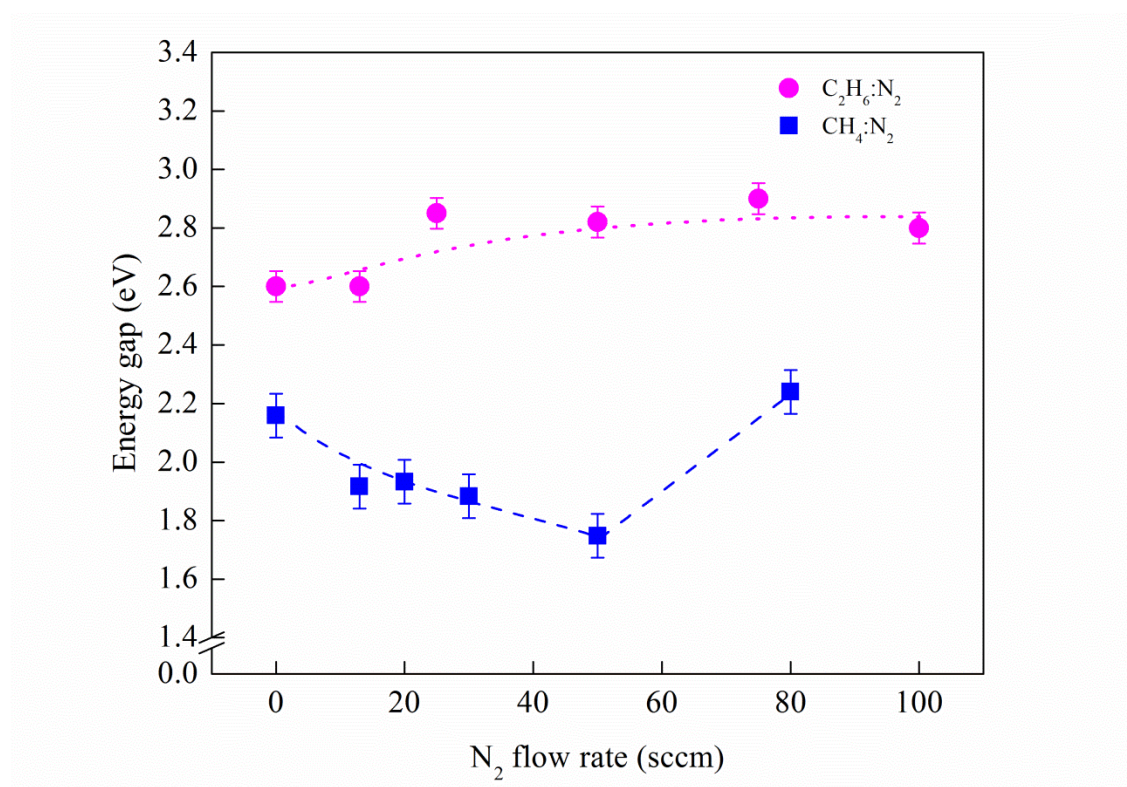


Figure 4.15 Variation in energy gap as a function of N_2 flow rate.

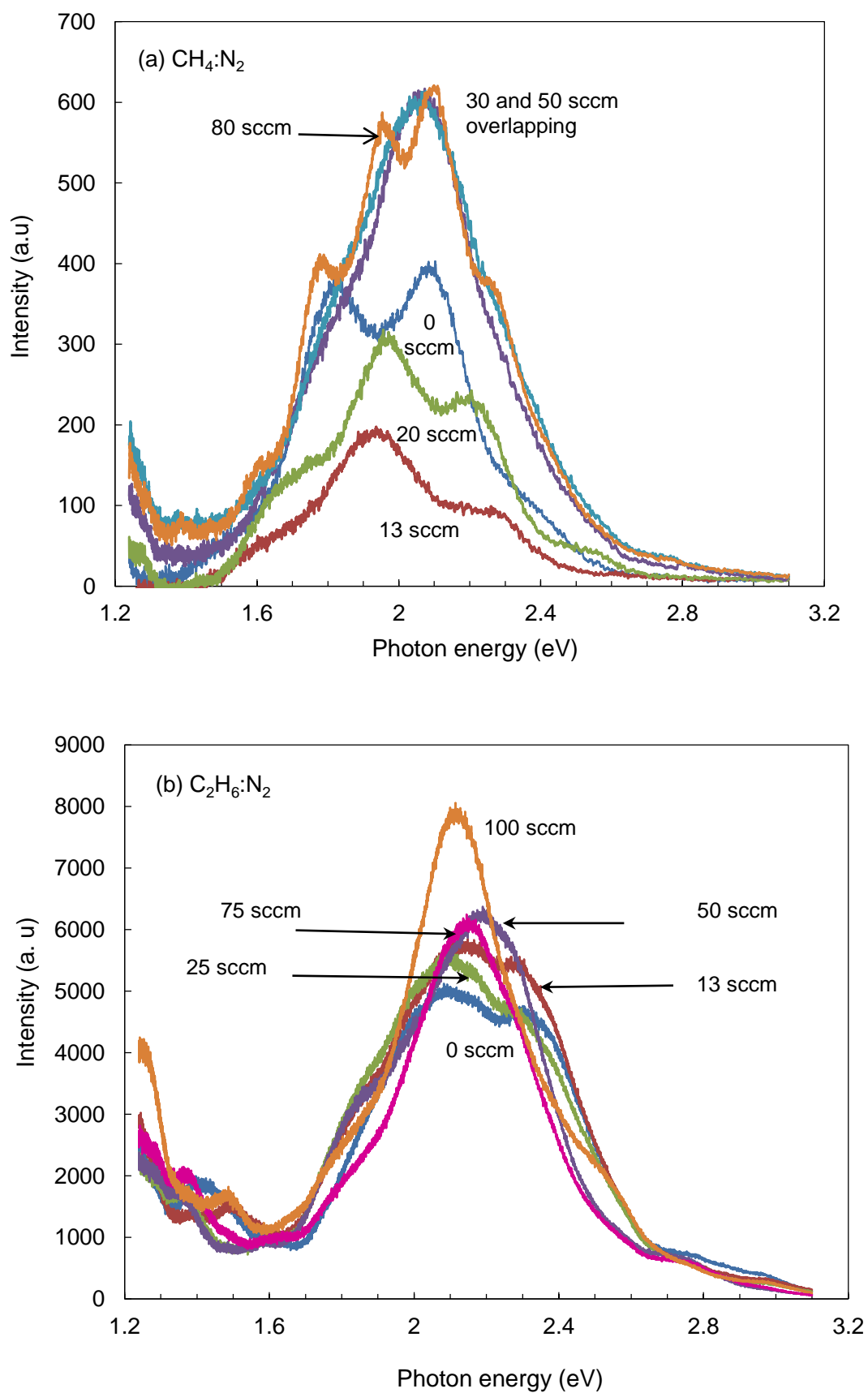
The sudden increased in E_g at 80 sccm may be due to the stabilizing effect of the sp^3 -hybridized C atom (Hellgren, Johansson, Broitman, Hultman, & Sundgren, 1999; Yap, Kida, Aoyama, Mori, & Sasaki, 1998) with further increase in N incorporation. In comparison, the films deposited using $C_2H_6:N_2$ generally exhibit higher E_g compared to those of $CH_4:N_2$. This coincides with the lower N incorporation observed from AES spectra of the former. Moreover, in line with the N/C ratio of these films, their E_g remains almost constant with the variation in N_2 flow rates. The high H content in the films keeps the sp^2 cluster size small and thus produces larger band gap.

The higher energy gap exhibited by the films produced from $C_2H_6:N_2$ in the range of 2 to 4 eV, together with their high H content at approximately 40 to 60 a.t %, classifies these films as polymeric-like $a-CN_x$ (Casiraghi, Ferrari, & Robertson, 2005; Robertson, 2002). On the other hand, the films produced from $CH_4:N_2$ shows lower band gap between approximately 1 and 2 eV, with intermediate H content in the range of 20 to 40 a.t % would identify them as graphite-like $a-CN_x$. These graphitic structure of films have lower overall sp^3 bonds which preferentially bonds as sp^3 C-C compared to the polymeric films, leading to have better mechanical properties (Robertson, 2002).

4.2.6 Photoluminescence

Figure 4.16 shows the PL spectra for both sets of samples as a function of N₂ flow rate. Both sets of spectra show broad strong PL emission peaks within the range of approximately 1.4 to 2.8 eV which corresponds to the wide visible region of approximately 440 to 885 nm. For further analysis these spectra were deconvoluted and shown in stacking progression as shown in Figure 4.17.

For the films produced from CH₄:N₂ there appears to be significant difference between the film produced from pure CH₄ and those with N incorporation. The film produced from pure CH₄ shows two strong peaks centered at approximately 1.8 ± 0.02 and $2.1 \text{ eV} \pm 0.01$ with two small shoulder peaks. With N₂ inclusion even with N₂ flow rate as low as 13 sccm a shift in the most prominent intensity is seen. The films produced at N₂ flow rate of 13 and 20 sccm show three emission peaks with the highest intensity emitted at photon energy centered at approximately 1.95 ± 0.02 eV and with shoulder peaks centered at approximately 1.70 ± 0.04 and 2.20 ± 0.02 eV. These peaks shift slightly with the increase in N incorporation at N₂ flow rate of 30 and 50 sccm. However, they still show three prominent peaks which shift slightly to 2.05 ± 0.02 eV for the highest intensity and 1.80 ± 0.02 eV and 2.30 ± 0.03 for the shoulder peaks. On the other hand, the film produced at the highest N₂ ratio of 80 sccm shows drastic change whereby the spectrum was composed of four prominent PL emission peaks. These are centered at 2.10 ± 0.02 eV for the most prominent peak and 1.94 ± 0.02 , 1.77 ± 0.03 and 2.40 ± 0.02 eV for the shoulder peaks listed in decreasing intensities.

Figure 4.16 Variation on PL spectra as a function of N_2 flow rate.

These PL emissions originate from the recombination of electrons and holes pairs at discrete radiative recombination centres within the energy level in the materials. The changes in this emission are subjected to the changes in these recombination centres which in turn are dependent on the bonding and structural characteristic of the film. Though the Raman and FTIR analysis may not reveal minute changes in the structure, these PL results indicate that there are slight changes in the structure of the films. This is seen particularly in the shift of the PL emission peaks from N₂ flow rate of 20 to 30 sccm and also at 50 to 80 sccm.

The variations in the PL intensities of the average energies of these deconvoluted peaks as a function of N₂ flow rate are shown in Figure 4.18 (a). In general, the intensity increases with N incorporation and is in line with the role of N incorporation in inducing the formation of sp² clusters in CN_x films. The most accepted model in the explanation of the relationship between sp² clusters and PL emission is the recombination of electron-hole pairs within sp² bonded clusters in the sp³ bonded amorphous matrix (Panwar et al., 2006). The sp³ bonded regions create a potential barrier which confines the π states of the sp² clusters. This result in the formation of highly localized sites which creates the π tail states and act as radiative recombination centers. Photo carriers can recombine inside the clusters themselves by phonon emission (Gharbi, Fathallah, Alzaied, Tresso, & Tagliaferro, 2008) and this produces PL emission. Thus the cluster size and distribution also affects the PL intensity. In this sense, N incorporation may help the increase in PL emission both in intensity and efficiency. N incorporation induces the formation of sp² clustering in the films and this increases the density of states within the π and π^* tails state. This in turn increases the radiative recombination centres for high PL emission. Apart from that, N incorporation also promotes formation of lone pairs through sp¹ C \equiv N bonds and this too has been

speculated to increase the radiative recombination centres in the films. Another contributing aspect could be the presence of O-H which is said to also contribute to the formation of lone pairs and decrease the stress in the material (Gharbi, et al., 2008). However, the effect of O-H on the PL emission is arguable since it has been said that its presence either increase radiative or non-radiative recombination centre which either increases or quenches PL emission (Fanchini, Ray, & Tagliaferro, 2003; Fanchini, Ray, Tagliaferro, & Laurenti, 2002).

The PL emission spectra of the films produced from $C_2H_6:N_2$ are different from those obtained from $CH_4:N_2$. The films produced from pure C_2H_6 show two prominent peaks at approximately 2.04 ± 0.02 and 2.36 ± 0.02 eV. Even with N_2 dilution these peaks do not vary significantly both in position and in width. This may be due to the low N incorporation in this set of film as supported by AES analysis. In this sense the incorporation of N into the C network might not significantly alter its recombination centres. The increase in the highest PL emission peak with the increase in N_2 flow rate as depicted in Figure 4.18 (b) is in line with the increase in the C=N content observed from FTIR analysis. This effectively increases the sp^2 clusters size due to the increase in the C=N bonds. Since the PL peak emission does not change, the increase in these clusters may only increase the efficiency of the recombination centres which corresponds to these peaks.

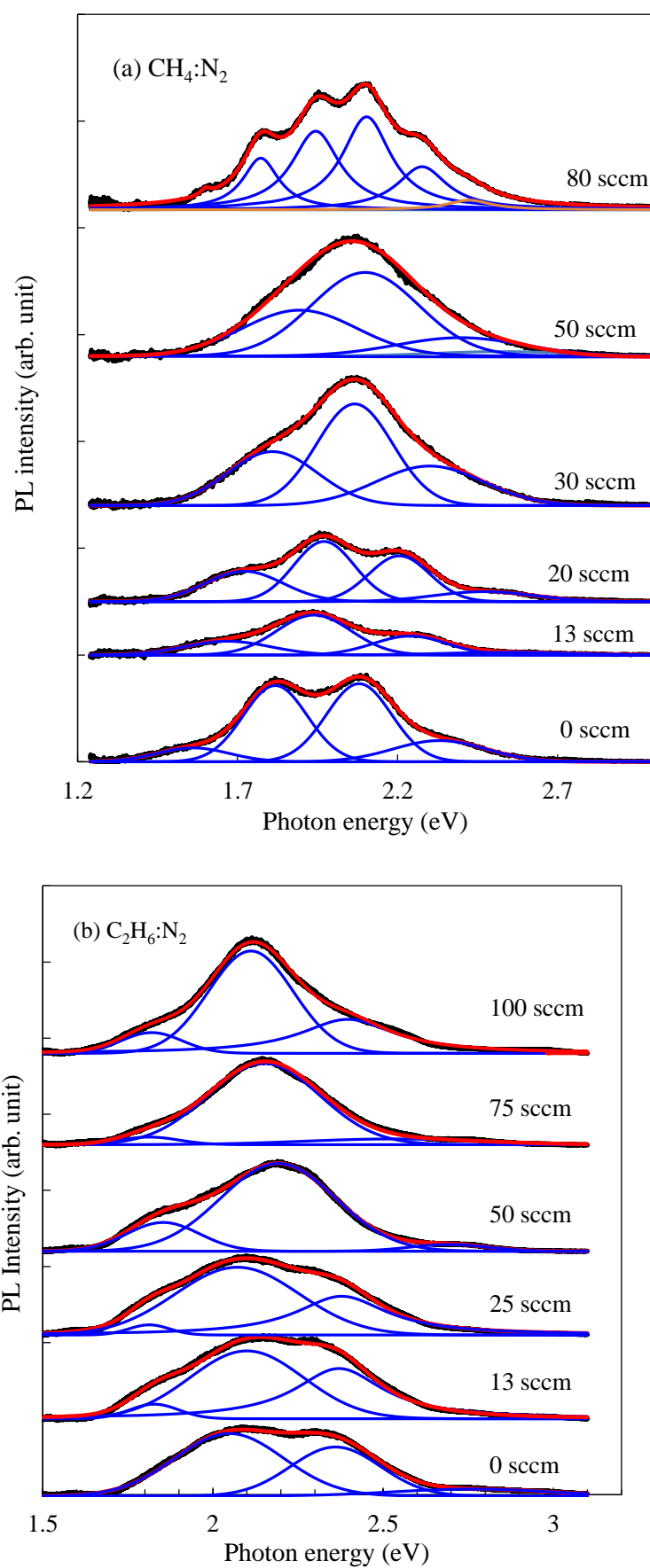


Figure 4.17 Gaussian fitting of PL spectra as a function of N_2 flow rate for a) CH_4 and b) C_2H_6 . The black line shows the cumulative fitting curve due to the best fit.

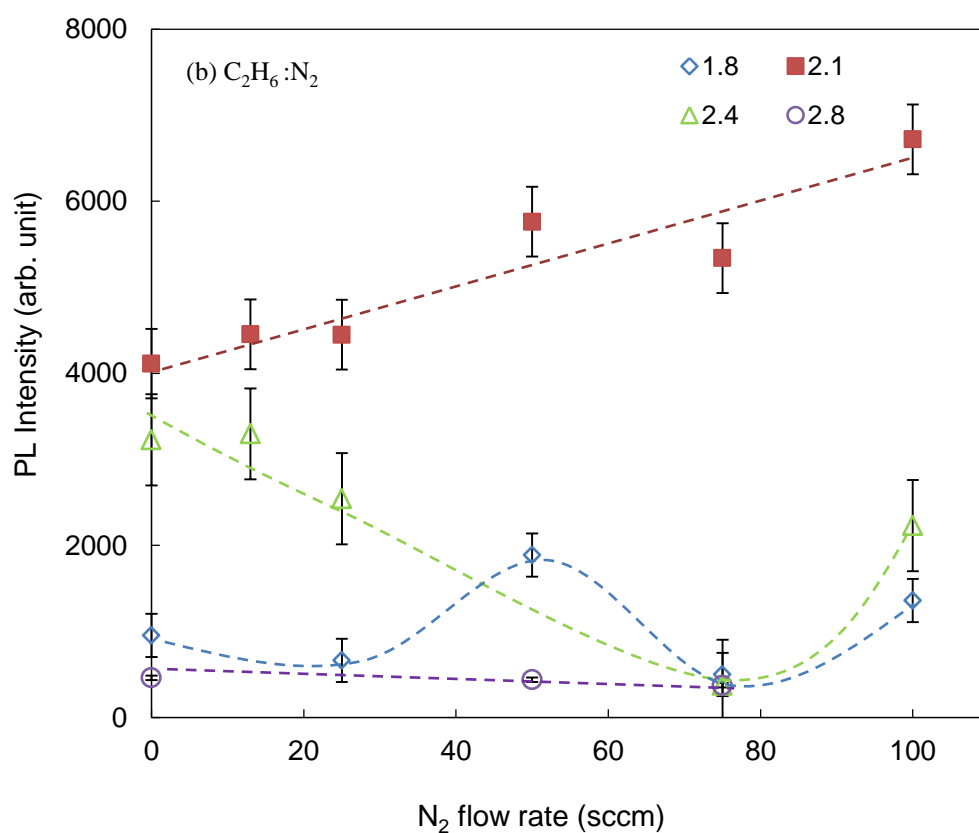
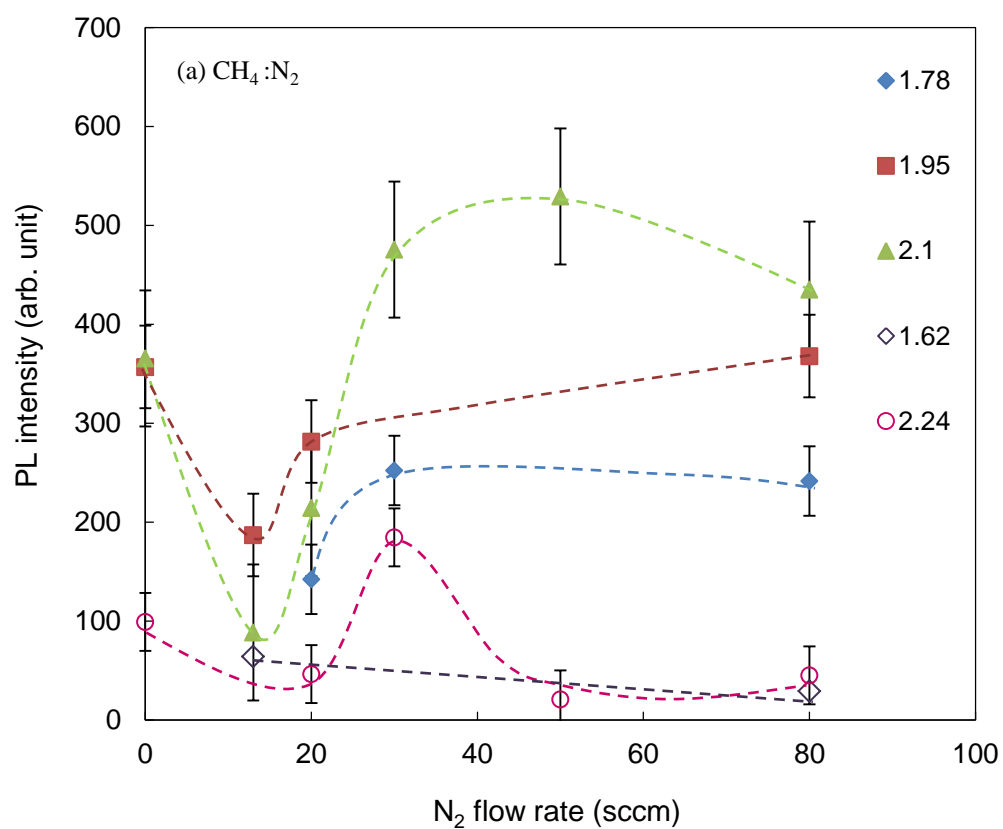


Figure 4.18 Variation in integrated PL intensities as a function of N_2 flow rate. Line is drawn as guide for eye.

It was also observed that the PL emission intensity for the films produced from $\text{C}_2\text{H}_6:\text{N}_2$ is almost ten times the value of the intensity of the films produce from $\text{CH}_4:\text{N}_2$. This is true even for the films produced from pure C_2H_6 as shown in Figure 4.19. When considering their FTIR and Raman results, this indicates that the increase may not be due to the N incorporation or the presence of O-H in the films. Instead it is believed that the H content and the structure of the films may play an important role. As the films produced from pure C_2H_6 and $\text{C}_2\text{H}_6:\text{N}_2$ shows high H content (48-55%) and are polymeric like, PL characteristic may be elevated by these characteristic rather than the graphite-like characteristic of the films produced from pure CH_4 and $\text{CH}_4:\text{N}_2$. Nevertheless, it is noted that N incorporation does increase PL emission in both sets of films due to its role in inducing the formation of sp^2 clustering.

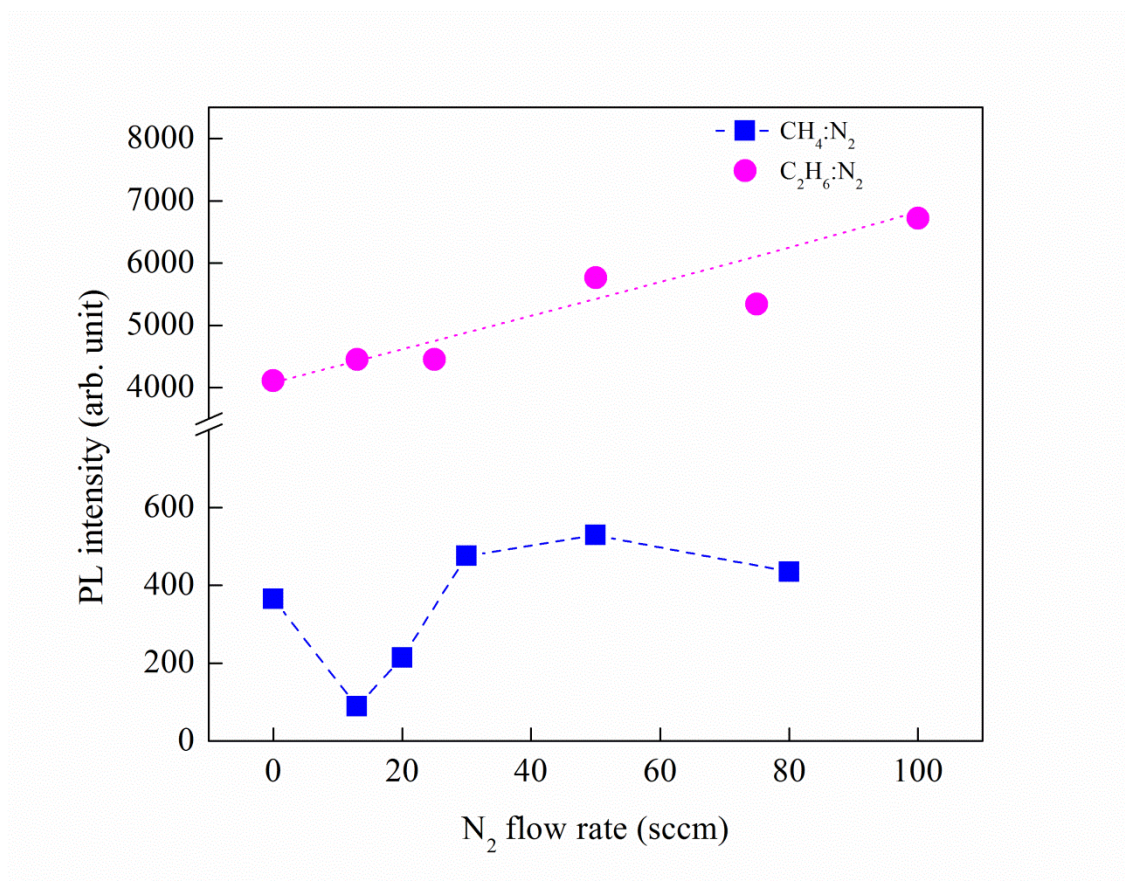


Figure 4.19 Variation in integrated PL intensities as a function of N_2 flow rate. Line is drawn as guide for eye.

4.3 Effects of Hydrogen Dilution on the Properties of Amorphous Carbon Nitride Films

In this part, hydrogen (H_2) gas was introduced into the C_2H_6 and N_2 gas mixture to study the effects of H_2 dilution on the properties of CN_x films. The C_2H_6 and N_2 flow rate were kept constant at 25 and 100 sccm. These flow rates were chosen as the film gives the highest PL emission intensity. H_2 dilution was carried out by introducing H_2 gas into this mixture in the flow rate range of 25 to 125 sccm. The resulting films were studied to determine the growth rate, chemical composition and bonding, structural characteristic, optical and PL properties of the films.

4.3.1 Growth Rate

Figure 4.20 shows the variation in films growth rate produced from $C_2H_6:N_2:H_2$ as a function of H_2 flow rate. The growth rate was calculated by dividing the films thickness with the deposition duration. The growth rate of the film produced without H_2 dilution that is from $C_2H_6:N_2$ was relatively low at approximately 5.7 ± 0.2 nm/min. With the initial introduction of H_2 into the gas mixture at as low as 25 sccm, a significant increase in growth rate is seen. The growth rate of the latter is almost three times higher than that of the former. The growth rate of the films produced from $C_2H_6:N_2:H_2$, then decreases almost linearly with further increase in H_2 flow rate.

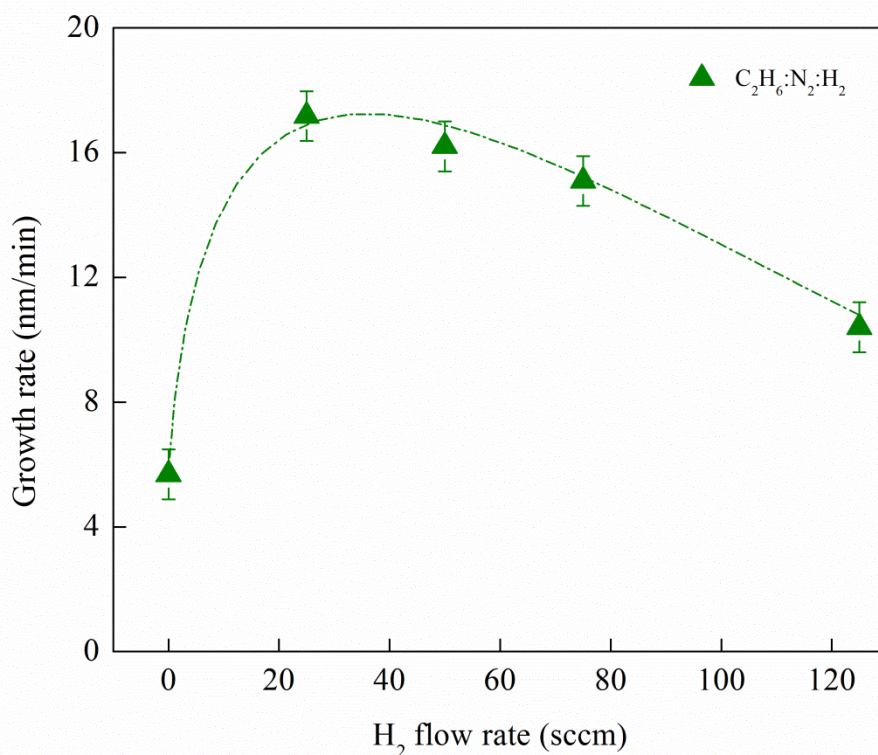


Figure 4.20 Variation in growth rate with H₂ flow rate. Line is as guide to the eye.

A possible explanation for the trend in the growth rate involves the role of H ions in the plasma. With the introduction of the H₂ dilution, the primary and secondary reaction together with the formation of the surface radical sites predominate the reaction in the plasma and deposition kinetics. By looking at the reaction in the first part of this study proposed by Legrand (Legrand, Damiy, Hrach, & Hrachová, 1999), the partial pressure of C₂H₆ is reduced at high N₂ flow rate resulting in lower concentration of H atoms in the secondary gas phase reaction and slower the formation of CH₃ radicals thus reduce the growth rate. In the initial introduction of the H₂ dilution, the activation of H₂ gas by the rf power would accelerate the formation of CH₃ radicals and leads to the increase in the film growth. The H ions radicals could also extract H from the films or substrate surface which forms surface radical sites. Though these sites could be re-terminate by the recombination of H atoms, occasionally some hydrocarbon radicals

could react with the sites. The latter results in chemisorption of the hydrocarbon species which result in increase in the films growth.

Although the increase of available H ions radicals would also increase the formation of hydrocarbon radicals and surface radical sites, with further increase in H_2 flow rate, the partial pressure of C_2H_6 in the mixture of $C_2H_6:N_2:H_2$ would decrease direct proportionate to the increase in H_2 flow rate. This is because the total pressure of the deposition was kept constant for all depositions. With the decrease C_2H_6 partial pressure, the available hydrocarbon species generated also decreases leading to the decrease in films deposition.

Another interesting aspect of the growth rate of these films could be seen when the trend in the growth rate of the films produced from $C_2H_6:N_2:H_2$ is compared with those of films produced from $CH_4:N_2$ and $C_2H_6:N_2$. This is shown in Figure 4.21. Note the difference in the axis and corresponding referencial trend. It is seen that while the growth rate of all three sets of films decreases at high N_2 or H_2 flow rate, the H_2 dilution of $C_2H_6:N_2:H_2$ genarally increase the relative growth rate of the resulting CN_x films. This shows the significant effects of H_2 dilution on the growth of the films and solves the disadvantage of the low growth rate of the films produced from $C_2H_6:N_2$ as compared to those produced from $CH_4:N_2$. The next question to be solved is whether the advantages of the structure and high PL emission of the former are sustained.

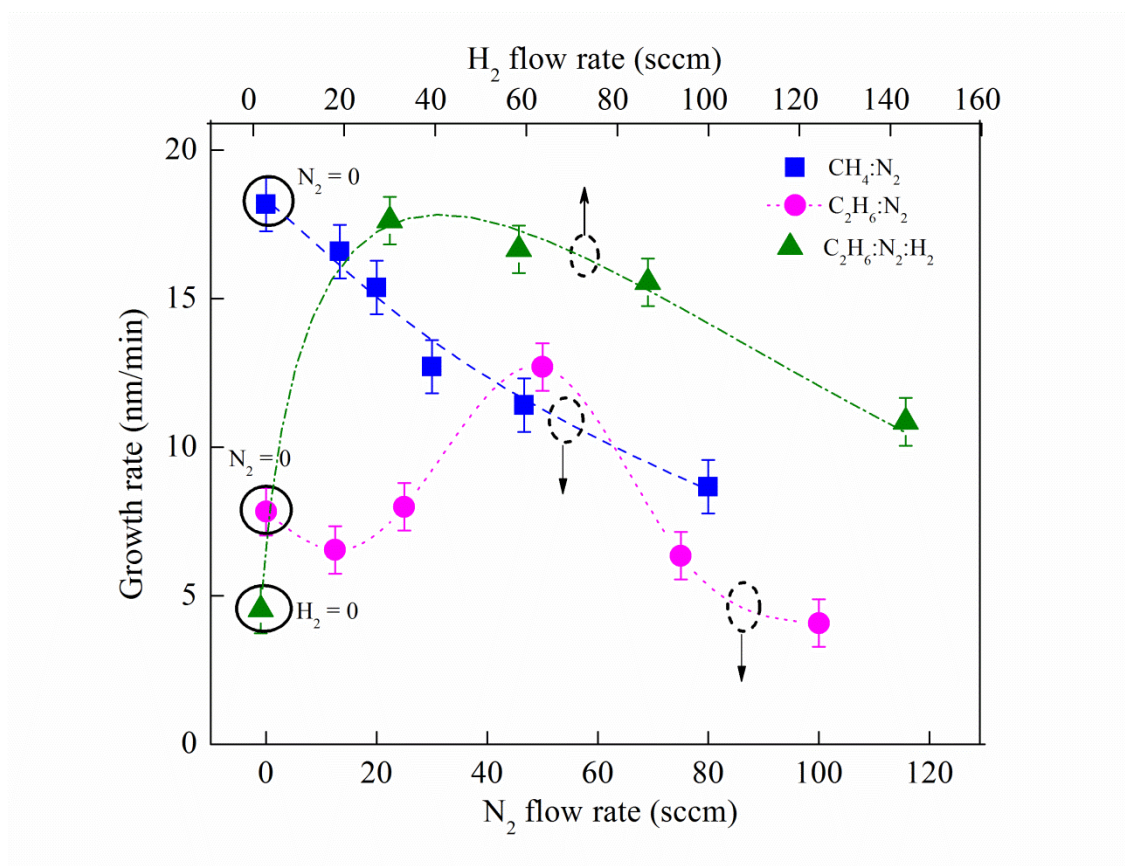


Figure 4.21 Variation of deposition rate with different flow rate of N₂ without inclusion of H₂ using CH₄ or C₂H₆, and deposition rate of CN_x with different flow rate of H₂ gas with a mixture of C₂H₆ and N₂. Line is as guide to the eye.

4.3.2 Auger Electron Spectroscopy

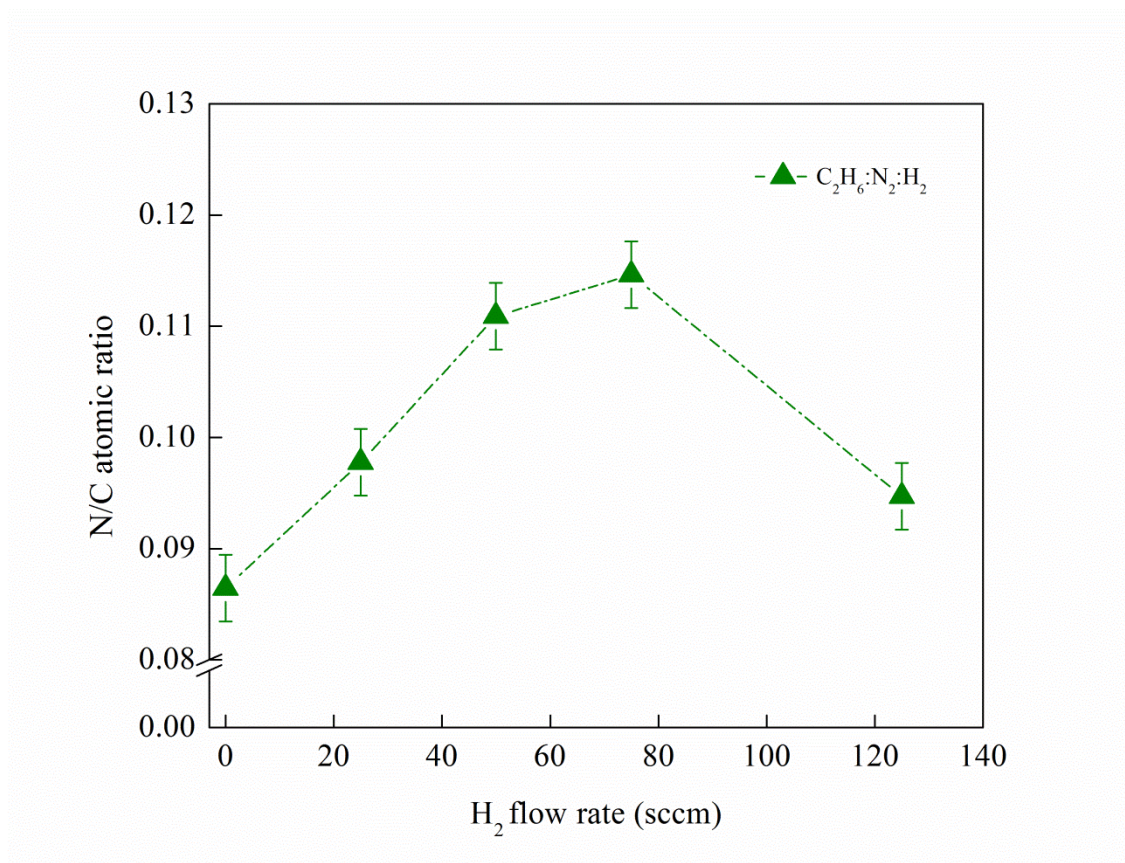


Figure 4.22 Variation of nitrogen to carbon N/C ratio as a function of H₂ flow rate. Line is as guide to the eye.

Figure 4.22 shows the variation in N/C ratio of CN_x films produced from C₂H₆:N₂:H₂ as a function of H₂ flow rate. N/C increased almost linearly with the increase in H₂ flow rate up to 75 sccm, and then decreases with the further increase in H₂ flow. The increase in N/C ratio and thus the N incorporation is attributed to the etching of H radicals on the film surface by H ions in the plasma. This increases the surface radical sites through the formation of dangling bonds that allows N and N containing radicals to be chemisorbed into the films. This effectively increases N content in the samples. As H₂ dilution is increased by increasing the flow rate, the generation of H ions increases and thus the etching effect also increases. Owing to this, N/C ratio increases with H₂ flow rate. However, this appears true only up to H₂ flow

rate of 75 sccm which is noted to be lower than the N_2 flow rate used at 100 sccm. Indeed N/C ratio decreases when H_2 flow rate was increased to 125 sccm. It is believed that this is caused by two reasons. Firstly, the high H_2 flow rate suppresses the formation of N containing radicals. N_2 would have to compete with the higher concentrated H_2 gas in the plasma. Secondly, with the high H ion concentration, the etching effects might not only be limited to H bonds but also may effectively breaks N bonds on the film surface. Consequently, H and N may be removed from the film resulting in the graphitization of the film. Graphitization of films with high H_2 dilution in PECVD is in line with the report by other researchers (Xu et al., 2004).

Figure 4.23 compares the N incorporation of the various gas mixtures used in these studies. It is seen that N incorporation of the film produced from $C_2H_6:N_2:H_2$ is still generally lower than the films produced from $CH_4:N_2$. However, they show higher N incorporation than the films produced from just $C_2H_6:N_2$. That is to say that H_2 dilution enhances N incorporation for the films produced from $C_2H_6:N_2$. As suggested above, H_2 dilution increases the formation of surface radical sites and encourages N chemisorption in the films. This shows the potential of increasing of N bonding in films produced from $C_2H_6:N_2$ through H_2 dilution.

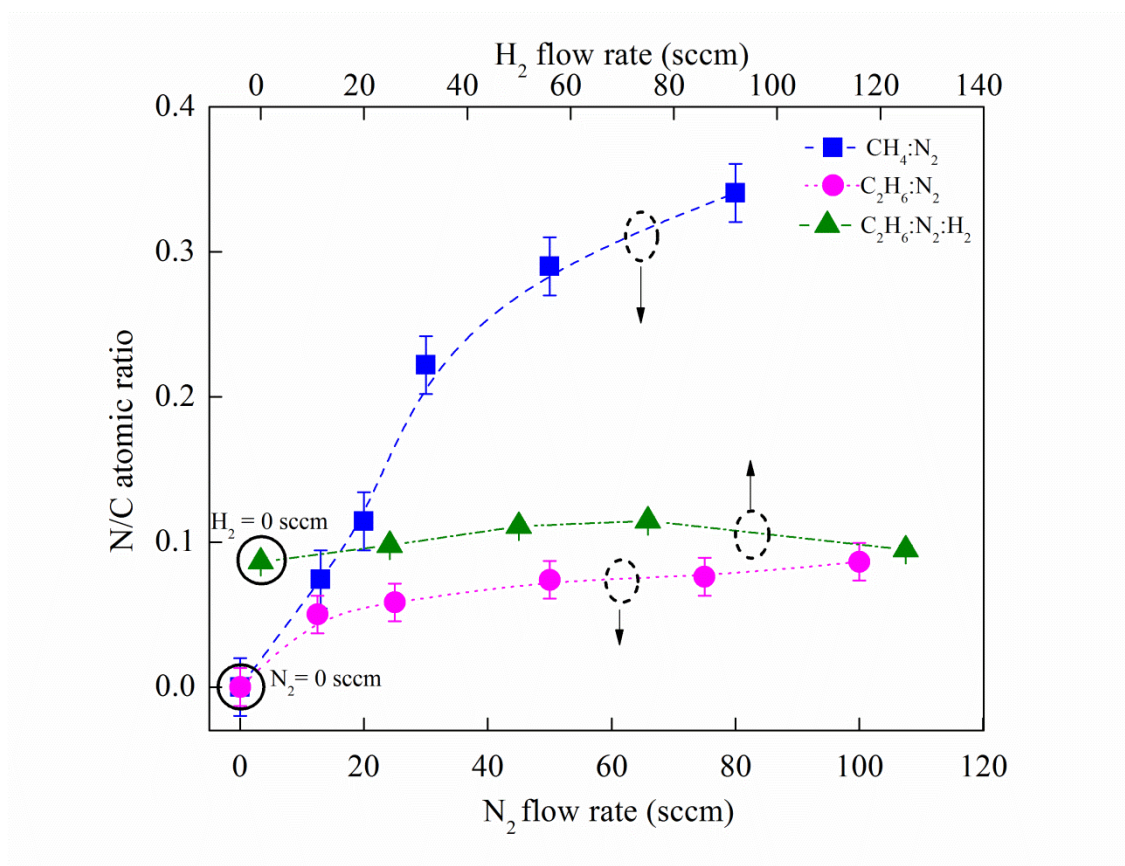


Figure 4.23 Variation in N/C ratio for films deposited as function of flow rate.

4.3.3 Fourier Transform Infrared

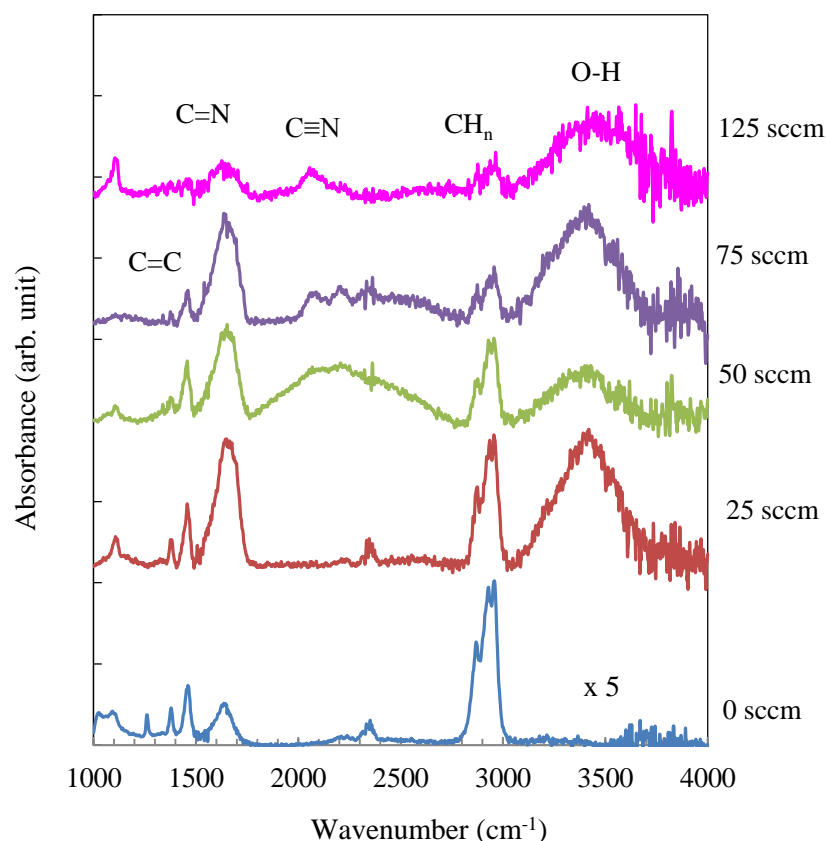


Figure 4.24 Variation in FTIR spectra for $C_2H_6:N_2:H_2$ as a function of H_2 flow rate. The height of the spectrum for film deposited at H_2 flow rate of 0 sccm is adjusted for clarification.

Figure 4.24 shows FTIR spectra of CN_x films prepared from $C_2H_6:N_2:H_2$ as a function of H_2 flow rate. For clearer representation of the changes, these spectra were separated into different region corresponding to the different functional groups as shown in Figure 4.25. Figure 4.25 (a) shows the variation in sp^2 C related bonds. It can be seen that as H_2 flow rate increases, the relative intensities of C=N compare to C=C increases up to H_2 flow rate of 75 sccm. However, both C=C and C=N peaks decreases when H_2 flow rate is increased from 25 to 125 sccm, indicating a general decrease in sp^2 bonds in the films. Figure 4.25 (b) which corresponds to the formation of sp^1 C related

bonds comprising of nitrile and isonitrile $C\equiv N$ bonds also varies with the change in H_2 flow rate. This peak appears for films deposited from the $C_2H_6:N_2:H_2$ with H_2 flow rate of 50 sccm and strengthen as the H_2 flow rate was increased.

Moreover, in contrast to the sp^2 C related bonds, this $C\equiv N$ bonds remain intact even at H_2 flow rate of 125 sccm. Generally it could be said that N related bonds increases for both $C=N$ and $C\equiv N$ bonds up to H_2 flow rate of 75 sccm and at H_2 flow rate of 125 sccm the $C\equiv N$ bonds are preferred. This is in line with the proposed initial increase in N incorporation due to the increase in surface radical sites. Furthermore, the loss of $C=N$ bonds at high H_2 flow rate supports the suggestion that at high H ion concentration, the etching effects also attack the N bonds on the surface. $C\equiv N$ bonds remain at high H_2 flow rate since these are stronger bonds and are harder to break. Moreover, the CH_n bonds shown in figure 4.25 (c) decreases progressively throughout the range of H_2 flow rate used. This further support the selective etching of H bonds on the surface of the film which creates radical sites and allows the incorporation of N into the films. This result strongly supports the variation seen in AES and the films growth rate, and the postulation made in those analysis.

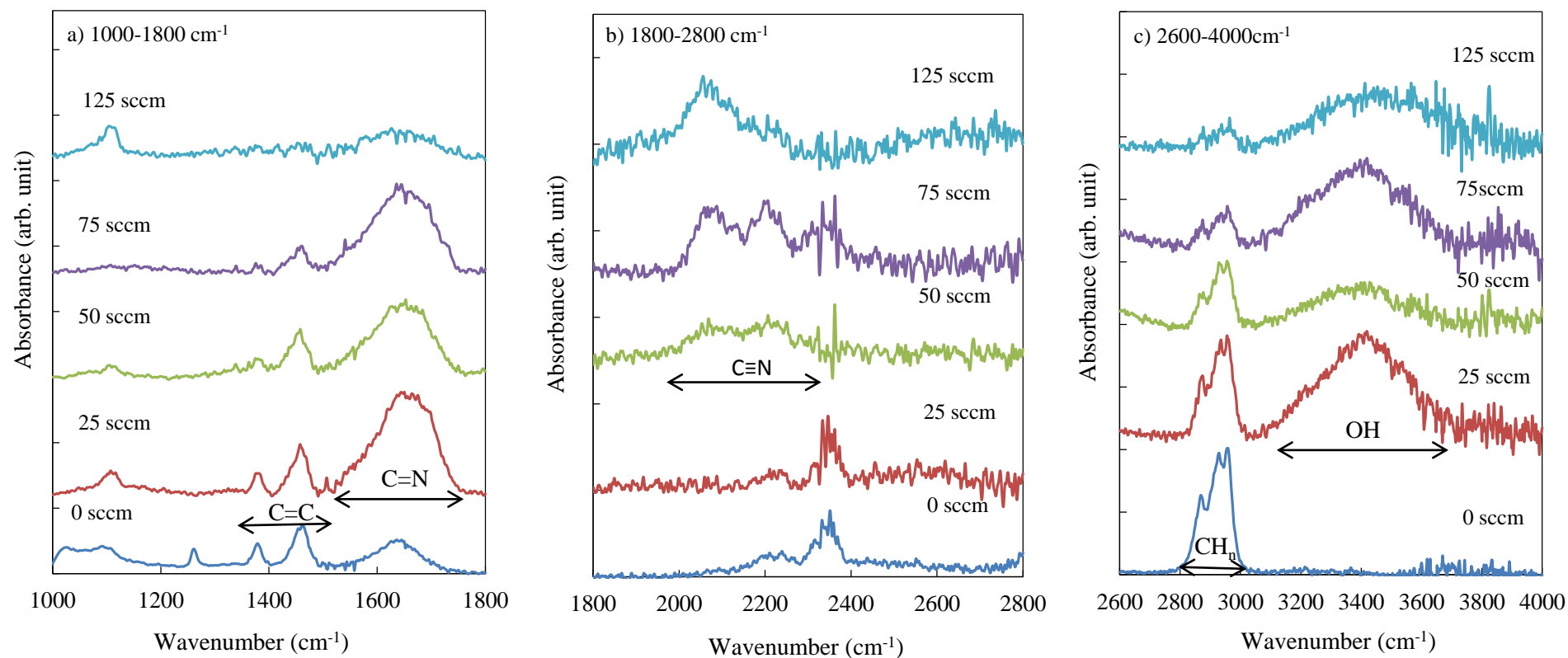


Figure 4.25 Fourier transform infrared spectra of CN_x films prepared from $\text{C}_2\text{H}_6:\text{N}_2:\text{H}_2$ as a function of H_2 flow rate separated into three different spectra range of (a) 1000-1800 cm^{-1} , (b) 1800-2800 cm^{-1} and (c) 2600-4000 cm^{-1} .

On the other hand, a marked difference in the spectra is seen in the appearance of the O-H bonds of the CN_x films when H_2 dilution is introduced. Indeed, from Figure 4.25 (c) the films produced from $\text{C}_2\text{H}_6:\text{N}_2$ (H_2 flow rate of 0 sccm) does not show this peak while all the films deposited from $\text{C}_2\text{H}_6:\text{N}_2:\text{H}_2$ shows strong broad absorption peak within the range of 3100 to 3800 cm^{-1} corresponding to the O-H bonds. This implies a certain similarity with the films produced from $\text{CH}_4:\text{N}_2$ whereby the presence of O-H bonds was attributed to the porosity of the material. It may be that the breaking of H bonds may also result in a structural rearrangement which create a certain degree of disorder and may also leave void within the films. To further explore this, the results of Raman measurements on these films are studied.

In general, these FTIR results show that with the increase in H_2 dilution the films produced from $\text{C}_2\text{H}_6:\text{N}_2:\text{H}_2$, a mark decrease in sp^2 -C bonds involving C=C and C=N bonds together with sp^3 -C involving various CH_n groups. In contrast, the increase in H_2 dilution brings about an increase in sp^1 -C involving the nitrile and/or isonitrile bonds together with the porosity and corresponding O-H peaks.

4.3.4 Raman Spectroscopy

The Raman spectra of the films produced from $\text{C}_2\text{H}_6:\text{N}_2:\text{H}_2$ are shown in Figure 4.26. These spectra were corrected from the raw Raman spectra shown in Figure 4.27. The raw spectra show the typical baseline with a positive slope up to flow rate of 75 sccm. However, at the highest flow rate the slope is almost horizontal. While the spectra below 75 sccm show the slope is typically seen for polymeric films (Chu & Li, 2006), the spectrum of the film produced at H_2 flow rate of 125 sccm resembles those of graphite-like $a\text{-CN}_x$ films. The deconvolution of the corrected spectra shown in

Figure 4.26 clearly shows the presence of the Raman D and G peaks. There appears to be an additional peak centered at 2000 cm^{-1} in the fitting which was correlated to the structural ordering in the films (Rodil, Ferrari, Robertson, & Milne, 2001). These peaks vanish when the H_2 flow rate was increased to 125 sccm. The disappearance of the peak is in line with the change in the structure as proposed earlier.

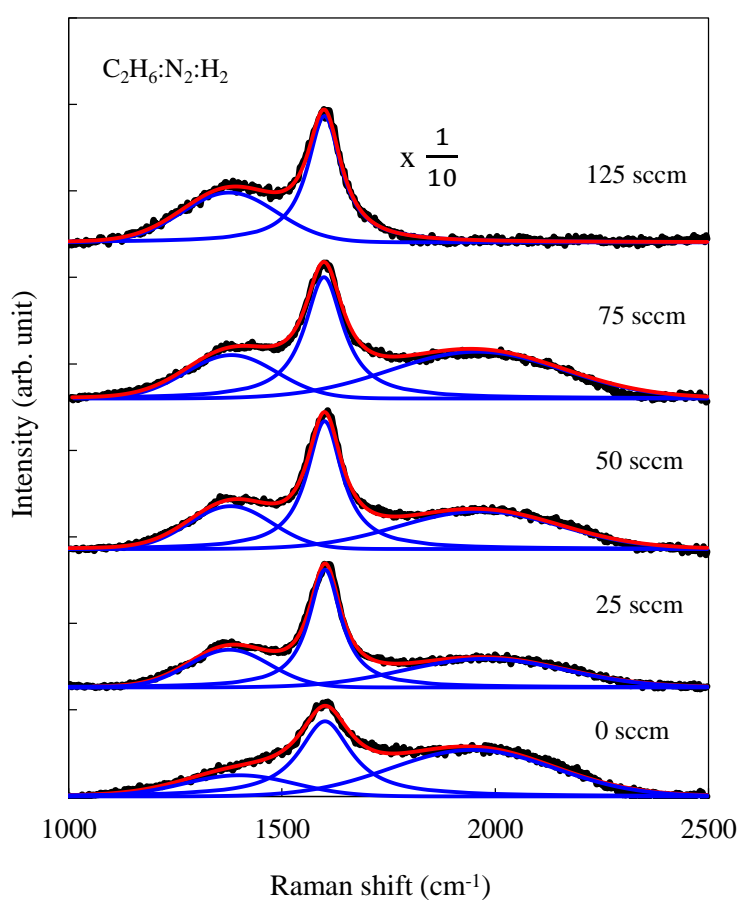
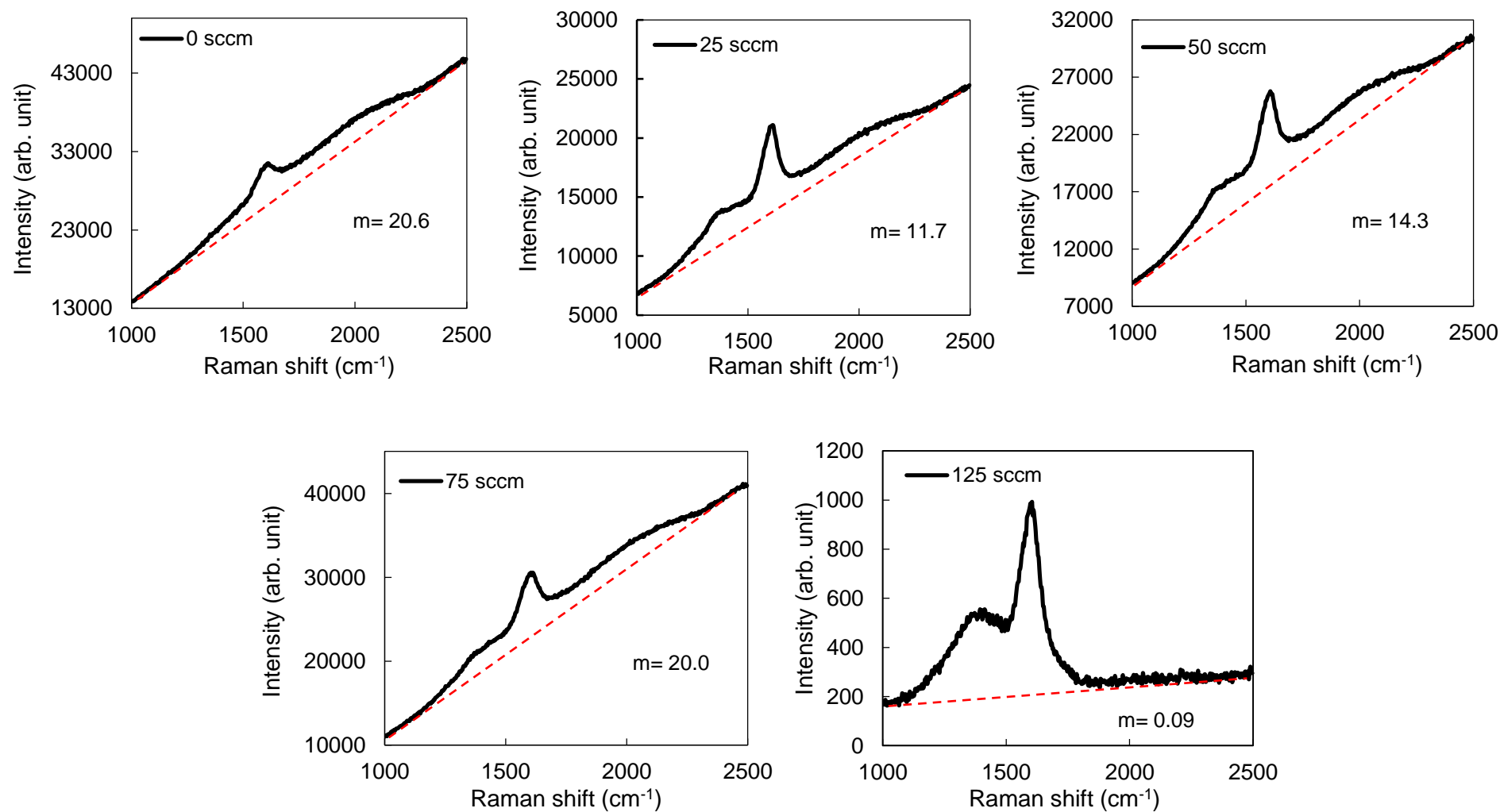


Figure 4.26 Variation in Raman spectra as a function of H_2 flow rate. The height of the spectrum for film deposited at H_2 flow rate of 125 sccm adjusted for classification.

Figure 4.27 Variation in original Raman spectra as a function of H_2 flow rate.

From the result of the deconvolution, the variations in G peak position and I_D/I_G are plotted as a function of H_2 flow rate which is shown in Figure 4.28. G peak position follows the trend in the corresponding I_D/I_G which is typically observed for such materials (A. C. Ferrari & J. Robertson, 2000). It is found that the G peak is blue shifted to lower wavenumber as hydrogen dilution increase up to 75 sccm. However, at the highest H_2 flow rate of 125 sccm the I_D/I_G suddenly increased. The decrease in G peak position between 0 to 75 sccm indicates a reduction in sp^2 cluster size with increasing H_2 dilution. It is well accepted that in microcrystalline graphite, the I_D/I_G is typically related to aromatic cluster size. As the I_D/I_G decreases, the grain size increases and vice versa (Tuinstra & Koenig, 1970a, 1970b). However, for amorphous C films, the opposite occurs since the disorder is so great that the I_D/I_G decreases with decrease in the 'grain' size (A. Ferrari & J. Robertson, 2000). On the other hand, since the presence of the D peak in amorphous C films indicates that the sp^2 sites are in the form of clustered aromatic rings, the decrease in I_D/I_G also suggests the suppression of the clustering of the sp^2 sites in the form of aromatic rings.

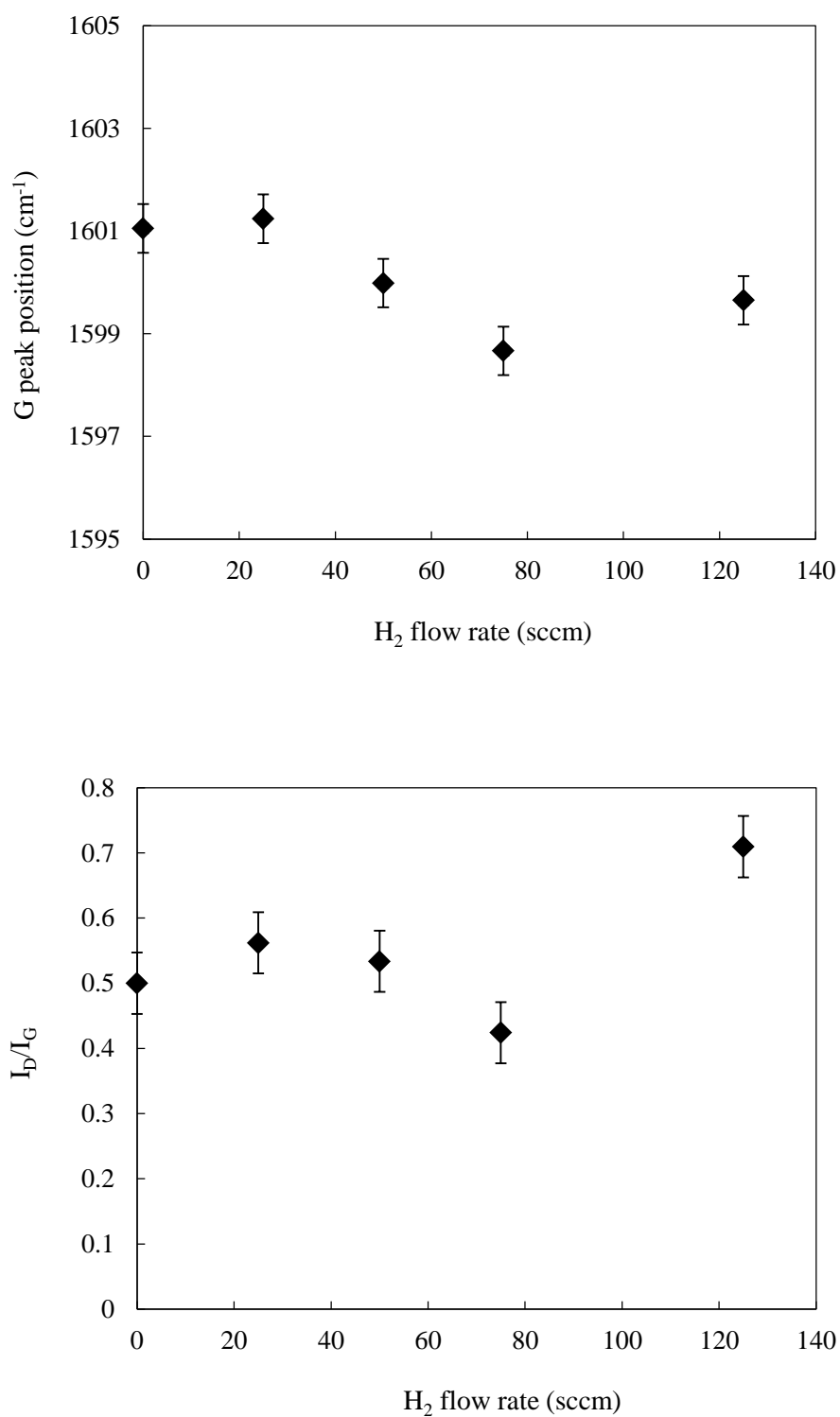


Figure 4.28 Variation in G peak position and I_D/I_G as a function of H₂ flow rate.

H content was estimated from the slope, m , of the raw Raman spectra as shown in Figure 4.29. The H content decrease gradually with the initial increase in H_2 flow rate up to 75 sccm, then decrease significantly when H_2 flow rate was increased to 125 sccm. This is in line with the FTIR result which shows a similar trend in the reduction of CH_n bonding group in the films. The decrease in H leads to the decrease in sp^3 -C bonds due to the fact that H incorporation favours the formation of sp^3 -C sites. Hence, the reduction of this sp^3 -C content should lead to the increase in either sp^2 -C or sp^1 -C bonds in these films. However, FTIR result shows that the formations of sp^1 -C bonds are favoured. At the highest H_2 flow rate, the significant decrease in H content to approximately 20 a.t % support the suggested structural changes in film from polymeric CN_x to graphite-like $a-CN_x$ films.

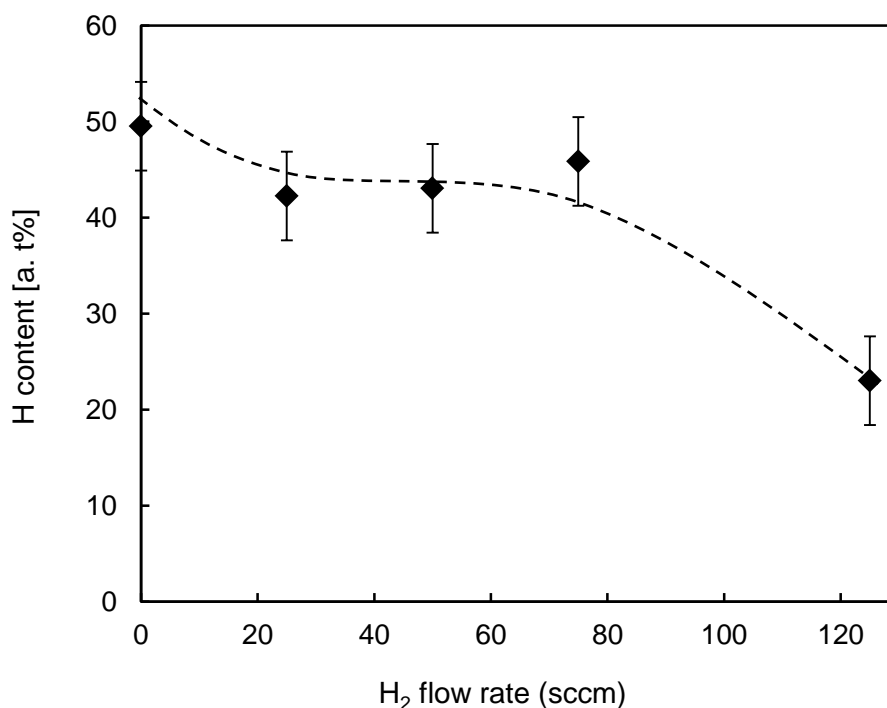


Figure 4.29 Variation in hydrogen content as a function of H_2 flow rate.

4.3.5 Optical

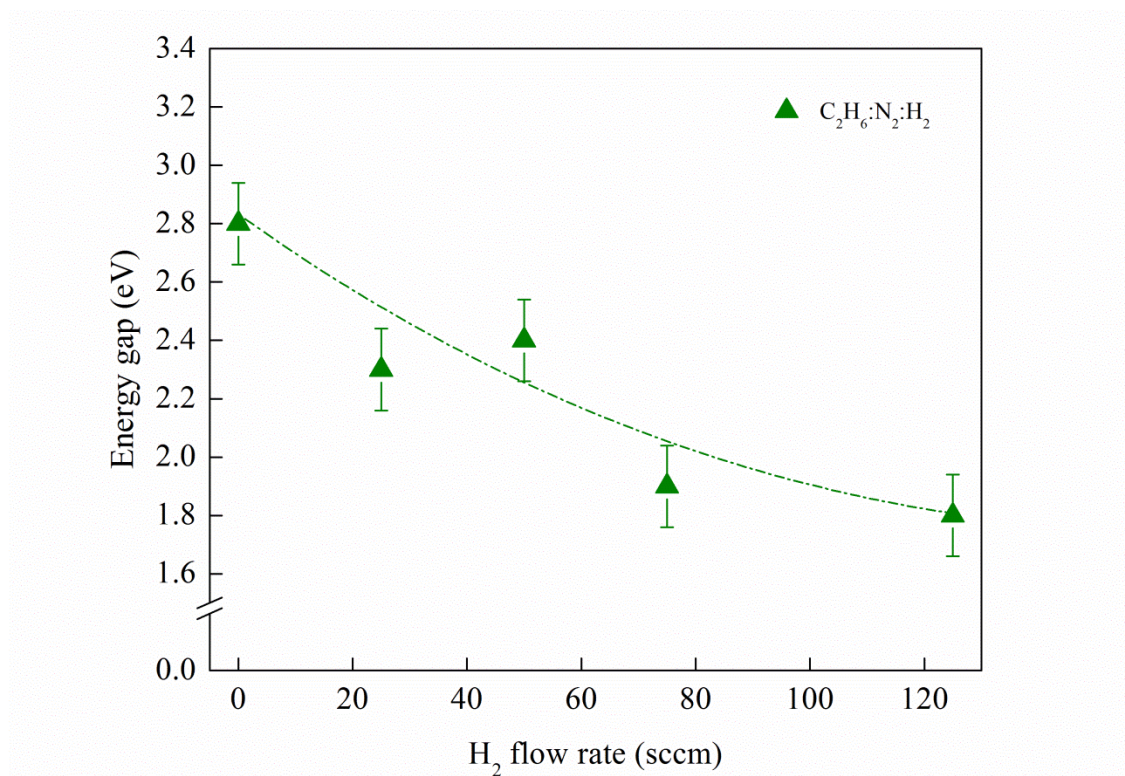


Figure 4.30 Variation in E_g as a function of H_2 flow rate.

The energy gap (E_g) of these CN_x films was calculated from Tauc plot obtained from the optical measurement. The variation in E_g as a function of H_2 flow rate is shown in Figure 4.30. The film produced from $C_2H_6:N_2$ without H_2 dilution shows an E_g of about 2.8 eV. This value decreases progressively with H_2 dilution to about 1.8 eV as the H_2 flow rate is increased from 0 to 125 sccm. According to the ‘cluster model’ for a-C: H films, E_g is determined by energy spacing between the π and π^* which in turn is determined by the size and distribution of sp^2 bonded cluster. A number of studies have shown that E_g decreases as the sp^2 content increases for all type of amorphous C films (Lejeune, Durand-Drouhin, Ballutaud, & Benlahsen, 2002). Some researchers have also shown that amorphous C films with lower H content display either high amount of distortion or large clustering of sp^2 -C sites (Robertson, 1995)

The opposite is seen for the results in this work. While E_g decreases with H_2 flow rate, both Raman and FTIR results indicate a decrease in sp^2 -C bonds and decreased in the size and clustering of these sp^2 -C sites. The decrease could be related to the obvious increase in sp^1 -C bonds in the material in the form of $C\equiv N$ bonds and the appearance of the O-H bonds as H_2 flow rate is increased. The $C\equiv N$ bonds may produce lone-pairs in the C network, while the presence of O-H indicates porosity and disorder in the films. Both of these would form disorder states which may broaden the π and π^* states of the films, thus reduces the E_g of the films.

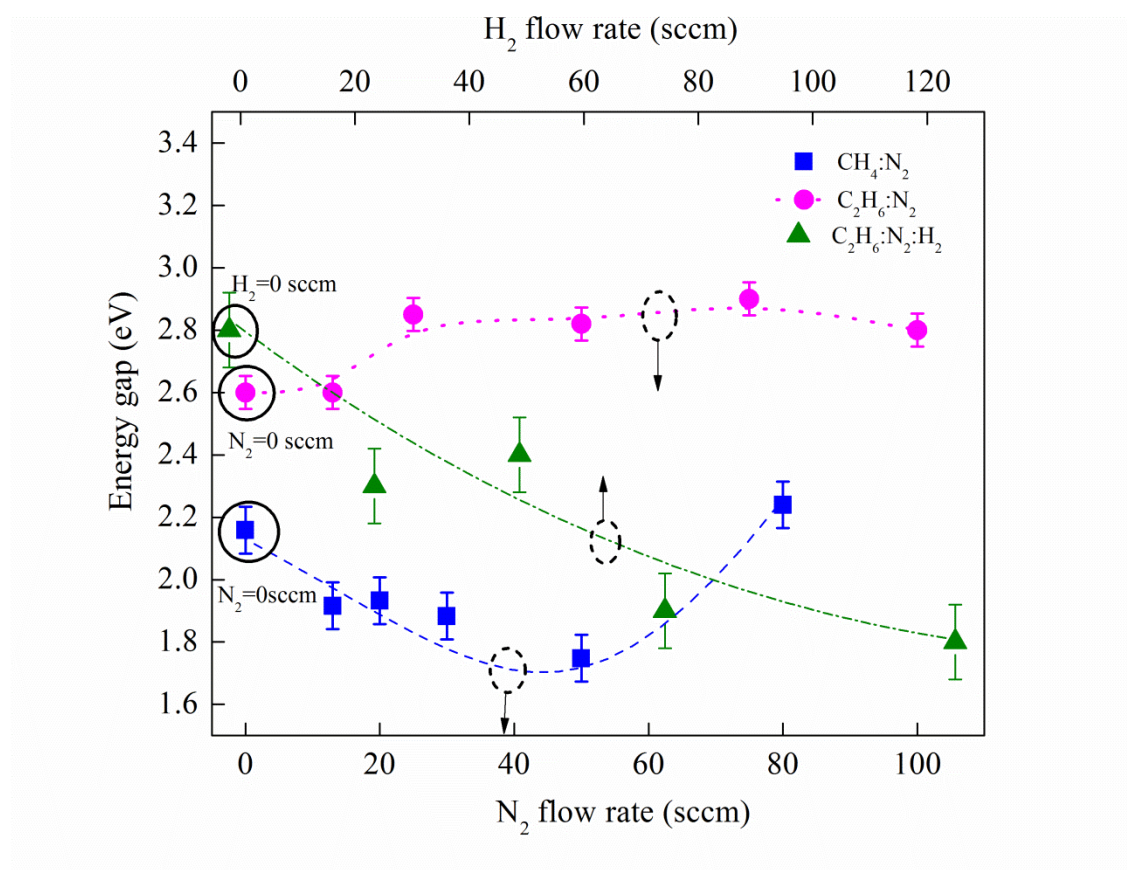


Figure 4.31 Variation in E_g as a function of N_2 and/or H_2 flow rate.

Figure 4.31 compares the variation of E_g for the various gas mixtures used to produce these CN_x films. The variation in E_g seen for films produced from $C_2H_6:N_2:H_2$ changes more drastically compared to the other mixtures. While it was suggested that the mechanism which contributes to the variation of the former is connected to the sp^1 -

C content and disorder, the variation in E_g for the other sets of films was related to the sp^2 -C content together with the size and distribution of its clusters. This in turn is related to the H content and the effects of the H etching on the growth surface. The figure also shows that the E_g of the films produced from $C_2H_6:N_2:H_2$ up to H_2 flow rate of 50 sccm is generally higher than those of $CH_4:N_2$. This might be the limit of H_2 dilution of the $C_2H_6:N_2$ if CN_x films with higher E_g are desired.

4.3.6 Photoluminescence

The variation in the PL spectra for the CN_x films produced from $C_2H_6:N_2:H_2$ as a function of H_2 flow rate is shown in Figure 4.32. The peak position of the emission spectra are almost the same independent of the H_2 flow rate, with changes observed only in the height of the emission intensities and the broadness of the emission band. The variations in the PL emission intensities and peak position as a function of the H_2 flow rate are shown in Figure 4.33. The peak position is taken as the center of the band corresponding to the highest peak intensity of each spectrum. The emission intensity decrease significantly with the H_2 flow rate and is almost quenched at H_2 flow rate of 125 sccm. At this H_2 flow rate, the peak position also shifted significantly corresponding to a change in the recombination center. This could be explained by the proposed change in structure of the material as seen in Raman results at this H_2 flow rate. The change in the structure would lead to a change in the profile of the energy band in the film. Indeed, the proposed graphitization of the film would lead to a smaller band gap due to the broadening of the extended states and the π and π^* states. This was also supported by the optical studies and coincides with the decrease in the PL emission energy at H_2 flow rate of 125 sccm seen in Figure 4.33.

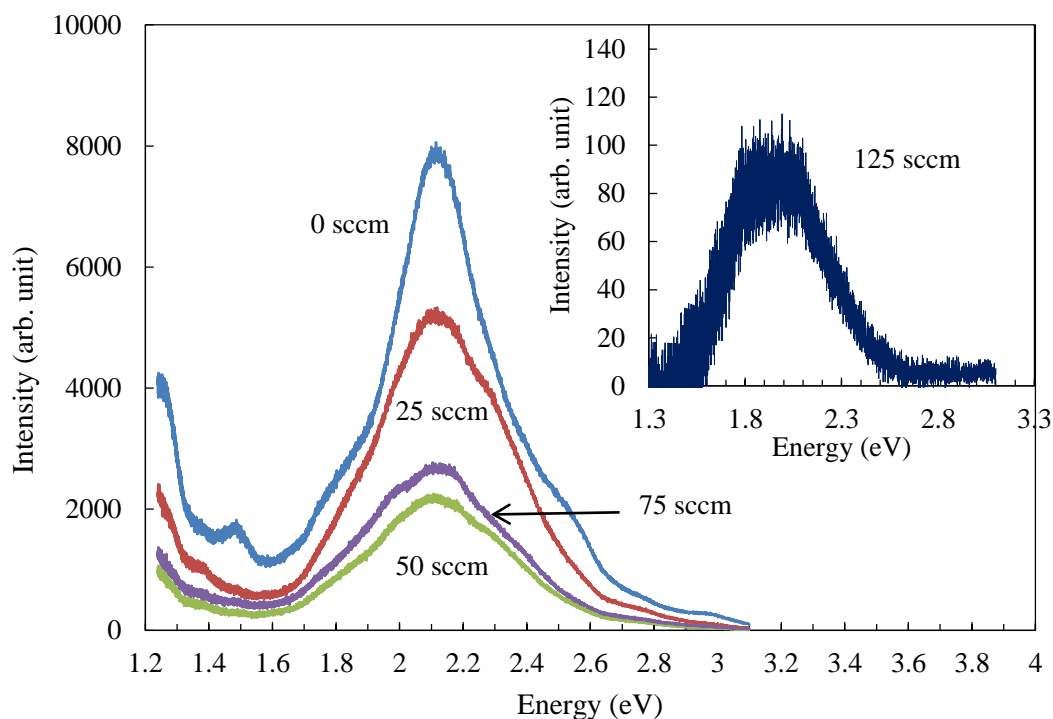


Figure 4.32 Variation in PL spectra as a function of H₂ flow rate

On the other hand the peak position of the emission peak remains almost constant for H₂ flow rate of 25 to 75 sccm, with only a slight decrease compared to the peak position of the film produced from (H₂-free) C₂H₆:N₂ mixture. Thus, this indicates that though the intensities of the PL emission decreases in this range of H₂ flow rate, the recombination centers remain almost the same. This is in line with the Raman results which show similar Raman profile indicating that the structures of the film are the same within this range. The fact that the structure remains the same may have led to the similarity in the recombination centers in the film due to the similarity in the profile of the energy band of the material.

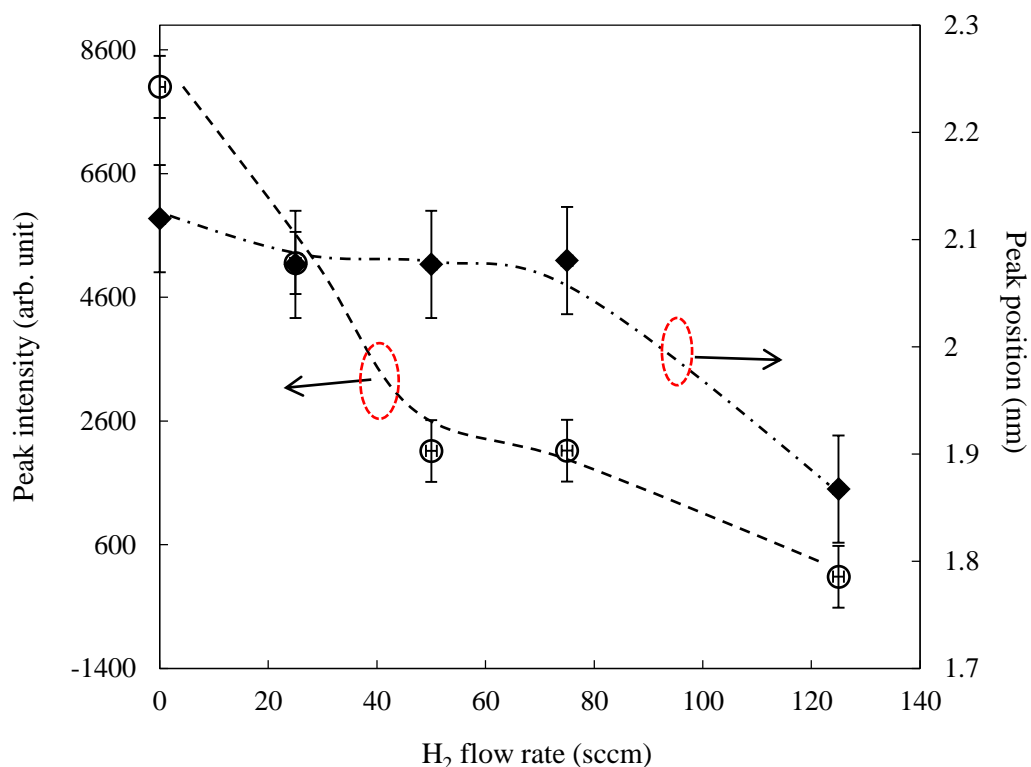


Figure 4.33 The PL intensity and peak position of CN_x films depending on H_2 flow rate.

The PL emission intensities decrease drastically with the increase in H_2 flow rate. The reduction in their intensities is even more pronounced than the changes seen for the variation of N_2 flow rate for the films produced from $\text{CH}_4:\text{N}_2$ and $\text{C}_2\text{H}_6:\text{N}_2$. This could be observed from the accumulated profiles seen in Figure 4.34. Apart from graphitization of the film at H_2 flow rate of 125 sccm, the drastic decrease in the PL emission is the cumulative effect of certain changes in the film with the variation in the H_2 flow rate. One aspect is the decrease in H bonded content in the film, which was discussed earlier in Raman analysis. These are related to the H in the CH_n functional groups that decreases with the increase in H_2 flow rate as was discussed in FTIR analysis. The relationship between the PL intensities and H content is clearly shown in Figure 4.35 where both the PL intensities and H content decreases with H_2 flow rate. However, the variation in the PL intensities does not seem to strictly follow the trend in the H content. Indeed, even as this relationship has been observed by other researchers

(Mutsukura, 2001) the changes in the PL intensities with the IR intensity of the C-H stretching in that work was not drastic. This indicates that other aspect may also contribute, whereby it is believed that two major contributors may include the variation in the sp^1 C \equiv N and the O-H bonds in the material. As discussed the O-H indicates the presence of porosity and disorder in the film. These aspects including C \equiv N, O-H and corresponding porosity and disorder contribute to the formation of lone-pairs in the film. Similar to the first part of this work, these lone-pairs are identified as non-recombination centers in the film resulting in the quenching of the PL emission. Thus with the increase in the H_2 flow rate and corresponding increase in the C \equiv N and O-H bonds observed in FTIR, the resulting quenching of the PL emission is observed.

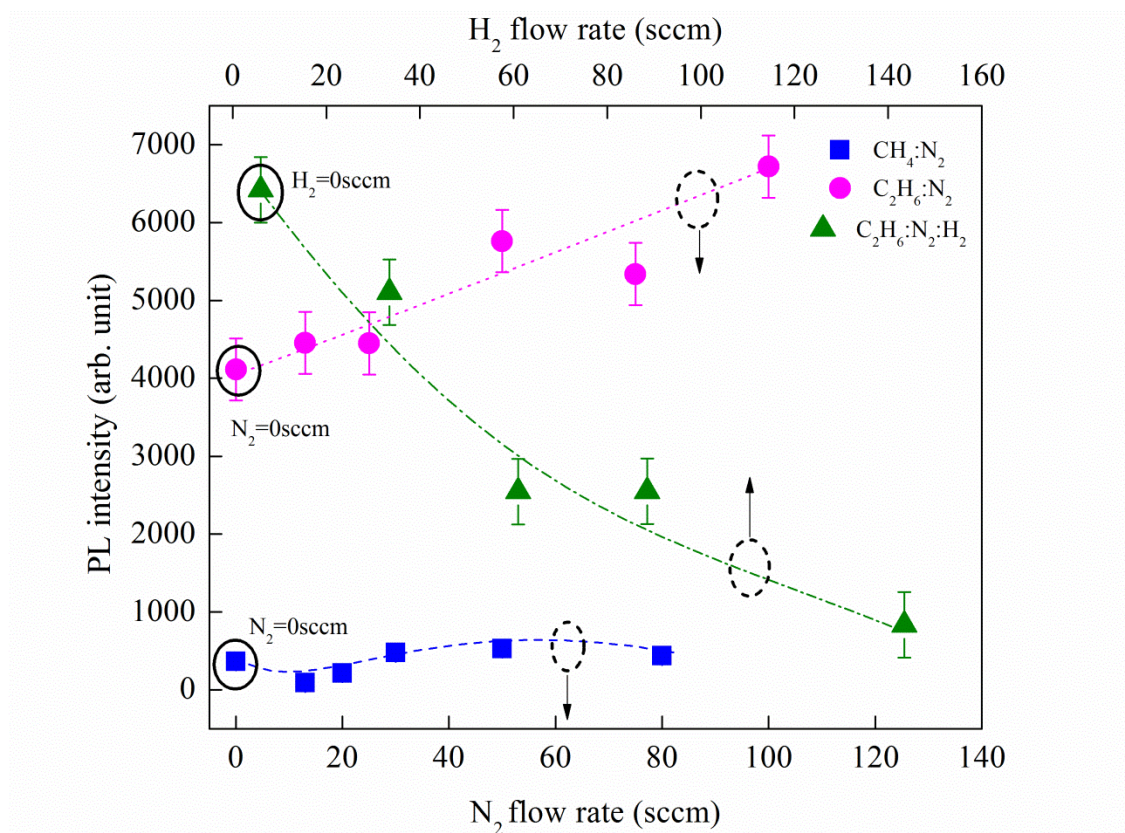


Figure 4.34 Variation in PL intensity as a function of N_2 flow rate for films produced from $CH_4:N_2$ and $C_2H_6:N_2$ together with the variation in PL intensity as a function of H_2 flow rate for the films produced from $C_2H_6:N_2:H_2$

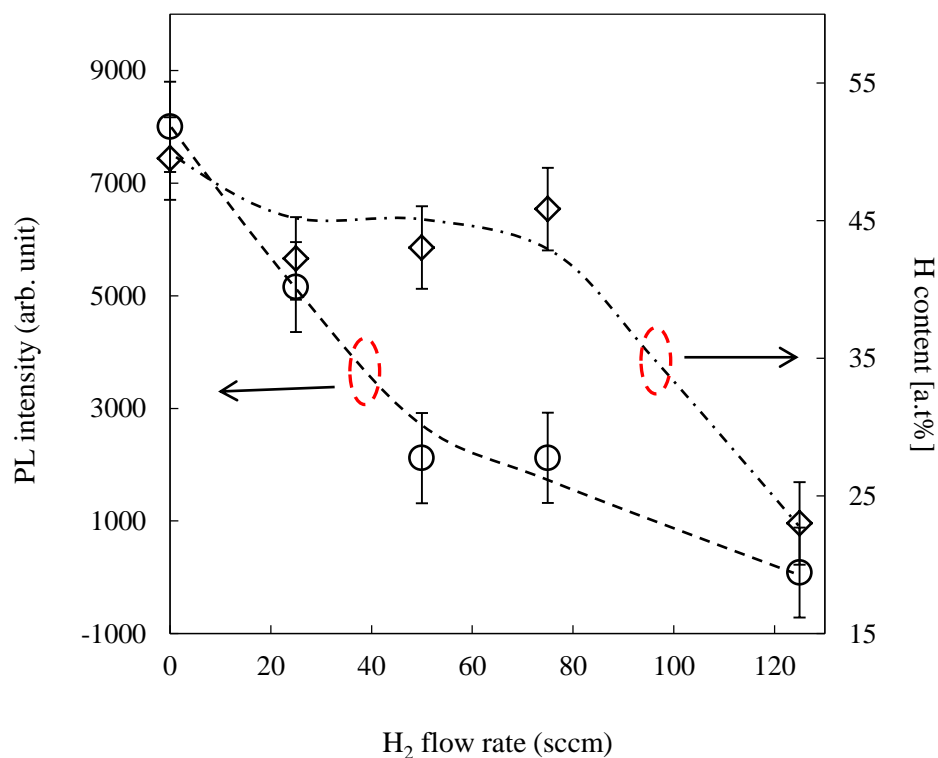


Figure 4.35 Variation in PL intensity and H content as a function of H₂ flow rate.

On the other hand, from Figure 4.34 it is also seen that the PL emission intensity for the films produced from C₂H₆:N₂:H₂, though decrease in intensity with the increase in H₂ flow rate and is generally lower than those of the films produced from C₂H₆:N₂, they are generally higher than those of the films produced from CH₄:N₂. In this aspect, even with the quenching of the PL emission due to H₂ dilution in C₂H₆:N₂, these mixture still produce films with higher PL intensities than that of CH₄:N₂.

CHAPTER 5 CONCLUSIONS AND FUTURE WORKS

5.1 Conclusions

This thesis reports the fabrication of CN_x films using rf PECVD technique from two different kinds of precursor gases. Good quality $\alpha\text{-CN}_x$ films with large surface area were successfully produced from a home built rf PECVD system. In the first part of this work, CN_x films were produced from different hydrocarbon precursors mixed with N_2 gas. The hydrocarbons used were CH_4 and C_2H_6 . N_2 gas flow rate was varied to study the effect of N incorporation. Varying N_2 flow rate significantly affects the CN_x film properties. The effects vary accordingly to the different reaction in CH_4 and C_2H_6 precursor gases. Though the films growth rate for both films decreased with the increase in N_2 flow rate, films produced from $\text{CH}_4\text{:N}_2$ exhibited higher growth rate compared to films produced from $\text{C}_2\text{H}_6\text{:N}_2$ mixture. For films produced from $\text{CH}_4\text{:N}_2$, the decrease in its growth rate was correlated to the decrease in partial pressure of CH_4 in the chamber resulting in a reduction of CH_x radicals. The increase in N_2 dilution also increases N incorporation in these films. N breaks the C network especially in rings which leads to the increase in the nitrile and/or isonitrile $\text{C}\equiv\text{N}$ bonds. The increase in this bonding influences the structure of the films to become more disordered. This disorder also coincide with the reduction in the films' E_g as the sp^2 sites increased with the increase in $\text{C}=\text{N}$ and $\text{C}=\text{C}$ bonds in the films. In contrast to films produced from $\text{C}_2\text{H}_6\text{:N}_2$, N acts as a dopant rather than an active species. Lower N was incorporated into these films and more ordered films were formed. These films exhibit high CH_n bonds which indicate more sp^3 sites in the films. This $\text{sp}^3\text{-C}$ bonds lead to higher E_g (2.8 eV) and the terminating H from this CH_n bond increase the H content which was found to be approximately 50 a.t% higher compared to films produced from $\text{CH}_4\text{:N}_2$. These values indicate that the films exhibit character of polymeric like CN_x films. On the other hand,

films produced from $\text{CH}_4:\text{N}_2$ which showed higher N incorporation exhibits lower E_g with average value of 1.9 eV and lower H content (~20 a.t%). Such properties categorized these films as graphite-like $\alpha\text{-CN}_x$. Both sets of films exhibit increase in PL intensity with the increase in N incorporation. However, films produced from $\text{C}_2\text{H}_6:\text{N}_2$ show much higher PL intensities compared to those produced from $\text{CH}_4:\text{N}_2$. The porosity and disorder in films produced from $\text{CH}_4:\text{N}_2$ which increase the presence of lone pairs in the films was identified as the main cause of their lower PL intensities. The lone pairs promote non-radiative centre and lead to the quenching of PL emission.

In second part of this work, H_2 gas was introduced into the C_2H_6 and N_2 gas mixture to study the effects of H_2 dilution on the CN_x films. The C_2H_6 and N_2 flow rates were kept constant at 25 and 100 sccm. The C_2H_6 precursor and the flow rates of C_2H_6 and N_2 gases were chosen due to the resulting high PL emission intensity of its film determined in the first part of this study. H_2 dilution strongly affects the properties of the CN_x films especially their structure and optical properties. At low H_2 dilution, films produced from $\text{C}_2\text{H}_6:\text{N}_2:\text{H}_2$ mixture show remarkable increase in their growth rate, almost three times higher than films produced from $\text{C}_2\text{H}_6:\text{N}_2$. However, with further increase in H_2 flow rate, the films growth rate decreased due to the etching effects of H_2 and reduction in growth radicals due to the decrease in related partial pressure of the C_2H_6 precursor. While films produced from $\text{CH}_4:\text{N}_2$ show higher growth rate than those of $\text{C}_2\text{H}_6:\text{N}_2$, by using H_2 dilution the growth rate of $\text{C}_2\text{H}_6:\text{N}_2:\text{H}_2$ could exceed even that of $\text{CH}_4:\text{N}_2$. H_2 increased the radical formation together with the increase in the surface radical sites. These sites increased due to the formation of dangling bonds and leads to the increase of the incorporation of N containing radicals. As N incorporation increased, the structure of the C network was distorted and the presence of $\text{sp}^1 \text{C}\equiv\text{N}$ also increased. In addition, the increased in N incorporation induced porosity of these films and

corresponding increase in disorder. The disorder and porosity leads to the reduction in films' E_g due to the broadening of π and π^* state. The reduction in films' E_g was also due to the decrease in sp^3 sites resulting from the decrease in H content. As the disorder, porosity and lone pairs in the films increases, the PL intensities also decrease. The reduction in PL emission intensities suggest that the unpaired electrons act as non-radiative centres, which leads to the decrease in PL efficiency, as proposed in both part of this study. For films produced at the highest H_2 flow rate; their properties changed due to the transition in the films structure. At this highest H_2 flow rate, the N incorporation and H content decreased due to the high H ion concentration which leads to high H_2 etching effects. This is in line with the significant increase in I_D/I_G resulting from the graphitization of the films. This also resulted in further decrease in films E_g . These characteristics show that at the highest H_2 flow rate, the structure of these CN_x films changed from polymeric to graphite-like. Besides ordering and lone pairs, the structures of the films also played an important part in the PL characteristic. This was ascertained from the quenching of PL intensity at the highest H_2 flow rate.

As a general conclusion, CN_x films produced from the $C_2H_6:N_2$ mixture exhibit enhanced PL properties compared to the $CH_4:N_2$ mixture. Apart from the enhancement in PL properties, their optical and structural properties, higher stability due to the absence of porosity makes $C_2H_6:N_2$ mixture more favorable than the $CH_4:N_2$. The disadvantage of lower growth rate using $C_2H_6:N_2$ mixture compared to $CH_4:N_2$ could be solved by introducing H_2 dilution at low flow rate. The films produced from these $C_2H_6:N_2:H_2$ mixture retains the enhanced and desirable properties of those produced from $C_2H_6:N_2$.

5.2 Future work

The used of C_2H_6 mixture in the production of CN_x films promises better films properties. However, there are many aspects that have yet to be investigated due to time limitation. The following suggestions are proposed as future works.

- Further characterization methods to be employed for these CN_x films such as electrical properties, hardness and high resolution (TEM) images.
- Study the effects of higher N_2 dilution particularly towards its contribution to their PL properties. Since the PL intensity of the CN_x films in this work continues to increase in the limited range of the increasing N_2 flow rate, the highest PL intensity which could be obtained as a function of the N_2 flow rate is yet to be determined.
- Focusing the study of H_2 dilution on low H_2 flow rate to determine the optimum value that gives the best CN_x properties while reducing the generation of porosity in the films.

REFERENCES

- Amir, O., & Kalish, R. (1991). Properties of nitrogen-doped amorphous hydrogenated carbon films. *Journal of Applied Physics*, 70(9), 4958-4962.
- Anita, V., Butuda, T., Maeda, T., Takizawa, K., Saito, N., & Takai, O. (2004). Effect of N doping on properties of diamond-like carbon thin films produced by RF capacitively coupled chemical vapor deposition from different precursors. *Diamond and Related Materials*, 13(11), 1993-1996.
- Badzian, A., Badzian, T., Roy, R., & Drawl, W. (1999). Silicon carbonitride, a new hard material and its relation to the confusion about 'harder than diamond' C₃N₄. *Thin Solid Films*, 354(1-2), 148-153.
- Beeman, D., Silverman, J., Lynds, R., & Anderson, M. R. (1984). Modeling studies of amorphous carbon. *Physical Review B*, 30(2), 870-875.
- Beghi, M., Ferrari, A., Teo, K., Robertson, J., Bottani, C., Libassi, A., et al. (2002). Bonding and mechanical properties of ultrathin diamond-like carbon films. *Applied Physics Letters*, 81, 3804.
- Bousetta, A., Lu, M., & Bensaoula, A. (1995). Physical properties of thin carbon nitride films deposited by electron cyclotron resonance assisted vapor deposition. *Journal of Vacuum Science and Technology A: Vacuum, Surfaces and Films*, 13(3), 1639-1643.
- Bull, S. (1995). Tribology of carbon coatings: DLC, diamond and beyond. *Diamond and Related Materials*, 4(5), 827-836.
- Camero, M., Gago, R., Gómez-Aleixandre, C., & Albella, J. (2003). Hydrogen incorporation in CN_x films deposited by ECR chemical vapor deposition. *Diamond and Related Materials*, 12(3), 632-635.
- Casiraghi, C., Ferrari, A. C., & Robertson, J. (2005a). Raman spectroscopy of hydrogenated amorphous carbons. *Physical Review B - Condensed Matter and Materials Physics*, 72(8), 1-14.
- Casiraghi, C., Piazza, F., Ferrari, A. C., Grambole, D., & Robertson, J. (2005b). Bonding in hydrogenated diamond-like carbon by Raman spectroscopy. *Diamond and Related Materials*, 14(3-7), 1098-1102.
- Carey, J. D., & Silva, S. R. P. (2004). Disorder, clustering, and localization effects in amorphous carbon. *Physical Review B - Condensed Matter and Materials Physics*, 70(23), 1-8.
- Chen, L., Bhusari, D., Yang, C., Chen, K., Chuang, T., Lin, M., et al. (1997). Si-containing crystalline carbon nitride derived from microwave plasma-enhanced chemical vapor deposition. *Thin Solid Films*, 303(1-2), 66-75.
- Chowdhury, A. K. M. S., Cameron, D. C., & Hashmi, M. S. J. (1998). Vibrational properties of carbon nitride films by Raman spectroscopy. *Thin Solid Films*, 332(1-2), 62-68.
- Chu, P. K., & Li, L. (2006). Characterization of amorphous and nanocrystalline carbon films. *Materials chemistry and physics*, 96(2), 253-277.
- Couderc, P., & Catherine, Y. (1987). Structure and physical properties of plasma-grown amorphous hydrogenated carbon films. *Thin Solid Films*, 146(1), 93-107.
- Cutiongco, E. C., Li, D., Chung, Y. W., & Bhatia, C. S. (1996). Tribological behavior of amorphous carbon nitride overcoats for magnetic thin-film rigid disks. *Journal of tribology*, 118, 543.
- Demichelis, F., Liu, Y. C., Rong, X. F., Schreiter, S., & Tagliaferro, A. (1995a). High energy photoluminescence in low tauc gap a-C : H : N. *Solid State Communications*, 95(7), 475-477.
- Demichelis, F., Schreiter, S., & Tagliaferro, A. (1995b). Photoluminescence in a-C:H films. *Physical Review B*, 51(4), 2143-2147.

- Donato, M., Galvagno, S., Messina, G., Milone, C., Pistone, A., & Santangelo, S. (2007). Optimisation of gas mixture composition for the preparation of high quality MWCNT by catalytically assisted CVD. *Diamond and Related Materials*, 16(4), 1095-1100.
- Donnet, C., Fontaine, J., Lefebvre, F., Grill, A., Patel, V., & Jahnes, C. (1999). Solid state C and H nuclear magnetic resonance investigations of hydrogenated amorphous carbon. *Journal of Applied Physics*, 85, 3264.
- Drabold, D. A., Fedders, P. A., & Stumm, P. (1994). Theory of diamondlike amorphous carbon. *Physical Review B*, 49(23), 16415-16422.
- Elinson, V., Sleptsov, V., Laymin, A., Potraysay, V., Kostuychenko, L., & Moussina, A. (1999). Barrier properties of carbon films deposited on polymer-based devices in aggressive environments. *Diamond and Related Materials*, 8(12), 2103-2109.
- Erdemir, A., Fenske, G., Terry, J., & Wilbur, P. (1997). Effect of source gas and deposition method on friction and wear performance of diamondlike carbon films. *Surface and Coatings Technology*, 94, 525-530.
- Escobar-Alarcón, L., Arrieta, A., Camps, E., Romero, S., & Camacho-Lopez, M. (2005). Infrared and Raman characterization of amorphous carbon nitride thin films prepared by laser ablation. *Superficies y vacío*(003), 9-12.
- Fanchini, G., Ray, S. C., Tagliaferro, A., & Laurenti, E. (2002a). Density and capture radius of 'defects': Quenching of the luminescent states in non-nitrogenated and nitrogenated amorphous carbon thin films. *Journal of Physics Condensed Matter*, 14(48), 13231-13240.
- Fanchini, G., Tagliaferro, A., Messina, G., Santangelo, S., Paoletti, A., & Tucciarone, A. (2002b). Vibrational properties and microstructure of reactively sputtered hydrogenated carbon nitrides. *Journal of Applied Physics*, 91, 1155.
- Fanchini, G., Ray, S. C., & Tagliaferro, A. (2003). Photoluminescence investigation of carbon nitride-based films deposited by reactive sputtering. *Diamond and Related Materials*, 12(3-7), 1084-1087.
- Fanchini, G., Mandracci, P., Tagliaferro, A., Rodil, S. E., Vomiero, A., & Della Mea, G. (2005). Growth and characterisation of polymeric amorphous carbon and carbon nitride films from propane. *Diamond and Related Materials*, 14(3-7), 928-933.
- Ferrari, A. C., & Robertson, J. (2000). Interpretation of Raman spectra of disordered and amorphous carbon. *Physical Review B - Condensed Matter and Materials Physics*, 61(20), 14095-14107.
- Ferrari, A. C., & Robertson, J. (2001). Resonant raman spectroscopy of disordered, amorphous, and diamondlike carbon. *Physical Review B - Condensed Matter and Materials Physics*, 64(7), 754141-7541413.
- Ferrari, A. C., Rodil, S. E., & Robertson, J. (2003). Interpretation of infrared and Raman spectra of amorphous carbon nitrides. *Physical Review B - Condensed Matter and Materials Physics*, 67(15), 1553061-15530620.
- Ferrari, A. C. (2008). Non-destructive characterisation of carbon films. *Tribology of Diamond-Like Carbon Films: Fundamentals and Applications*, Springer, 25-82.
- Gharbi, R., Fathallah, M., Alzaied, N., Tresso, E., & Tagliaferro, A. (2008). Hydrogen and nitrogen effects on optical and structural properties of amorphous carbon. *Materials Science and Engineering C*, 28(5-6), 795-798.
- Gilkes, K., Sands, H., Batchelder, D., Robertson, J., & Milne, W. (1997). Direct observation of sp bonding in tetrahedral amorphous carbon using ultraviolet Raman spectroscopy. *Applied Physics Letters*, 70, 1980.
- Grill, A., & Patel, V. (1992). Characterization of diamondlike carbon by infrared spectroscopy? *Applied Physics Letters*, 60(17), 2089-2091.

- Godet, C., Heitz, T., Bourée, J., Dré villon, B., & Clerc, C. (1998). Growth and composition of dual-plasma polymer-like amorphous carbon films. *Journal of Applied Physics*, 84, 3919.
- Gulino, G., Vieira, R., Amadou, J., Nguyen, P., Ledoux, M. J., Galvagno, S., et al. (2005). C₂H₆ as an active carbon source for a large scale synthesis of carbon nanotubes by chemical vapour deposition. *Applied Catalysis A: General*, 279(1), 89-97.
- Hammer, P., Victoria, N. M., & Alvarez, F. (1998). Electronic structure of hydrogenated carbon nitride films. *Journal of Vacuum Science and Technology A: Vacuum, Surfaces and Films*, 16(5), 2941-2949.
- Hammer, P., Lacerda, R. G., Droppa Jr, R., & Alvarez, F. (2000). Comparative study on the bonding structure of hydrogenated and hydrogen free carbon nitride films with high N content. *Diamond and Related Materials*, 9(3-6), 577-581.
- Hassan, M. K., Pramanik, B. K., & Hatta, A. (2006). Electrical Resistivities of the Diamond-Like Carbon Films Fabricated from Methane and Acetylene Using RF Plasma. *New Diam Front Carbon Technol*, 16(4), 211-219.
- Hayashi, Y., Ishikawa, S., Soga, T., Umeno, M., & Jimbo, T. (2003). Photovoltaic characteristics of boron-doped hydrogenated amorphous carbon on n-Si substrate prepared by rf plasma-enhanced CVD using trimethylboron. *Diamond and Related Materials*, 12(3), 687-690.
- Hayashi, Y., Kamio, T., Soga, T., Kaneko, K., & Jimbo, T. (2005). Efficient nitrogen incorporation into amorphous carbon films by double beam method. *Diamond and Related Materials*, 14(3), 970-974.
- Heitz, T., Dré villon, B., Godet, C., & Bourée, J. E. (1998). Quantitative study of C-H bonding in polymerlike amorphous carbon films using in situ infrared ellipsometry. *Physical Review B - Condensed Matter and Materials Physics*, 58(20), 13957-13973.
- Hellgren, N., Johansson, M. P., Broitman, E., Hultman, L., & Sundgren, J. E. (1999). Role of nitrogen in the formation of hard and elastic CN_x thin films by reactive magnetron sputtering. *Physical Review B - Condensed Matter and Materials Physics*, 59(7), 5162-5169.
- Ilie, A., Harel, O., Conway, N. M. J., Yagi, T., Robertson, J., & Milne, W. I. (2000). Photoconductivity of nitrogen-modified hydrogenated tetrahedral amorphous carbon. *Journal of Applied Physics*, 87(2), 789-794.
- Iwasaki, T., Aono, M., Nitta, S., Habuchi, H., Itoh, T., & Nonomura, S. (1999). Structural and electronic properties of highly photoconductive amorphous carbon nitride. *Diamond and Related Materials*, 8(2-5), 440-445.
- Kim, B., & Grotjohn, T. (2000). Comparison of aC: H films deposited from methane-argon and acetylene-argon mixtures by electron cyclotron resonance-chemical vapor deposition discharges. *Diamond and Related Materials*, 9(1), 37-47.
- Kleinsorge, B., Ferrari, A. C., Robertson, J., Milne, W. I., Waidmann, S., & Hearne, S. (2000). Bonding regimes of nitrogen in amorphous carbon. *Diamond and Related Materials*, 9(3), 643-648.
- Köhler, T., Frauenheim, T., & Jungnickel, G. (1995). Stability, chemical bonding, and vibrational properties of amorphous carbon at different mass densities. *Physical Review B*, 52(16), 11837-11844.
- Kresse, G., Furthmüller, J., & Hafner, J. (1995). Ab initio force constant approach to phonon dispersion relations of diamond and graphite. *EPL (Europhysics Letters)*, 32, 729.
- Kumar, S., Dixit, P., Sarangi, D., & Bhattacharyya, R. (1996). Diamond-like carbon films grown by very high frequency (100 MHz) plasma enhanced chemical vapor deposition technique. *Applied Physics Letters*, 69, 49.

- Kuo, M., May, P., Gunn, A., Ashfold, M., & Wild, R. (2000). Studies of phosphorus doped diamond-like carbon films. *Diamond and Related Materials*, 9(3), 1222-1227.
- Lacerda, R., Marques, F., & Freire, F. (1999). The subimplantation model for diamond-like carbon films deposited by methane gas decomposition. *Diamond and Related Materials*, 8(2), 495-499.
- Lazar, G., Zellama, K., Vascan, I., Stamate, M., Lazar, I., & Rusu, I. (2005). Infrared absorption properties of amorphous carbon films. *Journal of Optoelectronics and Advanced Materials*, 7(2), 647-652.
- Lee, K. R., Baik, Y. J., Eun, K. Y., & Han, S. (1994). Precursor gas effect on the structure and properties of diamond-like carbon films. *Diamond and Related Materials*, 3(10), 1230-1234.
- Lee, S., Park, S. J., Oh, S. G., Kim, W. M., Bae, J. H., Cheong, B. K., et al. (1997). Optical and mechanical properties of amorphous CN films. *Thin Solid Films*, 308-309(1-4), 135-140.
- Legrand, J. C., Damiy, A. M., Hrach, R., & Hrachová, V. (1999). Mechanisms of methane decomposition in nitrogen afterglow plasma. *Vacuum*, 52(1-2), 27-32.
- Lejeune, M., Durand-Drouhin, O., Ballutaud, D., & Benlahsen, M. (2002). Optical investigations of the microstructure of carbon nitride films deposited by magnetron sputtering. *Surface and Coatings Technology*, 151, 242-246.
- LIN, V., Colthup, N. B., Fateley, W. G., & Grasselli, J. G. (1991). Handbook of infrared and raman characteristic frequencies of organic molecules. *Recherche*, 67, 02.
- Liu, A. Y., & Cohen, M. L. (1990). Structural properties and electronic structure of low-compressibility materials: β -Si₃N₄ and hypothetical β -C₃N₄. *Physical Review B*, 41(15), 10727.
- Liu, Y., Demichelis, F., & Tagliaferro, A. (1996). The effect of nitrogen on the microstructure and the luminescence properties of a-C : H thin films. *Solid State Communications*, 100(8), 597-602.
- Mapelli, C., Castiglioni, C., Zerbi, G., & Müllen, K. (1999). Common force field for graphite and polycyclic aromatic hydrocarbons. *Physical Review B - Condensed Matter and Materials Physics*, 60(18), 12710-12725.
- Marchon, B. (1997). Photoluminescence and Raman Spectroscopy in Hydrogenated Carbon Films. *IEEE Transactions on Magnetics*, 33(5 PART 1), 3148-3150.
- Mariotto, G., Freire Jr, F. L., & Achete, C. A. (1994). Raman spectroscopy on nitrogen-incorporated amorphous hydrogenated carbon films. *Thin Solid Films*, 241(1-2), 255-259.
- Mendoza, D., Aguilar-Hernández, J., & Contreras-Puente, G. (1992). Graphite-like bonding induced in hydrogenated amorphous carbon films with high nitrogen content. *Solid State Communications*, 84(11), 1025-1027.
- Motta, E. F., & Pereyra, I. (2004). Amorphous hydrogenated carbon-nitride films prepared by RF-PECVD in methane-nitrogen atmospheres. *Journal of Non-Crystalline Solids*, 338-340(1 SPEC. ISS.), 525-529.
- Muhl, S., & Méndez, J. M. (1999). A review of the preparation of carbon nitride films. *Diamond and Related Materials*, 8(10), 1809-1830.
- Mutsukura, N. (2001). Photoluminescence and infra-red absorption of annealed a-CN_x:H films. *Diamond and Related Materials*, 10(3-7), 1152-1155.
- Mutsukura, N., & Akita, K.-i. (1999a). Deposition of hydrogenated amorphous CN_x film in CH₄/N₂ RF discharge. *Diamond and Related Materials*, 8(8-9), 1720-1723.
- Mutsukura, N., & Akita, K. I. (1999b). Infrared absorption spectroscopy measurements of amorphous CN_x films prepared in CH₄/N₂ r.f. discharge. *Thin Solid Films*, 349(1-2), 115-119.

- Nemanich, R. J., & Solin, S. A. (1979). First- and second-order Raman scattering from finite-size crystals of graphite. *Physical Review B*, 20(2), 392-401.
- Neuhaeuser, M., Hilgers, H., Joeris, P., White, R., & Windeln, J. (2000). Raman spectroscopy measurements of DC-magnetron sputtered carbon nitride (a-C:N) thin films for magnetic hard disk coatings. *Diamond and Related Materials*, 9(8), 1500-1505.
- Neuhaeuser, M., Hilgers, H., Joeris, P., White, R., & Windeln, J. (2000). Raman spectroscopy measurements of DC-magnetron sputtered carbon nitride (a-C:N) thin films for magnetic hard disk coatings. *Diamond and Related Materials*, 9(8), 1500-1505.
- Panwar, O. S., Khan, M. A., Bhattacharjee, B., Pal, A. K., Satyanarayana, B. S., Dixit, P. N., et al. (2006). Reflectance and photoluminescence spectra of as grown and hydrogen and nitrogen incorporated tetrahedral amorphous carbon films deposited using an S bend filtered cathodic vacuum arc process. *Thin Solid Films*, 515(4), 1597-1606.
- Pappas, D. L., Saenger, K. L., Bruley, J., Krakow, W., Cuomo, J. J., Gu, T., et al. (1992). Pulsed laser deposition of diamond-like carbon films. *Journal of Applied Physics*, 71(11), 5675-5684.
- Pereira, J., Géraud-Grenier, I., Massereau-Guilbaud, V., & Plain, A. (2005). Characterization of hydrogenated amorphous carbon nitride particles and coatings obtained in a CH₄/N₂ radiofrequency discharge. *Thin Solid Films*, 482(1-2), 226-231.
- Piscanec, S., Lazzeri, M., Mauri, F., Ferrari, A. C., & Robertson, J. (2004). Kohn anomalies and electron-phonon interactions in graphite. *Physical Review Letters*, 93(18), 185503-185501-185503-185504.
- Polo, M. C., Andújar, J. L., Hart, A., Robertson, J., & Milne, W. I. (2000). Preparation of tetrahedral amorphous carbon films by filtered cathodic vacuum arc deposition. *Diamond and Related Materials*, 9(3), 663-667.
- Popescu, B., Verney, C., Davis, E., Paret, V., & Brunet-Bruneau, A. (2000). Optical properties of sputtered hydrogenated amorphous carbon. *Journal of Non-Crystalline Solids*, 266, 778-782.
- Ristein, J., Stief, R. T., Ley, L., & Beyer, W. (1998). A comparative analysis of a-C:H by infrared spectroscopy and mass selected thermal effusion. *Journal of Applied Physics*, 84(7), 3836-3847.
- Robertson, J., & O'reilly, E. (1987). Electronic and atomic structure of amorphous carbon. *Physical Review B*, 35(6), 2946.
- Robertson, J. (1995). Structural models of a-C and a-C:H. *Diamond and Related Materials*, 4(4), 297-301.
- Robertson, J., & Davis, C. A. (1995). Nitrogen doping of tetrahedral amorphous carbon. *Diamond and Related Materials*, 4(4), 441-444.
- Robertson, J. (1996a). Photoluminescence mechanism in amorphous hydrogenated carbon. *Diamond and Related Materials*, 5(3-5), 457-460.
- Robertson, J. (1996b). Recombination and photoluminescence mechanism in hydrogenated amorphous carbon. *Physical Review B - Condensed Matter and Materials Physics*, 53(24), 16302-16305.
- Robertson, J. (1997). Gap states in diamond-like amorphous carbon. *Philosophical Magazine B*, 76(3), 335-350.
- Robertson, J. (2002). Diamond-like amorphous carbon. *Materials Science and Engineering: R: Reports*, 37(4-6), 129-281.
- Rodil, S. E., Ferrari, A. C., Robertson, J., & Milne, W. I. (2001a). Raman and infrared modes of hydrogenated amorphous carbon nitride. *Journal of Applied Physics*, 89(10), 5425-5430.

- Rodil, S. E., Milne, W. I., Robertson, J., & Brown, L. M. (2001b). Dual ion plasma-beam sources used to maximise sp³ C-C bonds in carbon nitride. *Diamond and Related Materials*, 10(3-7), 1125-1131.
- Rodil, S., & Muhl, S. (2004). Bonding in amorphous carbon nitride. *Diamond and Related Materials*, 13(4), 1521-1531.
- Rodil, S. E., Muhl, S., Maca, S., & Ferrari, A. C. (2003). Optical gap in carbon nitride films. *Thin Solid Films*, 433(1-2 SPEC.), 119-125.
- Santos, M., Silvestre, A., & Conde, O. (2002). Laser-assisted deposition of rB< sub>4</sub> C coatings using ethylene as carbon precursor. *Surface and Coatings Technology*, 151, 160-164.
- Sattel, S., Robertson, J., & Ehrhardt, H. (1997). Effects of deposition temperature on the properties of hydrogenated tetrahedral amorphous carbon. *Journal of Applied Physics*, 82, 4566.
- Schwan, J., Dworschak, W., Jung, K., & Ehrhardt, H. (1994). Microstructures and mechanical properties of amorphous hydrogenated carbon-nitrogen films. *Diamond and Related Materials*, 3(7), 1034-1039.
- Schwan, J., Batori, V., Ulrich, S., Ehrhardt, H., & Silva, S. R. P. (1998). Nitrogen doping of amorphous carbon thin films. *Journal of Applied Physics*, 84(4), 2071-2081.
- Shiao, J., & Hoffman, R. W. (1996). Studies of diamond-like and nitrogen-containing diamond-like carbon using laser Raman spectroscopy. *Thin Solid Films*, 283(1-2), 145-150.
- Shinohara, M., Kawazoe, H., Inayoshi, T., Kawakami, T., Matsuda, Y., Fujiyama, H., et al. Dependences of growth process of amorphous carbon films on the different source gases: methane and acetylene.
- Silva, S. R. P., Robertson, J., Amaratunga, G. A. J., Rafferty, B., Brown, L. M., Schwan, J., et al. (1997). Nitrogen modification of hydrogenated amorphous carbon films. *Journal of Applied Physics*, 81(6), 2626-2634.
- Sjöström, H., Stafström, S., Boman, M., & Sundgren, J. E. (1995). Superhard and elastic carbon nitride thin films having fullerenelike microstructure. *Physical Review Letters*, 75(7), 1336-1339.
- Sjöström, H., Hultman, L., Sundgren, J. E., Hainsworth, S. V., Page, T. F., & Theunissen, G. S. A. M. (1996). Structural and mechanical properties of carbon nitride CN_x (0.2≤x≤0.35) films. *Journal of Vacuum Science and Technology A: Vacuum, Surfaces and Films*, 14(1), 56-62.
- Smith, S. M., Voight, S. A., Tompkins, H., Hooper, A., Talin, A. A., & Vella, J. (2001). Nitrogen-doped plasma enhanced chemical vapor deposited (PECVD) amorphous carbon: processes and properties. *Thin Solid Films*, 398, 163-169.
- Souto, S., & Alvarez, F. (1997). The role of hydrogen in nitrogen-containing diamondlike films studied by photoelectron spectroscopy. *Applied Physics Letters*, 70, 1539.
- Spaeth, C., Kühn, M., Kreissig, U., & Richter, F. (1997). Preparation of CN_x films by ion beam assisted filtered cathodic arc deposition. *Diamond and Related Materials*, 6(5-7), 626-630.
- Suzuki, T., Manita, Y., Yamazaki, T., Wada, S., & Noma, T. (1995). Deposition of carbon films by electrolysis of a water-ethylene glycol solution. *Journal of materials science*, 30(8), 2067-2069.
- Swain, B. P. (2006). The analysis of carbon bonding environment in HWCVD deposited a-SiC: H films by XPS and Raman spectroscopy. *Surface and Coatings Technology*, 201(3), 1589-1593.
- Swain, B. P., Gundu Rao, T., Roy, M., Gupta, J., & Dusane, R. (2006). Effect of H< sub>2</sub> dilution on Cat-CVD a-SiC: H films. *Thin Solid Films*, 501(1), 173-176.

- Szörényi, T., Fuchs, C., Fogarassy, E., Hommet, J., & Le Normand, F. (2000). Chemical analysis of pulsed laser deposited a-CN_x films by comparative infrared and X-ray photoelectron spectroscopies. *Surface and Coatings Technology*, 125(1), 308-312.
- Takada, N., Arai, K., Nitta, S., & Nonomura, S. (1997). Preparation and properties of reactive-sputtered amorphous CN_x films. *Applied Surface Science*, 113-114, 274-277.
- Tamor, M. A., Haire, J. A., Wu, C. H., & Hass, K. C. (1989). Correlation of the optical gaps and Raman spectra of hydrogenated amorphous carbon films. *Applied Physics Letters*, 54(2), 123-125.
- Tsai, H., & Bogy, D. (1987). Characterization of diamondlike carbon films and their application as overcoats on thin-film media for magnetic recording. *Journal of Vacuum Science & Technology A: Vacuum, Surfaces, and Films*, 5(6), 3287-3312.
- Tuinstra, F., & Koenig, J. L. (1970a). Raman Spectrum Of Graphite. *Journal of Chemical Physics*, 53(3), 1126-1130.
- Tuinstra, F., & Koenig, J. L. (1970b). Roman spectrum of graphite. *The Journal of Chemical Physics*, 53(3), 1280-1281.
- Veerasamy, V. S., Yuan, J., Amaratunga, G. A. J., Milne, W. I., Gilkes, K. W. R., Weiler, M., et al. (1993). Nitrogen doping of highly tetrahedral amorphous carbon. *Physical Review B*, 48(24), 17954-17959.
- Von Keudell, A., Meier, M., & Hopf, C. (2002). Growth mechanism of amorphous hydrogenated carbon. *Diamond and Related Materials*, 11(3), 969-975.
- Walters, J. K., Kühn, M., Spaeth, C., Dooryhee, E., & Newport, R. J. (1998). X-ray diffraction studies of the effects of N incorporation in amorphous CN_x materials. *Journal of Applied Physics*, 83(7), 3529-3534.
- Wang, C., Yang, S., & Zhang, J. (2008a). Correlation between nitrogen incorporation and structural modification of hydrogenated carbon nitride films. *Journal of Non-Crystalline Solids*, 354(15-16), 1608-1614.
- Wang, C., Yang, S., & Zhang, J. (2008b). The infrared characteristics investigation of carbon nitride films. *Diamond and Related Materials*, 17(2), 174-179.
- Wang, H., Shen, M. R., Ning, Z. Y., Ye, C., & Zhu, H. S. (1997). Pulsed electrodeposition of diamond-like carbon films. *Journal of materials research*, 12(11), 3102-3105.
- Wang, J., Huang, N., Yang, P., Leng, Y., Sun, H., Liu, Z., et al. (2004). The effects of amorphous carbon films deposited on polyethylene terephthalate on bacterial adhesion. *Biomaterials*, 25(16), 3163-3170.
- Wang, Y., Alsmeyer, D. C., & McCreery, R. L. (1990). Raman spectroscopy of carbon materials: Structural basis of observed spectra. *Chemistry of Materials*, 2(5), 557-563.
- Weber, F. R., & Oechsner, H. (1999). Low-energy plasma beam deposition of carbon nitride layers with β-C₃N₄-like fractions. *Thin Solid Films*, 355, 73-78.
- Wei, B., Zhang, B., & Johnson, K. E. (1998). Nitrogen-induced modifications in microstructure and wear durability of ultrathin amorphous-carbon films. *Journal of Applied Physics*, 83(5), 2491-2499.
- Widawski, G., Rawiso, M., & François, B. (1994). Self-organized honeycomb morphology of star-polymer polystyrene films.
- Wood, P., Wydeven, T., & Tsuji, O. (1995). Influence of reactant gas composition on selected properties of N-doped hydrogenated amorphous carbon films. *Thin Solid Films*, 258(1), 151-158.
- Xie, E., Jin, Y., Wang, Z., & He, D. (1998). Formation of C-N compounds by N-implantation into diamond films. *Nuclear Instruments and Methods in Physics*

- Research Section B: Beam Interactions with Materials and Atoms*, 135(1), 224-228.
- Xu, J., Mei, J., Huang, X., Li, W., Li, Z., Li, X., et al. (2004). The change of photoluminescence characteristics of amorphous carbon films due to hydrogen dilution. *Journal of Non-Crystalline Solids*, 338, 481-485.
- Yap, Y. K., Kida, S., Aoyama, T., Mori, Y., & Sasaki, T. (1998). Influence of negative dc bias voltage on structural transformation of carbon nitride at 600 °C. *Applied Physics Letters*, 73(7), 915-917.
- Yeh, T. A., Lin, C. L., Sivertsen, J. M., & Judy, J. H. (1991). Durability and structure of RF sputtered carbon-nitrogen thin film overcoats on rigid disks of magnetic thin film media. *Magnetics, IEEE Transactions on*, 27(6), 5163-5165.
- Zhang, M., Nakayama, Y., & Harada, S. (1999a). Photoluminescence of hydrogenated amorphous carbon nitride films after ultraviolet light irradiation and thermal annealing. *Journal of Applied Physics*, 86(9), 4971-4977.
- Zhang, M., Nakayama, Y., & Kume, M. (1999b). Room-temperature electroluminescence from hydrogenated amorphous carbon nitride film. *Solid State Communications*, 110(12), 679-683.
- Zhang, M., Nakayama, Y., Miyazaki, T., & Kume, M. (1999c). Growth of amorphous hydrogenated carbon nitride films in radio-frequency plasma. *Journal of Applied Physics*, 85, 2904.
- Zhang, P., Tay, B., Sun, C., & Lau, S. (2002). Microstructure and mechanical properties of nanocomposite amorphous carbon films. *Journal of Vacuum Science & Technology A: Vacuum, Surfaces, and Films*, 20, 1390.
- Zhang, Y., Gu, Y., Chang, X., Tian, Z., Shi, D., & Zhang, X. (2000). On the structure and composition of crystalline carbon nitride films synthesized by microwave plasma chemical vapor deposition. *Materials Science and Engineering B*, 78(1), 11-15.
- Zhao, X. A., Ong, C. W., Tsang, Y. C., Wong, Y. W., Chan, P. W., & Choy, C. L. (1995). Reactive pulsed laser deposition of CN_x films. *Applied Physics Letters*, 66, 3368.